IAEA
International Atomic Energy Agency

Assessment of High Wind and External Flooding (Excluding Tsunami) Hazards in Site Evaluation for Nuclear Installations

IAEA SAFETY STANDARDS AND RELATED PUBLICATIONS

IAEA SAFETY STANDARDS

Under the terms of Article III of its Statute, the IAEA is authorized to establish or adopt standards of safety for protection of health and minimization of danger to life and property, and to provide for the application of these standards.

The publications by means of which the IAEA establishes standards are issued in the **IAEA Safety Standards Series**. This series covers nuclear safety, radiation safety, transport safety and waste safety. The publication categories in the series are **Safety Fundamentals**, **Safety Requirements** and **Safety Guides**.

Information on the IAEA's safety standards programme is available on the IAEA Internet site

http://www-ns.iaea.org/standards/

The site provides the texts in English of published and draft safety standards. The texts of safety standards issued in Arabic, Chinese, French, Russian and Spanish, the IAEA Safety Glossary and a status report for safety standards under development are also available. For further information, please contact the IAEA at: Vienna International Centre, PO Box 100, 1400 Vienna, Austria.

All users of IAEA safety standards are invited to inform the IAEA of experience in their use (e.g. as a basis for national regulations, for safety reviews and for training courses) for the purpose of ensuring that they continue to meet users' needs. Information may be provided via the IAEA Internet site or by post, as above, or by email to Official.Mail@iaea.org.

RELATED PUBLICATIONS

The IAEA provides for the application of the standards and, under the terms of Articles III and VIII.C of its Statute, makes available and fosters the exchange of information relating to peaceful nuclear activities and serves as an intermediary among its Member States for this purpose.

Reports on safety in nuclear activities are issued as **Safety Reports**, which provide practical examples and detailed methods that can be used in support of the safety standards.

Other safety related IAEA publications are issued as **Emergency Preparedness and Response** publications, **Radiological Assessment Reports**, the International Nuclear Safety Group's **INSAG Reports**, **Technical Reports** and **TECDOCs**. The IAEA also issues reports on radiological accidents, training manuals and practical manuals, and other special safety related publications.

Security related publications are issued in the **IAEA Nuclear Security Series**.

The **IAEA Nuclear Energy Series** comprises informational publications to encourage and assist research on, and the development and practical application of, nuclear energy for peaceful purposes. It includes reports and guides on the status of and advances in technology, and on experience, good practices and practical examples in the areas of nuclear power, the nuclear fuel cycle, radioactive waste management and decommissioning.

ASSESSMENT OF HIGH WIND
AND EXTERNAL FLOODING
(EXCLUDING TSUNAMI)
HAZARDS IN SITE EVALUATION
FOR NUCLEAR INSTALLATIONS

The following States are Members of the International Atomic Energy Agency:

AFGHANISTAN
ALBANIA
ALGERIA
ANGOLA
ANTIGUA AND BARBUDA
ARGENTINA
ARMENIA
AUSTRALIA
AUSTRIA
AZERBAIJAN
BAHAMAS
BAHRAIN
BANGLADESH
BARBADOS
BELARUS
BELGIUM
BELIZE
BENIN
BOLIVIA, PLURINATIONAL
    STATE OF
BOSNIA AND HERZEGOVINA
BOTSWANA
BRAZIL
BRUNEI DARUSSALAM
BULGARIA
BURKINA FASO
BURUNDI
CABO VERDE
CAMBODIA
CAMEROON
CANADA
CENTRAL AFRICAN
    REPUBLIC
CHAD
CHILE
CHINA
COLOMBIA
COMOROS
CONGO
COSTA RICA
CÔTE D'IVOIRE
CROATIA
CUBA
CYPRUS
CZECH REPUBLIC
DEMOCRATIC REPUBLIC
    OF THE CONGO
DENMARK
DJIBOUTI
DOMINICA
DOMINICAN REPUBLIC
ECUADOR
EGYPT
EL SALVADOR
ERITREA
ESTONIA
ESWATINI
ETHIOPIA
FIJI
FINLAND
FRANCE
GABON
GAMBIA
GEORGIA

GERMANY
GHANA
GREECE
GRENADA
GUATEMALA
GUINEA
GUYANA
HAITI
HOLY SEE
HONDURAS
HUNGARY
ICELAND
INDIA
INDONESIA
IRAN, ISLAMIC REPUBLIC OF
IRAQ
IRELAND
ISRAEL
ITALY
JAMAICA
JAPAN
JORDAN
KAZAKHSTAN
KENYA
KOREA, REPUBLIC OF
KUWAIT
KYRGYZSTAN
LAO PEOPLE'S DEMOCRATIC
    REPUBLIC
LATVIA
LEBANON
LESOTHO
LIBERIA
LIBYA
LIECHTENSTEIN
LITHUANIA
LUXEMBOURG
MADAGASCAR
MALAWI
MALAYSIA
MALI
MALTA
MARSHALL ISLANDS
MAURITANIA
MAURITIUS
MEXICO
MONACO
MONGOLIA
MONTENEGRO
MOROCCO
MOZAMBIQUE
MYANMAR
NAMIBIA
NEPAL
NETHERLANDS,
    KINGDOM OF THE
NEW ZEALAND
NICARAGUA
NIGER
NIGERIA
NORTH MACEDONIA
NORWAY
OMAN
PAKISTAN

PALAU
PANAMA
PAPUA NEW GUINEA
PARAGUAY
PERU
PHILIPPINES
POLAND
PORTUGAL
QATAR
REPUBLIC OF MOLDOVA
ROMANIA
RUSSIAN FEDERATION
RWANDA
SAINT KITTS AND NEVIS
SAINT LUCIA
SAINT VINCENT AND
    THE GRENADINES
SAMOA
SAN MARINO
SAUDI ARABIA
SENEGAL
SERBIA
SEYCHELLES
SIERRA LEONE
SINGAPORE
SLOVAKIA
SLOVENIA
SOUTH AFRICA
SPAIN
SRI LANKA
SUDAN
SWEDEN
SWITZERLAND
SYRIAN ARAB REPUBLIC
TAJIKISTAN
THAILAND
TOGO
TONGA
TRINIDAD AND TOBAGO
TUNISIA
TÜRKİYE
TURKMENISTAN
UGANDA
UKRAINE
UNITED ARAB EMIRATES
UNITED KINGDOM OF
    GREAT BRITAIN AND
    NORTHERN IRELAND
UNITED REPUBLIC OF TANZANIA
UNITED STATES OF AMERICA
URUGUAY
UZBEKISTAN
VANUATU
VENEZUELA, BOLIVARIAN
    REPUBLIC OF
VIET NAM
YEMEN
ZAMBIA
ZIMBABWE

The Agency's Statute was approved on 23 October 1956 by the Conference on the Statute of the IAEA held at United Nations Headquarters, New York; it entered into force on 29 July 1957. The Headquarters of the Agency are situated in Vienna. Its principal objective is "to accelerate and enlarge the contribution of atomic energy to peace, health and prosperity throughout the world".

SAFETY REPORTS SERIES No. 120

ASSESSMENT OF HIGH WIND AND EXTERNAL FLOODING (EXCLUDING TSUNAMI) HAZARDS IN SITE EVALUATION FOR NUCLEAR INSTALLATIONS

INTERNATIONAL ATOMIC ENERGY AGENCY
VIENNA, 2024

COPYRIGHT NOTICE

FOREWORD

All natural and human induced hazards that could affect the safety of nuclear installations are identified and incorporated into design bases established during the site characterization stage. The scope of the work necessary for the evaluation of the site varies according to the type and size of the nuclear installation, and a well established graded approach is used to ensure that efforts comply with requirements.

Meteorological and hydrological hazards are two of the most important types of natural hazard. This publication covers hazards related specifically to high winds and external flooding (excluding tsunamis). These phenomena are assessed during the site characterization stage to ensure that the nuclear installation is designed to be able to withstand their effects without losing its capability to perform safety functions.

In recent years, significant experience of the effects of high winds and flooding on nuclear installations has been gained worldwide. These phenomena may simultaneously affect all structures, systems and components important to safety at a site. This could lead to common cause failure of systems important to safety, affect communication and transport networks around the site of a nuclear installation, and jeopardize the implementation of emergency response actions.

This publication provides detailed information on hazard evaluation for high winds and external flooding and offers a comprehensive review of the relevant literature. Wind hazards relating to tropical cyclones, tornadoes, extratropical storms, thunderstorms and wind-borne debris are discussed. External flooding hazards (excluding tsunamis) relating to wind induced coastal flooding, wind generated waves on rivers, extreme precipitation and runoff events, and the sudden release of impounded water are also covered.

This publication supports IAEA Safety Standards Series No. SSG-18, Meteorological and Hydrological Hazards in Site Evaluation for Nuclear Installations.

The IAEA officer responsible for this publication was A. Altinyollar of the Division of Nuclear Installation Safety.

EDITORIAL NOTE

CONTENTS

1. INTRODUCTION

1.1. BACKGROUND

The accident at the Fukushima Daiichi nuclear power plant of 11 March 2011 reinforced the importance — and the challenges — of ensuring the safety of nuclear installation sites against multiple external hazards. The Great East Japan Earthquake and subsequent tsunami affected the safety systems of the Fukushima Daiichi nuclear power plant and caused a severe multi-unit accident, highlighting the importance of protecting safety systems, such as emergency power supply systems, decay heat removal systems and other vital systems, from common cause failures.

The adequate evaluation of all possible hazards is a fundamental step in the safety evaluation of nuclear installation sites. As seen at the Fukushima Daiichi nuclear power plant, meteorological and hydrological phenomena have the potential to simultaneously affect structures, systems and components that are important for the safety of nuclear installations.

IAEA Safety Standards Series No. SSG-18, Meteorological and Hydrological Hazards in Site Evaluation for Nuclear Installations [1], provides recommendations on how to comply with safety requirements when assessing the hazards associated with meteorological and hydrological phenomena. It also makes recommendations on how to establish a design basis appropriate for these natural hazards, as well as providing steps to protect nuclear installations from them.

1.2. OBJECTIVE

The objective of this publication is to support SSG-18 [1] by detailing the methodologies used to evaluate hazards and providing case studies demonstrating the evaluation of meteorological and hydrological hazards during site evaluation for nuclear installations.

This publication can be used by nuclear regulatory bodies and other organizations that oversee the evaluation of meteorological and hydrological hazards for nuclear installation sites.

Guidance and recommendations provided here in relation to identified good practices represent expert opinion but are not made on the basis of a consensus of all Member States.

1.3. SCOPE

This publication addresses the assessment of external flooding (excluding tsunami related flooding) and high wind hazards for the purposes of site evaluation for existing and prospective nuclear installations.

The following hazards are covered:

(a) High wind hazards:
    (i)   Tropical cyclones;
    (ii)   Tornado winds;
    (iii) Extratropical storms, thunderstorms and other winds;
    (iv)   Wind-borne projectiles.
(b) External flooding hazards (excluding tsunamis):
    (i)   Wind induced coastal flooding;
    (ii)   Wind generated waves on rivers;
    (iii) Extreme precipitation and runoff events;
    (iv)   Flooding due to the sudden release of impounded water.

Although this publication was developed for nuclear power plants, the methodology presented can be applied to all nuclear installations.

1.4. STRUCTURE

This publication comprises 11 sections, with this introduction being the first section. Section 2 discusses general considerations on wind hazards caused by different phenomena for nuclear installations. It reviews the current state of the practice methods for wind hazard modelling and discusses the approaches most frequently used to develop wind hazard information for different meteorological phenomena. Section 3 presents information on tropical cyclones, including their modelling, data resources and modelling uncertainty. Section 4 summarizes information on tornadoes, including statistics and databases, and hazard modelling and uncertainties. Section 5 focuses information on extratropical storms, including thunderstorms and other winds, statistical methods for their analysis, estimating uncertainties, combined straight line wind hazards and tail limited distributions. Section 6 provides information on wind-borne debris, including deterministic and probabilistic methods of analysis, missile impact effects, atmospheric pressure change (APC) loads and missile surveys. Section 7 presents general information on flood hazard assessment and discusses uncertainties in flood hazard evaluation, flood effects and specificities to consider for risk assessment, as well as elements of probabilistic flood hazard

assessment (PFHA). Section 8 focuses information on wind induced coastal flooding, including data sources and their deterministic and probabilistic hazard assessment. Section 9 provides information on wind generated waves on rivers, including deterministic and probabilistic hazard assessment. Section 10 discusses information on extreme precipitation and runoff events, including data resources and deterministic and probabilistic hazard assessment. Finally, Section 11 presents information on floods caused by the sudden release of impounded water, including data resources and deterministic and probabilistic hazard assessment.

2. GENERAL CONSIDERATIONS ON WIND HAZARDS

The wind hazard at a site can result from hurricanes (tropical cyclones), tornadoes, extratropical storms, thunderstorms and other extreme winds, including downslope winds (a type of wind created by the movement of air from high elevations down a slope) and the shamals (a type of wind occurring in and around the Arabian Peninsula characterized by high levels of sand and dust in the air). These wind generating phenomena are formed by different meteorological and sea conditions, occur in different regions of the world, are accompanied by different meteorological events and cover small to large distances. Tornado wind speeds of more than 34 m/s are capable of producing missiles from objects in the wind's path, such as debris from damaged buildings. Sections 3–6 of this publication address the various types of wind hazard.

Information on the wind hazard, typically provided in the form of a hazard curve presenting wind speed as a function of annual exceedance probabilities, needs to be convolved with wind fragility functions to arrive at damage frequencies.

The state of the practice method for designing wind hazard models in the case of tornadoes and tropical cyclones is to use simulations. Other wind hazards typically have their hazard curves established using historical data and various extreme value distribution models. The state of the practice approach for modelling wind hazard curves using historical data involves separating the wind speed data by meteorological type. For example, in the United States of America (USA), the non-tropical cyclone wind hazard is developed by considering thunderstorm and non-thunderstorm winds separately.

3. TROPICAL CYCLONES

3.1. GENERAL CONSIDERATIONS

A tropical cyclone is a warm core storm with a low central pressure that forms over the warm waters of the Earth's oceans, typically in the tropics. Tropical cyclones are known as 'hurricanes' in the Atlantic Ocean, 'typhoons' in the Northwest Pacific Ocean and 'tropical cyclones' or simply 'cyclones' in the Bay of Bengal, the Indian Ocean and the South Pacific Ocean. Tropical cyclones gain their energy from the latent heat released when warm water evaporates from the ocean's surface and condenses as it rises within the core of the cyclone. The terms 'hurricane' and 'tropical cyclone' have been used interchangeably in this publication.

Figure 1 shows tropical cyclone tracks for two regions as an example [2]. Each tropical cyclone track line connects the six-hourly best track positions[1], with red squares indicating a hurricane force landfall location point and blue circles indicating overland observations of tropical storm strength (wind speeds between 34 kn (63 km/h) and 63 kn (117 km/h)).

The central pressure in cyclones varies from about 1000 hPa for weak cyclones to less than 880 hPa for very intense cyclones. Cyclones typically have diameters of approximately 300 km but can be much larger. The highest winds are found in the eyewall area of the cyclone, surrounding the cyclone's centre. Figure 2 shows a cross-section of a typical tropical cyclone, showing the variation of wind speeds and pressures as a function of distance from the centre of the cyclone.

Since tropical cyclones affect a given location infrequently, a simulation approach is used to determine the wind hazard, rather than standard statistical methods that use historical records of measured wind speeds.

The tropical cyclone simulation approach relies on historical records of cyclone tracks to provide data on annual occurrence rates, storm heading, translation speed and storm strength, which is often determined by maximum wind speed or minimum atmospheric pressure. Hurricane simulation is a commonly used method for estimating wind speeds for structural design and hurricane risk assessment. In the USA [3–5], the Caribbean [6] and Australia [7], the simulation technique is used to produce design wind speed charts. Wind field based storm

---

[1]   The best track of a tropical cyclone refers to the estimated centre location and intensity of the storm, typically determined through a combination of satellite imagery and ground based observations. It can also be used to help identify trends in tropical cyclone behaviour, as well as to evaluate the performance of forecasting models.

surge models are applied to make flood forecasts for coastal regions, assist in setting flood insurance rates and determine minimum floor elevation levels for structures along the USA's hurricane prone coastal areas. Most structures and bridges constructed in hurricane or cyclone areas have been wind tunnel tested and their data linked with the results of hurricane hazard models. Reliable risk based engineering analysis has become a critical component of structural design as modern design practice continues to drive the performance criteria for infrastructure in hazard prone regions. Hurricane models have progressed to meet this need.
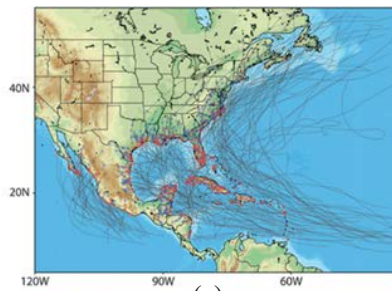
(a)
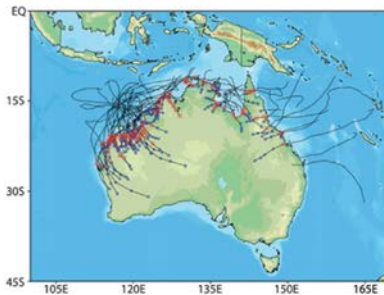
(b)

FIG. 1. *Tropical cyclone tracks and landfall location points for storms that make landfall at hurricane intensity (maximum 1 min sustained ≥ 64 kn (118 km/h)) for (a) the North Atlantic and East Pacific and (b) the Australian region. The American Meteorological Society has the ownership of these maps, which have been reproduced with its permission from Ref. [2].*
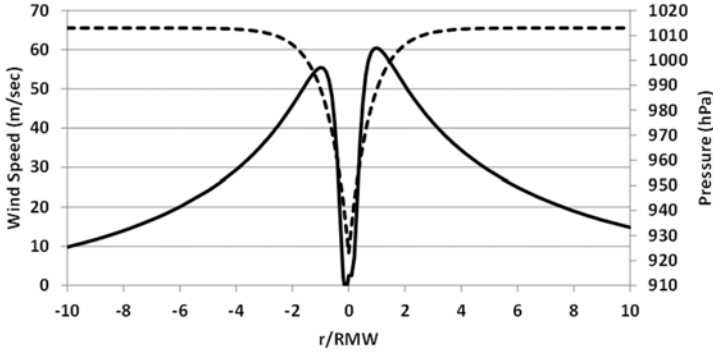
FIG. 2. Cross-section of model tropical cyclone showing axisymmetric surface pressure (dashed line) and upper level wind speeds (solid line). The wind speeds are not symmetric and are higher on the right owing to the effect of translation speed. RMW — radius to maximum wind; r — radial distance from the centre of the cyclone.

Since the inception of modelling in the late 1960s and early 1970s, modelling techniques have vastly improved [8–10]. The basic principle has remained the same since the original work [8], but the specifics have changed, especially in hurricane wind field modelling. The advancements were made possible using more advanced physics based models. The most significant model advancements have mainly been due to the tremendous increase in the quality and quantity of observed data. They can now be used to construct and evaluate physical and mathematical models applied to depict hurricane risk using the increased available computational power. The physical and mathematical models used in the modelling process, the adjustments and improvements made to the various components, and the expectations for the next generation of hazard models are discussed in the following subsections.

In addition to the wind hazard, other hazards associated with hurricanes include wind driven waves and storm surges, as well as inland flooding resulting from heavy rainfall. Examples of hurricane induced rain models include those described in Refs [11–14]. These rainfall rate models can be coupled with hydrological models to estimate inland flooding.

The overall objective of the tropical cyclone simulation methodology is to develop wind speed hazard curves that can be used to estimate wind speeds for annual exceedance probabilities as low as 10^{-7}. The methodology and results of such an effort for the USA are presented in Ref. [15].

3.2. TROPICAL CYCLONE MODELLING

3.2.1. Single point probabilistic models

References [8, 9] were the first publications to present the simulation process. Others have since extended and developed this initial modelling technique for US applications (e.g. Refs [10, 16–20]). The basic method used is similar to the methods used in Refs [8, 9], in that site specific statistics of key hurricane parameters, such as central pressure deficit, radius to maximum winds (RMW), heading, translation speed and coast crossing location or closest approach distance, are obtained first. Given the statistical distributions of these hurricane parameters, a Monte Carlo approach is used to sample from each distribution. A mathematical representation of a hurricane is passed along the straight line path satisfying the sampled data while the simulated wind speeds are recorded. The hurricane's strength is kept steady until it makes landfall, at which point it decays using a filling rate model. Since the required statistics are generated using site specific data that centre on the sample circle or coastline segments, this method is only applicable for a single site or small regions.

Figure 3, which is reproduced from Ref. [21], illustrates the overall simulation approach. Reference [21] presents an overview of past and present work in hurricane modelling including the evolution and current state of wind field modelling, modelling uncertainties, and possible future directions of the hurricane risk modelling process.

The implementation of the simulation modelling process (site specific modelling) is similar, with the main variations being the physics based models used (e.g. filling rate models, wind field models). Other variations include the size of the area for which hurricane climatology (statistical distributions) can be considered accurate, as well as whether a coast segment crossing approach [9, 10, 16] or a circular subregion approach [17–20] is used.

The probability distributions used to match a given parameter (e.g. central pressure (or central pressure difference), RMW, translation speed) differ among the studies. The study described in Ref. [19] created a risk model that varies from the others. Instead of modelling the hurricane's central pressure, the Hurricane Database (HURDAT) was used to model the hurricane's maximum surface wind speed [22]. Perhaps the first attempt to integrate wind tunnel data with simulated hurricane wind speeds was described in Ref. [10] to establish design wind loads for individual structures. Similarly, the model described in Ref. [16] was developed for the USA's hurricane prone coastal areas. However, none of the studies described in Refs [8, 10, 16] tried to replicate the wind speeds and directions observed in historical hurricanes. Reference [18] describes possibly the first study to make such a wind field model validation. In Ref. [23], a slightly
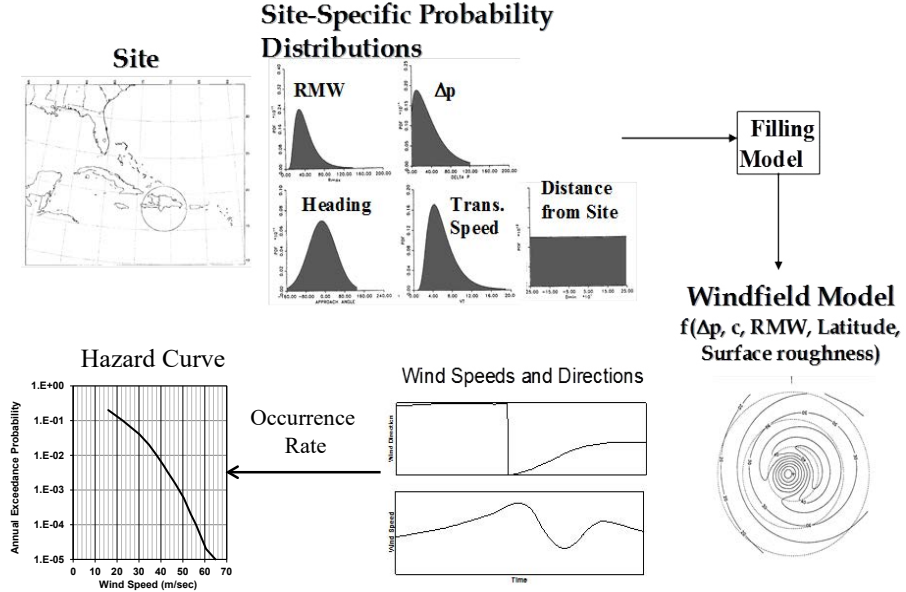
FIG. 3. An overview of the simulation modelling process (site specific modelling) (reproduced from Ref. [21] with permission).

different approach to evaluate hurricane risk is proposed. Instead of developing statistical distributions for central pressure, the model was applied to hurricane risk in the Miami (Florida) region of the USA. The relative strength of a storm (as determined by wind speed or central pressure) is a comparison of the storm's theoretical maximum potential intensity (as defined by wind speed or central pressure). Reference [24] defines the maximum potential intensity that was used in Ref. [23]. Since the maximum potential intensity placed a physical limit on the minimum central pressure of a simulated storm, it removed the need (at least for South Florida) to artificially truncate the distribution of central pressure.

3.2.2. Track modelling

The first method for modelling the tracks of tropical cyclones was presented in Ref. [25] and incorporated the relative intensity technique introduced in Ref. [23]. A notable contribution of the track modelling study described in Ref. [25] was the capacity to model the hurricane hazard for the entire coastline of a continent, rather than simply a single spot or a limited area. The Holland B parameter [26] was included as a random variable in Ref. [25], which added an additional parameter. This track modelling approach was subsequently extended

in studies described in Refs [27, 28], [29, 30] and [31, 32] for North America, Australia and eastern Asia, respectively. The track model presented in Ref. [33] coupled a stochastic track model with a deterministic axisymmetric equilibrium model and a one dimensional ocean mixing model to explain the life cycle of a hurricane. A database of synthetic hurricane wind speeds for historical hurricanes may be useful for developing hurricane damage models [34].

Reference [35] describes in full the axisymmetric balance model presented in Ref. [33]. With data on sea surface temperature, tropopause temperature, humidity, and other parameters, as well as a training set of historical storms, the model is able to simulate the strengthening and weakening of hurricanes as they move along the modelled tracks, accounting for the effects of wind shear and ocean mixing, without using statistical models to model the changes in hurricane intensity.

Rather than central pressures, the model in Ref. [35] is 'calibrated' to suit US National Hurricane Center forecasts of sustained wind speeds (maximum 1 min average), which is one of the main differences between it and the models presented in Refs [25, 27, 36, 37]. Reference [37] presents a hybrid model that incorporates some of the features of the models presented in Refs [33, 36].

3.2.3.   Joint probability method

A method favoured by the US government agencies (e.g. the Federal Emergency Management Agency (FEMA), the US Army Corps of Engineers (USACE)) for performing coastal flood hazard analyses for hurricanes is known as the joint probability method. The name was chosen because the modelling approach correlates the key hurricane parameters, namely the RMW and central pressure. All coastal flood studies performed for FEMA since 2006 have used the joint probability method. The approach entails developing suites of storm tracks with fixed shapes (track history and approach angles). These comprise sets of tracks representing landfalling hurricanes and bypassing hurricanes. Each track (or group of tracks) has an assigned value, or values, of translation speed, central pressure, RMW, and, possibly, the Holland B parameter. The parameters are chosen such that they cover the full range of parameters necessary to develop estimates of the hurricane induced flood hazard representative of annual exceedance probabilities of 0.01–0.002. The approach has not yet been used to assess wind speed or wind induced flood hazards representative of annual exceedance probabilities of 10^{-6} or less. Some examples of the implementation of the joint probability method along the Gulf of Mexico coast of the USA are given in Refs [38, 39].

The US Nuclear Regulatory Commission guidance document JLD-ISG-2012-06 [40] provides background information on hurricane hazard modelling as it pertains to coastal flood (storm surge and wave) modelling,

rather than the wind hazard alone. It summarizes the joint probability method for hurricane simulations, as well as an approach known as the empirical simulation technique (EST), which is essentially a hurricane track shifting method. The technique was widely used by USACE and FEMA, before becoming less popular in the late 2000s following Hurricane Katrina. The EST approach is now no longer used by FEMA for modelling hurricane induced flood.

3.2.4. Wind field modelling

A three step procedure is typically used to model tropical cyclone wind fields:

(1) An approximation of the wind speed at gradient height is obtained using the main input values (e.g. central pressure, RMW). The average wind speed over a span of 10 min to 1 h is used to calculate the mean wind speed. In Refs [25, 37], the modelled mean wind speed was assumed to be indicative of 1 h, whereas in Ref. [41], a 30 min averaging time was assumed. The height above ground at which the wind speed is in gradient equilibrium with the Coriolis, centripetal and pressure gradient forces is known as the gradient height. Tropical cyclone gradient height varies with storm size and strength, ranging from a few hundred metres to more than 1000 m. Most wind field models presume that the wind speed at gradient height is a mean wind speed.
(2) Using atmospheric boundary layer principles and assuming neutral equilibrium, this gradient wind speed is modified to a mean surface wind speed value at a given height.
(3) Using gust factors, the mean surface wind speed is calibrated for terrain and averaging time.

The evolution and current state of each of these three steps are addressed in the following subsections.

3.2.4.1. Gradient wind field modelling

The gradient wind field models applied in hazard simulation models have been continuously improving since the 1970s.

The maximum gradient wind speed in the model presented in Ref. [16] was modelled as:

$$V_{Gmax} = K\sqrt{\Delta p - \frac{RMWf}{2}} \approx K\sqrt{\Delta p} \tag{1}$$

where

K is an empirical constant that includes air density;

RMW is the radius to maximum winds;

f is the Coriolis parameter;

and p is the central pressure difference, which is defined as the difference between the pressure at the storm's centre and the far field pressure, usually taken as the pressure associated with the first anticyclonically (in the northern hemisphere) curved isobar.

A nomograph was used to explain the difference in wind speed away from the maximum. The studies in Refs [8, 42] both used similar basic models. The maximum gradient wind speed in the model mentioned in Ref. [10] was proportional to $\sqrt{\Delta p}$ as well, but instead of using a nomograph method as in Ref. [16], an analytic representation of the entire wind area was used. Reference [26] presented a description of the gradient hurricane wind field that has been used in several hurricane risk studies (e.g. Refs [17, 34, 43]). In Ref. [26], an additional parameter, now known as the Holland B parameter, was added to describe the maximum wind speed in a hurricane. At a distance of r from the storm's core, the pressure, $p(r)$, is given as:

$$p(r) = p_{\mathrm{c}} + \Delta p \, \exp\left[-\left(\frac{\mathrm{RMW}}{r}\right)^{B}\right] \tag{2}$$

where p_{c} is the pressure in the storm's core.

For a stationary storm, the gradient balance velocity, V_{G}, is therefore:

$$V_{\mathrm{G}} = \left[\left(\frac{\mathrm{RMW}}{r}\right)^{B} \frac{B\Delta p \, \exp\left[-\left(\frac{\mathrm{RMW}}{r}\right)^{B}\right]}{\rho} + \frac{r^{2} f^{2}}{4}\right]^{\frac{1}{2}} - \frac{fr}{2} \tag{3}$$

where ρ is the density of air. At RMW, the maximum wind speed is:

$$V_{\mathrm{Gmax}} \approx \sqrt{\frac{B\Delta p}{\mathrm{e}^{p}}} \tag{4}$$

where e is the base of natural logarithms. As a result, the hurricane's maximum velocity is directly proportional to $\sqrt{B\Delta p}$, rather than being proportional to $\sqrt{\Delta p}$ alone as in many simulations.

When Georgiou [18] integrated the model presented in Ref. [44] with the Holland model in Ref. [26] to define the wind speeds at gradient height, he was the first to apply a numerical model of the hurricane wind field for risk assessment. The value of the Holland B parameter, B, was restricted to be equivalent to 1 in Georgiou's implementation. In Ref. [36], a computational approach was also used to describe the hurricane wind field model, using a model similar to that in Ref. [41]. The pressure field defined in Eq. (2) is used to drive the wind field model, but B is not set to 1. Two dimensional (2-D) slab models were utilized in the simulations [18, 36, 45], and procedures were applied in such a way that precomputed solutions to the equations of motion of a translating storm were used. Super gradient winds (i.e. wind speeds larger than those recorded using the gradient balancing equations) can be modelled using a 2-D numerical model, as can the effect of the sea–land interface (produced by changes in surface friction) and the augmented inflow generated by surface friction.

Surface roughness variations can be better modelled with three dimensional (3-D) numerical models to describe changes in the vertical structure of the storm boundary layer, including changes in the boundary layer height, as well as localized convective dynamics including boundary layer roll formation [46]. At the time of publication, no peer reviewed published hurricane risk studies had used 3-D models. Such models, however, are increasingly likely to be used in the future as computational power improves. The use of 3-D models does not eliminate the requirement for comprehensive validation utilizing data from surface level anemometers. In each of the above situations, the calculated gradient wind speed is associated with a longer duration averaging period of 10 min to 1 h. In each of the gradient level wind field models discussed, the driving pressure field is assumed to be axisymmetric, which is a significant oversimplification.

3.2.4.2. Boundary layer, sea–land transition and gust factors

An atmospheric boundary layer model or a wind speed reduction factor V_{10}/V_G is used to change the mean wind speed at gradient height (V_G). This wind speed is then applied to the surface (10 m above water or land, V_{10}). Basic reduction factors used in the past for winds over the ocean vary from as high as 0.950 in Ref. [42] to a low of about 0.650 in Ref. [47]. A value of 0.865 was used in Ref. [16], and a value of 0.825 near the eyewall, reducing to 0.750 away from the eyewall, was used in Ref. [18].

For the overland cases linked with the four investigations discussed in Refs [16, 18, 42, 47], the average wind speed ratios are, respectively, 0.845 at the shore and 0.745 at 19 km inland [42]; 0.450 [47]; 0.620 [18]; and 0.740 [16]. These wind speed ratios lead to immediate 11–22% reductions in mean wind speed as the wind travels from sea to land [42]; 30% reductions in Ref. [48];

16–25% reductions over 50 km in Ref. [18]; and a 15% reduction over 50 km in Ref. [16]. In Ref. [16], the roughness of the land is defined as a surface roughness length of 0.005 m. The authors of Ref. [47] imply open terrain when they say that the 0.45 ratio refers to an airport located a few kilometres inland. Open terrain may also benefit from wind speed reduction [18]. The only mention of terrain hardness is in Ref. [18], where it is stated that the terrain is not hard.

In Ref. [25], a hurricane boundary layer model based on the Monin–Obukov similarity theory with an ocean drag coefficient model was used, with the drag coefficient C_d linearly growing with wind to obtain wind speed ratios that varied with both wind speed and the air–sea temperature differential. An empirical increase of 10% in the wind speed ratio near the eyewall was implemented. The standard V_{10}/V_G ratios near the eyewall for relatively violent storms with a zero air–sea temperature differential were in the range of 0.70–0.72. Because an unlimited[2] drag coefficient model was used to estimate ocean surface roughness, it was then combined with wind speed transition models from the Engineering Sciences Data Unit (ESDU) [50, 51] to estimate mean wind speed in open terrain; the reduction in wind speed as the wind moves from the sea to the land is dependent on the severity of the storm. The consequent decrease in mean wind speed ranged from 14% for severe storms to 20% for less severe storms.

In Ref. [27], the mean surface (10 m) wind speed was calculated to be 80% of the boundary layer average wind speed (mean wind speed over the lowest 500 m), resulting in $V_{10}/V_G \approx 0.73$, but this varied with wind speed. The model has been updated to use a 78% factor instead of an 80% factor in the recent version [27]. An uncapped drag coefficient model was used to estimate the over water surface roughness presented in Ref. [27], and then the terrain transition model mentioned in Ref. [52] was used to calculate the reduced over land mean wind speeds, yielding reductions in the mean wind speed similar to those calculated in Ref. [25]. Table 1 summarizes the V_{10}/V_G values for a selection of hurricane 'boundary layer' models found in the literature.

The examination of dropsonde data obtained from 1997 to the present has enhanced knowledge of the overall characteristics of a hurricane marine boundary layer, but it has also highlighted new problems. The results of the study in Ref. [49] were as follows:

— Over the lower 200 m, the marine boundary layer is logarithmic.
— At a height of 10 m, the mean wind speed is 78% of the mean boundary layer wind speed (vertically averaged wind over the lower 500 m).

----

[2]   Prior to theory presented in Ref. [49], it was incorrectly theorized by many that the wind speed dependent surface drag coefficient was unlimited or that it continued to increase monotonically with wind speed without limit.

— At 10 m, the mean wind speed is 71% of the maximum (or gradient) wind speed. The maximum wind speed and RMW affect the height of the maxima.
— The drag coefficient of the sea surface increases with wind speed up to around 40 m/s mean wind speed (at 10 m), after which it levels off or even decreases with increasing wind speed.
— With rising wind speed, the height of the boundary layer decreases.

TABLE 1. EXAMPLE MODEL VALUES OF V_{10}/V_{G} AND SEA–LAND WIND SPEED REDUCTIONS[a]

Source	V_{10}/V_{G} over water (near eyewall)	Sea–land transition (% reduction of mean wind speed at 10 m)
Reference [42]	0.95 (PMH[b]), 0.90 (SPH[c])	11% at coast, 22% 19 km inland
Reference [16]	0.865	15% at coast
Reference [18]	0.825 $r < 2$ RMW, 0.75 $r > 5$ RMW	0% at coast, 25% 50 km inland
Reference [25]	~0.70 to 0.72	14–20% at coast, 23–28% 50 km inland
Reference [47]	0.65	30% a few km inland
Reference [27]	~0.73	15–20% at coast
Reference [49]	~0.71	n.a.[d]
Reference [45]	~0.71 (varies from 0.67 to 0.74)	18–20% at coast

[a] Adapted from Ref. [21] with permission.
[b] PMH: probable maximum hurricane, a term used in the USA and defined as a hypothetical steady state hurricane with a combination of values of meteorological parameters that will give the highest sustained wind speed that can probably occur at a specified coastal location.
[c] SPH: standard project hurricane, a term used in the USA and defined as a steady state hurricane with a severe combination of values of meteorological parameters that will give high sustained wind speeds reasonably characteristic of a specified coastal location.
[d] n.a.: not applicable.

The study described in Ref. [45] separated the dropsonde data by storm size and wind speed and combined them with a simplified version of the linearized hurricane model presented in Ref. [53]. The data showed that as inertial stability increases, the boundary layer height decreases, which is consistent with Ref. [53]. The data also showed that the boundary layer is logarithmic over the lower 200–300 m, which agrees with Ref. [49]. Figure 4 depicts the variance of mean wind speed with height derived from dropsonde analysis for a range of mean boundary layer wind speeds and storm radii [21]. For all mean boundary layer scenarios, mean and fitted logarithmic profiles are shown for drops near the RMW. The horizontal error bars show the 95th percentile error on the mean wind speed calculation. For the 20–200 m event, least squares fits are used. Mean boundary layer events are 20–29 m/s, 30–39 m/s, 40–49 m/s, 50–59 m/s, 60–69 m/s and 70–85 m/s. Figure 4 shows all the profiles that were taken at or near the RMW.

In Ref. [45], $U(z)$, the variance of mean wind speed with height z in the hurricane boundary layer, was empirically modelled using:

$$U(z) = \frac{u_*}{k}\left[\ln\left(\frac{z}{z_0}\right) - 0.5\left(\frac{z}{H}\right)^2\right] \tag{5}$$

where

k is the von Kármán coefficient, which has a value of 0.4;
u_* is the friction velocity;
z_0 is the aerodynamic roughness length (m);

and H is the boundary layer height (m), which decreases as inertial stability increases, as follows:

$$H = 431 + 0.32 / I \tag{6}$$

Here, the inertial stability I is defined as:

$$I = \sqrt{\left(f + \frac{2V}{r}\right)\left(f + \frac{V}{r} + \frac{\partial V}{\partial r}\right)} \tag{7}$$

where

V is the tangential gradient wind speed azimuthally averaged;
f is the Coriolis parameter;

and r is the radial distance from the storm's centre.
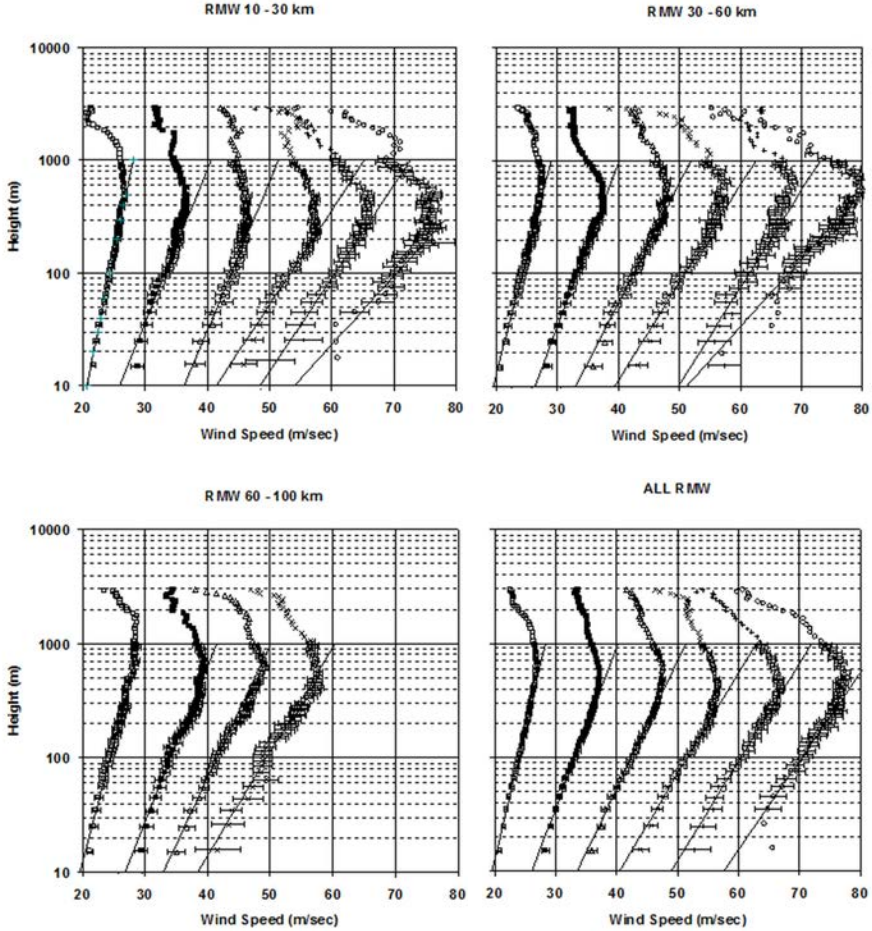
FIG. 4. Variance of mean wind speed with height derived from dropsonde analysis for a range of mean boundary layer wind speeds and storm radii (reproduced from Ref. [21] with permission).

Reference [45] defines an azimuthally averaged boundary layer model that ignores the expected variance in the shape of the hurricane boundary layer as a function of hurricane azimuth predicted in Ref. [53].

The sea surface drag coefficient calculated from the dropsondes mentioned in Ref. [45] increases with mean wind speed in a manner similar to that modelled in Ref. [54], reaches a maximum value and then levels off or decreases, as shown in Fig. 5. The mean wind speed at 10 m (U_{10}), at which the sea surface drag coefficient exceeds this limit, is only around 25 m/s (less than the 40 m/s in Ref. [49]), but this varies with storm radius. Although few measurements were taken at wind speeds above 25 m/s, this lower threshold is consistent with the

16
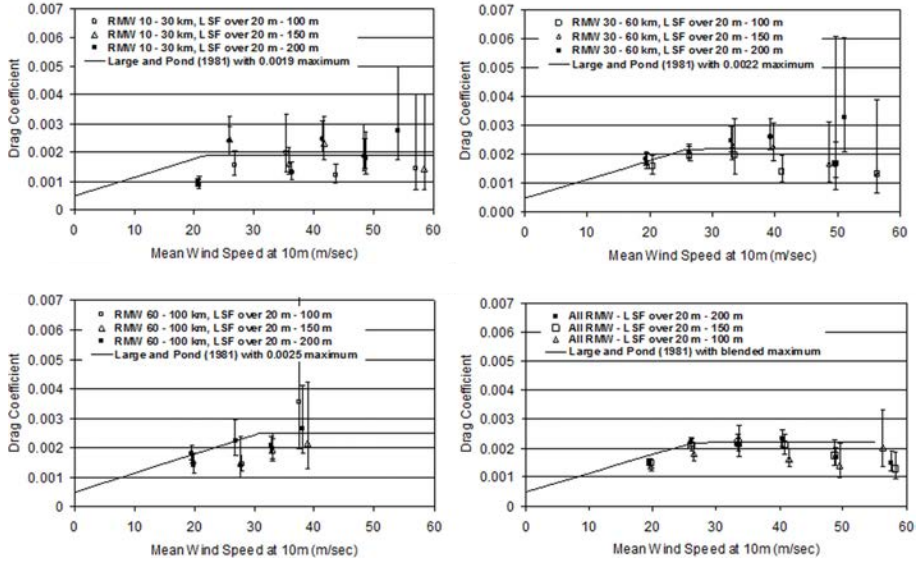
FIG. 5. *Variation of the sea surface drag coefficient with* U_{10} *near the radius to maximum winds (reproduced from Ref. [21] with permission). LSF — least squares fit.*

values estimated in Ref. [55] of around 23 m/s. The empirical boundary layer model combined with the variable limit on the sea surface drag coefficient yields U_{10}/U_G ratios of 0.67–0.74 over the ocean, varying with storm size and strength.

Figure 6 shows a comparison of the modelled and observed marine wind speed profiles computed using the drag coefficients shown in Fig. 5, as well as the boundary layer model defined by Eqs (5–7), with the maximum (gradient) wind speed and distance from the storm's centre as the only inputs.

Models are increasingly being used to assess the properties of the storm boundary layer over land because dropsonde data for velocity profiles over land are limited. The conventional engineering technique for modelling terrain change impacts is to assume that the top of the boundary layer wind speed remains constant (but the boundary layer height is free to change) and then update the winds in the boundary layer to represent the new roughness length. The boundary layer height change was calculated in Ref. [45] using the linear boundary layer theory presented in Ref. [53], but the boundary layer height increase expected in the model presented in Ref. [53] was increased further so that the mode's predicted reduction in surface level winds matched ESDU values for high boundary layer height. Using the method described in Ref. [45], approximate boundary layer height increases (from marine to open terrain) are 60–100%, meaning overland boundary layer heights of 800–3000 m, depending on wind speed and RMW. As
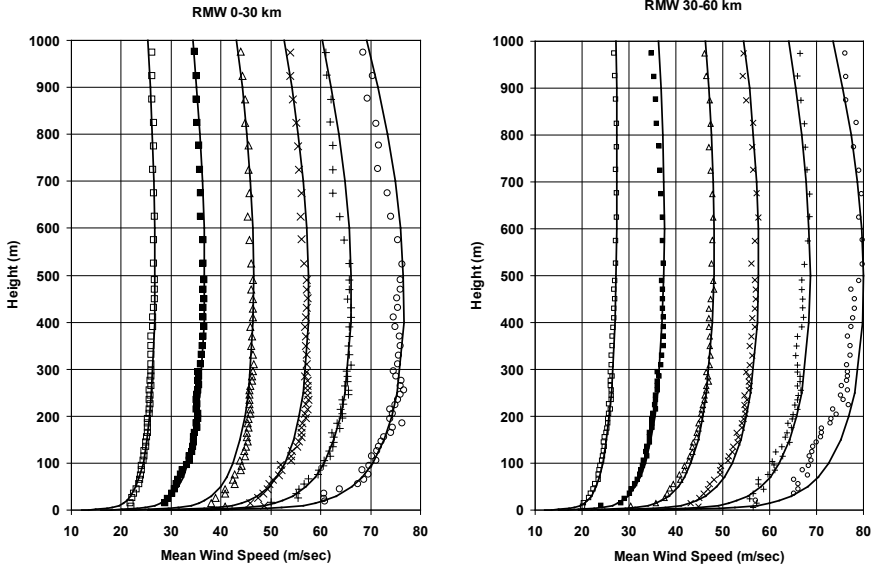
FIG. 6. Hurricane mean velocity profiles over the open ocean, modelled and observed for a variety of wind speeds (reproduced from Ref. [21] with permission).
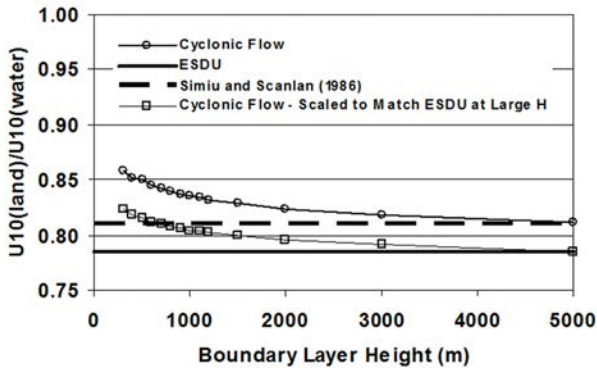
FIG. 7. Ratio of the fully transitioned mean wind speed over land ($z_0 = 0.03$ m) to the mean wind speed over water ($z_0 = 0.0013$ m) as a function of boundary layer height (H) (reproduced from Ref. [21] with permission). See Ref. [21] for information reflected in the figure.

the wind transitioned from sea to land in Ref. [27], the boundary layer height was increased by 100%.

Figure 7 compares the results of the boundary layer height increase used in Ref. [45] with the decrease in surface level winds caused by the combined effects of increased boundary layer height and increased surface roughness as wind transitions from marine to open terrain. The reduction in wind speed computed using the boundary layer height method in Ref. [53] is shown by the upper curve, denoted 'cyclonic flow'. Additional conversions are required to convey the effect of different land terrain conditions (e.g. open, residential), as well as averaging times after the wind field has been converted from gradient height to 10 m surface level. The creation and application of gust factors is a popular approach.

3.2.4.3.   Hurricane gust factors

In certain situations, the final application requires estimates of wind speeds associated with averaging times other than those provided by the simple hurricane wind field model (e.g. 1 min average winds, peak gust wind). Different representations of a gust factor model have been used in various hurricane risk models. References [16] and [56] both used and represented the gust factor model. The winds associated with hurricanes are 'gustier' than those associated with non-hurricanes, according to a gust factor model built for hurricane winds presented in Ref. [57]. It was also proposed in Refs [58, 59] that hurricane gust factors are greater than those associated with extratropical storms, based on wind speed data obtained during Hurricane Bonnie.

In Ref. [60], a large number of wind speed records were examined and no evidence was found that the gust variables associated with hurricanes differ from those associated with extratropical storms. The data were reanalysed in Ref. [61], along with additional data from Ref. [57], and it was determined that there was no proof that hurricane gust factors differed from extratropical storm gust factors. Formulations by ESDU [50, 51] for atmospheric turbulence developed for extratropical storms were found to be adequate for describing the mean gust factors in hurricanes in Ref. [61] (which did not look at the distribution of gust factors around the mean).

The larger gust factors were attributed in Refs [60] and [61] to surface roughness greater than that usually associated with open terrain (i.e. $z_0 = 0.03$ m), as seen in the Krayer and Marshall model [57]. Reference [62] contained the same conclusions as Ref. [61]. Reference [63] provides an overview of a large database of 10 m land based measurements of several landfalling hurricanes in the USA. The study revealed that there was no difference between hurricane gust factors and those calculated using non-hurricane winds. Figure 8 shows a comparison of the gust factors derived from the ESDU model with those
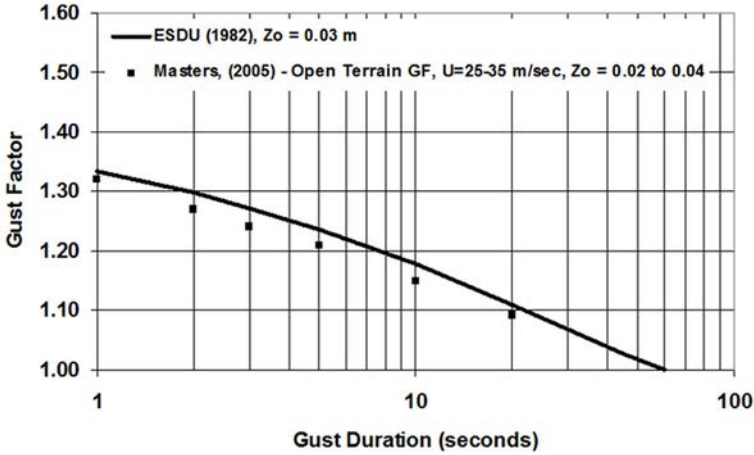
FIG. 8. Comparison of the ESDU [50] model gust factors with those derived from hurricane winds as reported by Masters in Ref. [63]. The gust factor here is defined as the ratio of the gust wind speed to the 1 min mean wind speed (reproduced from Ref. [21] with permission). Z_0 — surface roughness; GF — gust factor; U — wind speed.

presented in Ref. [63], indicating that the mean gust factors associated with hurricanes are comparable to those expected using ESDU models (with respect to a 60 s averaging time wind speed).

According to hurricane wind speed records, the near surface gust factors are similar to those in non-hurricanes for the most part. However, other types of turbulence may result in uncommon and small scale high winds that are substantially larger than the ESDU gust factor model predicts. Wind swirls caused by horizontal shear vorticity on the inner edge of the eyewall [64], coherent linear features such as rolls in the boundary layer [46, 65] or other convective features of the storms may be associated with these anomalous gusts. Despite the fact that the ESDU gust factor model appears to be able to characterize the gust factors associated with hurricane winds near the surface, more research is needed to allow modelling of additional small scale, but potentially significant, meteorological phenomena.

3.2.4.4.   Wind field model validation

The capacity of the wind field model used in the simulation procedure to replicate wind speeds measured physically in the field is a significant and crucial phase in the hurricane risk modelling process. Reference [18], which looked at the time variance of both wind speeds and wind directions, was probably the

first attempt to validate a hurricane wind field model used in a simulation model. In Refs [61, 65], similar validation studies were conducted and the comparisons of wind speed were expanded to include both mean and gust wind speeds. References [34, 43] both present similar but selective validation studies for models to be used for hurricane risk assessment. In Ref. [45], comparisons for wind speeds, wind directions and surface pressures are made to ensure that the wind model can replicate the observed winds without jeopardizing the model's ability to model the pressure field. Figure 9 shows pressures, gust and average wind speeds and wind directions for a comparison of modelled and observed wind speeds. Despite the fact that Ref. [66] conducted validation investigations comparing both pressures and wind speeds, pressure verification has not been incorporated into any other model verification research in the literature.

Although wind field model comparisons are important for detecting any biases in the wind model phase of the simulation process, successful validation comparisons could also be the consequence of other mistakes that compensate for model limitations. For example, the high gust factors associated with the Krayer–Marshall gust factors utilized in Ref. [67] contributed to an overall underestimation of mean surface wind speed. Similarly, even though the wind field model's main input is theoretically a gradient level wind, the validation process for hurricane wind models uses surface level winds. The verification of surface winds does not imply that the upper level winds have been verified. When hurricane simulation results are combined with wind tunnel test data for high rise buildings, this difference in the height at which the validation is performed may be significant. In Refs [18, 67], using a Holland B parameter of unity in conjunction with the Shapiro 2-D slab model [44] results in an underestimation of gradient wind speed. A boundary layer model that was too shallow (i.e. V_{10}/V_G ratios that were too high) compensated for the underestimation, resulting in fair estimates of surface level wind speeds and underestimations of gradient level wind speeds.

The maximum peak gust wind speeds computed using the wind field model mentioned in Ref. [45] are compared with observations for both marine and land based anemometers in Fig. 10. Figure 10 shows a total of 245 comparisons (165 land based measurements and 80 marine based measurements). Although there is strong agreement between the model and measured wind speeds, only a few measured gust wind speeds are greater than 45 m/s. The highest gust wind speed recorded was only 57 m/s. The inability of the wind field model to be described adequately by a single value of B and RMW, errors in the modelled boundary layer, errors in height, terrain and averaging time adjustments applied to measured wind speeds (if required), as well as storm track position errors and errors in the estimated values, all contribute to the differences between modelled and observed wind speeds. The knowledge obtained from the comparisons
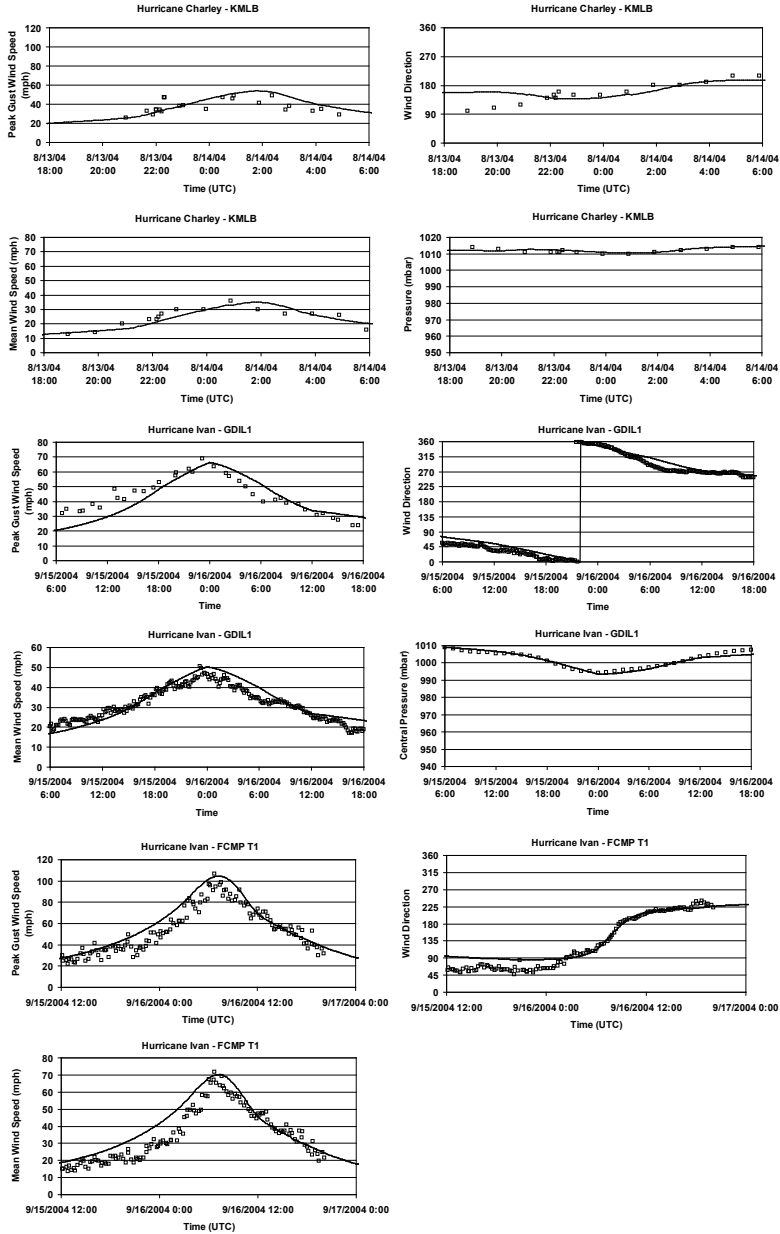
FIG. 9. Example comparisons of model and observed wind speeds, directions and pressures (reproduced from Ref. [21] with permission). FCMP — Florida Coastal Monitoring Program; KMLB — Melbourne, Florida, ASOS Anemometer; GDIL1 — National Data Buoy Centre Fixed Platform Anemometer).
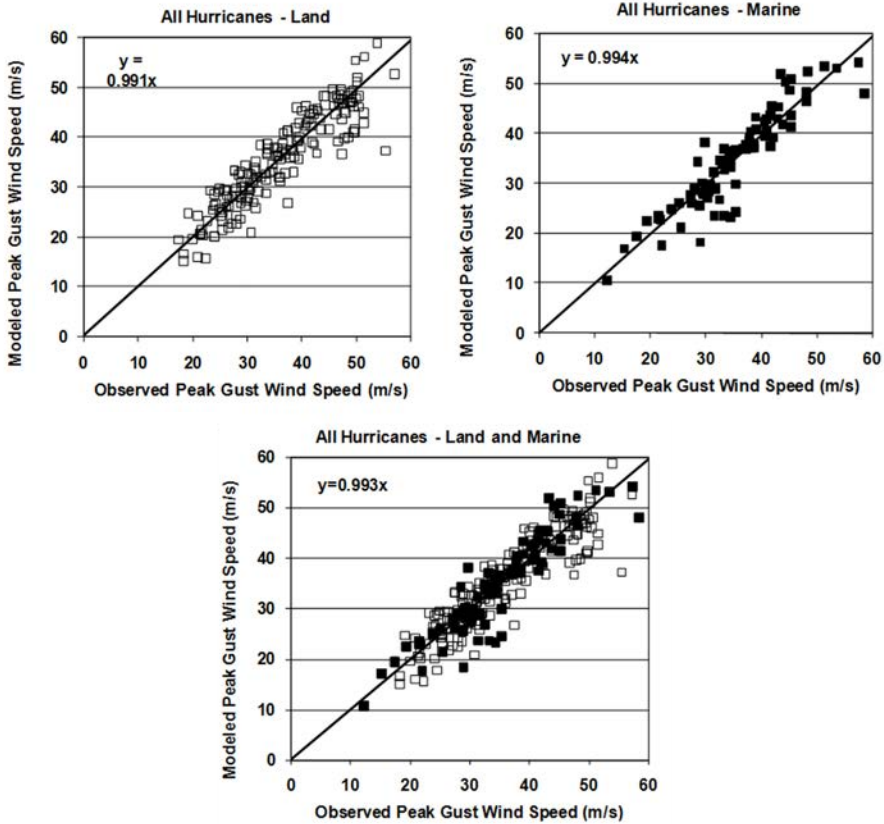
FIG. 10. Example comparisons of modelled and predicted maximum surface level peak gust wind speeds in open terrain from US landfalling hurricanes; wind speeds measured on land are given for open terrain (open squares) and wind speeds measured over water are given for marine terrain (filled squares) (reproduced from Ref. [21] with permission).

about model observed error is useful for assessing the overall uncertainty of the simulation phase, but it does not pinpoint the source(s) of errors that need to be refined further.

In conference papers discussing hurricane models for a variety of purposes, the validation of the wind field model is often overlooked. Such models, as well as the conclusions drawn from studies based on wind field models that have not been properly validated, need to be treated with caution.

It is important to emphasize that the wind field model validation task can be carried out with any good quality surface measurements, and it does not have to be performed at the site or even in the same country. The vast volume of data

available for landfalling storms in the USA provide an extremely useful source of validation for wind field models.

3.2.5. Other important model components

The RMW, the Holland B parameter (for some models) and hurricane weakening after landfall are all significant modelling components of the whole simulation process, as previously indicated. The Holland B parameter, as well as Δp, plays an important role in estimating maximum wind speeds, as shown in Eq. (4). The value of B can range from about 0.5 to about 2.5, according to Holland [26]; however, variations in the range of about 0.7 to 2.2 [27, 68, 69] are more common and rational. Modelling B variance has become an important part of hurricane simulation, affecting both the magnitude of maximum wind speeds and the aerial extent of these powerful winds.

The magnitude of maximum wind speeds is unaffected by the RMW (all else being equal). In contrast, the RMW has a major impact on the storm affected region. In the case of a single site wind risk analysis, RMW modelling influences the probability of the site experiencing heavy winds in the event of a near miss. Storm surge and wave modelling, as well as calculating potential maximum damages for insurance modelling, all require RMW modelling. The central pressure differential is assumed to be negatively connected to the amplitude of the RMW, with stronger storms (greater central pressure difference) having lower RMW than weaker storms. The RMW rises in tandem with increasing latitude. In most models, the RMW is modelled as a log-normally distributed function of central pressure and/or latitude, with the median value as a function of both. There is much variation in field data when it comes to the modelled relationships of RMW and Δp.

3.2.5.1. Statistical model for Holland B parameter

The Holland B parameter can be very useful for estimating the maximum wind speeds in a hurricane. B is a linear function of central pressure p_c (hPa) for Australian cyclones, according to Ref. [70], which is modelled as:

$$B = 2.0 - \left(p_c - 900\right)/160 \tag{8}$$

so that as the central pressure decreases (i.e. Δp increases), B increases.

According to Ref. [25], B has a poor association with both RMW and Δp, with B dropping as RMW grows and increasing as Δp climbs.

The values of B were used in Ref. [27] to model the Holland B parameter as a function of RMW and latitude, and flight level data of wind speeds were used in Ref. [68] to model the Holland B parameter as a function of RMW and latitude ψ as follows.

$$B = 1.881 - 0.00557 \text{RMW} - 0.01097 \ \psi r^2 = 0.200$$
$$\sigma_B = 0.286 \tag{9}$$

where

RMW is in kilometres;
ψ is latitude expressed as degrees;

and σ_B is the standard deviation. No relationship was found between B and central pressure in Ref. [27].

The same flight level data as in Refs [68] and [71] were used in Ref. [69], but the radial pressure profiles were fitted instead of the radial velocity profiles. B can be described as a function of a non-dimensional parameter A [69], as shown in Fig. 11 and defined as:

$$A = \frac{\text{RMW}f}{\sqrt{2R_d T_s \ln\left(1 + \dfrac{\Delta p}{p_c e}\right)}} \tag{10}$$

where

the numerator indicates the contribution of the Coriolis force to angular velocity and is equal to the product of RMW (in metres) and f;
the denominator is a rough estimate of a hurricane's overall strength (as measured by wind speed);
R_d is the dry air gas constant;
p_c is the central pressure (Pa);

and T_s is the sea surface temperature in degrees K.
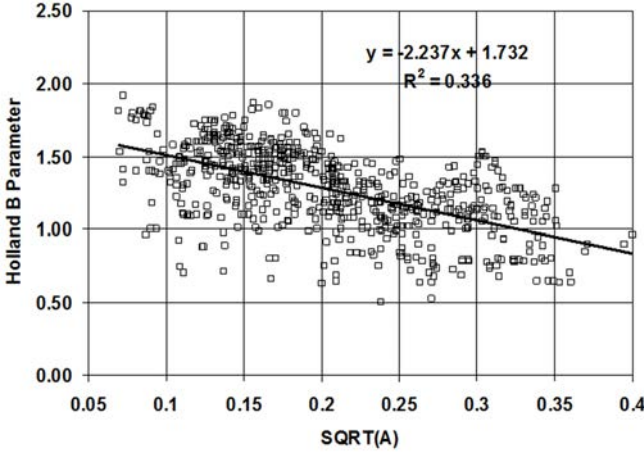
FIG. 11. *Relationship between the Holland B parameter and the dimensionless parameter A (reproduced from Ref. [21] with permission).*

The units of velocity appear in the numerator and denominator of A. Parameters B and A have the following relationship:

$$B = 1.732 - 2.237\sqrt{A}$$
$$r^2 = 0.336 \tag{11}$$
$$\sigma_B = 0.225$$

where r^2 is the distance from the storm's core and σ_B is the standard deviation.

In contrast to the relationship suggested in Ref. [70], it was found in Refs [27, 69] that B drops as RMW and latitude increase, and it is only weakly (if at all) reliant on the central pressure.

Incorporating B into the simulation phase is a major improvement over using a single, constant value of B (usually unity for Atlantic storms). A single value of B cannot model all storms at all times, as discussed in Refs [41, 68, 71]. The simple single parameter model is incapable of simulating the wind fields associated with eyewall replacement cycles, and it also has a tendency to underestimate wind speeds far from the centre of the storm. In most circumstances, however, as shown in Figs 9 and 10, modelling hurricanes with a single B value is adequate. Hurricane Wilma, which hit South Florida, USA, in 2005, was an example of a landfalling hurricane that was inadequately modelled using a single B value. Figure 10 depicts the wind speed comparisons for Hurricane Wilma. According to both surface level anemometer data and remotely sensed data, the strongest

surface level winds occurred on the storm's left side, not the right, as expected by an axisymmetric pressure field modelled using single B and RMW values. In most circumstances, B will suffice.

3.2.5.2. Filling models

As the central pressure rises, storms either fill or weaken once they reach land. This filling is not to be confused with the additional wind speed reduction caused by increased land friction. Accurate filling figures are critical for estimating wind speeds at inland locations, and they become even more critical as the distance inland increases. The rate of filling is affected by geography, topography, climatology and the characteristics of individual cyclones. Filling models based on statistics cannot be used in areas other than those that were used to create the models.

The storms are weakened as a function of time after landfall in most filling models (e.g. Refs [20, 72]). A typical filling model is as shown in Eq. (12):

$$\Delta p(t) = \Delta P_0 \exp(-at) \tag{12}$$

where

$\Delta p(t)$ is the central pressure difference;
t is hours after landfall;
ΔP_0 is the central pressure difference at the time of landfall;

and a is an empirically derived decay constant.

In Ref. [18], it was decided to depart from this approach and to consider the weakening of the storms as a function of distance from landfall. The rate of filling of storms affecting the coastal USA was revisited in Ref. [73], and it was discovered that the decay constant, a, is better modelled as a function of $c\Delta P_0/\text{RMW}$, where c is the hurricane's translation speed at landfall and ΔP_0 is the central pressure difference at landfall. The dependence of the filling rate on translation speed at landfall is consistent with findings in Ref. [18], which indicated that inland distance is a better measure of filling than time after landfall.

In Ref. [74], a filling model for tropical cyclones hitting the South China coast was created. The authors proposed three models, all in the form of Eq. (12): (i) with a being a function of ΔP_0 alone; (ii) with a being a function of $c\Delta P_0$; and (iii) with a as a function of $c\Delta P_0/\Phi_m$, where Φ_m is the 850 hPa moist static energy at landfall and c is the translation speed (m/s). Reference [74] revealed that using

only the component of c normal to the coast produced higher r^2 values than using the full value of c. In Ref. [74], there were no RMW results.

3.3. DATA SOURCES

3.3.1. Track modelling

The most reliable historical database containing information on the track and intensity of tropical cyclones is HURDAT [22], which applies to tropical cyclones in the North Atlantic. The HURDAT database, now HURDAT2, contains information on tropical cyclones dating back to 1885. The database contains data on storm position, maximum wind speed and central pressure in six hour increments. Central pressure data from before the 1980s are missing at many points, and are almost always missing prior to the mid-1940s. The reliability and quality of the data increases significantly from the mid-1940s, when aircraft reconnaissance flights began, and direct estimates of the pressure in the centre of the storm were made. Prior to this time, estimates of wind speed and position were developed using ship reports (using wind speed and atmospheric pressure) and other ground based measurement platforms. Since the launch of meteorological satellites in the early 1970s, the accuracy of storm position data in areas without aircraft reconnaissance flights has increased significantly. Using the Dvorak technique described in Ref. [75], estimates of central pressure and maximum wind speed can be obtained from satellite imagery. These estimates of wind speed and/or central pressure are subject to much greater uncertainties and errors than those obtained from aircraft or surface measurements of wind speed. As discussed in Ref. [75], reviews of the Dvorak estimates have demonstrated that the historical data sets have inherited biases that are implicit in the technique. These biases vary with both basin and era. Dvorak intensity estimates are the primary source of intensity data for most of the historical record, excluding the near coastal USA, Canada, Mexico and the Caribbean, where aircraft are able to obtain data.

Outside the USA, tropical cyclone information from reconnaissance flights is usually not available, and thus prior to the satellite era, the quality of the data is generally considered to be less reliable.

The International Best Track Archive for Climate Stewardship (IBTrACS) is a tropical cyclone database available online[3]. Reference [76] provides a worldwide database of tropical cyclone tracks, pressures and maximum wind

---

[3]   Available online at https://climatedataguide.ucar.edu/climate-data/ibtracs-tropical-cyclone-best-track-data; http://www.ncdc.noaa.gov/ibtracs/

speeds. IBTrACS provides global tropical cyclone best track data in a centralized location to aid understanding of the distribution, frequency and intensity of tropical cyclones worldwide. The World Meteorological Organization (WMO) Tropical Cyclone Programme has endorsed IBTrACS as an official archiving and distribution resource for tropical cyclone best track data. The data are available in many formats. The IBTrACS data set adjusts the maximum wind speeds given in the database so that all basins reflect the same definition of maximum wind speed, chosen as a 10 min average. This adjustment is required because different regions of the world use different definitions of the maximum wind speed. For example, in the North Atlantic and Eastern and Central Pacific basins, a 1 min wind speed is used, in Australia and Asia a 10 min wind speed is used, and the India Meteorological Department uses a maximum 3 min wind speed. In all cases, these maximum wind speeds are estimated and not actually measured. These wind speed adjustments were performed using the conversion factors and form the basis of WMO guidelines in Ref. [77].

The IBTrACS–WMO version of the data set uses data from the WMO sanctioned Regional Specialized Meteorological Centre or Tropical Cyclone Warning Centre in each basin. The database includes archived tropical cyclone data from 12 different agencies, including the Joint Typhoon Warning Centre (JTWC), the Chinese Meteorological Association (CMA), the Japan Meteorological Agency (JMA), Hong Kong Observatory (HKO), the India Meteorological Department, among others. In cases where basins are covered by multiple agencies, such as the Northwest Pacific Ocean (which is covered by JTWC, HKO, JMA and CMA), there are often discrepancies in the storm intensity, location or even the existence of a particular storm. Overall, users of the database need to be aware that changing operational procedures and observing systems have led to significant heterogeneities in the best track record, and storms may have conflicting data from multiple sources.

Only historical hurricane track (heading, position and translation speed), frequency and intensity data appropriate to the basin(s) bordering the coastline(s) under investigation can be used when developing the track model. If needed, information on storm size, Holland B or other profile parameters obtained from other basins can be used to supplement local basin data.

3.3.2. Hurricane parameterization

Historical information on the RMW, pressure–wind relationships and radial profile information is largely limited to the archived aircraft reconnaissance data obtained from flights into North Atlantic hurricanes (e.g. Ref. [32]). A database was developed in Ref. [31] for RMW applicable to Japan using surface pressure data recorded at or near the time when the typhoons made landfall in Japan.

Models developed using these data are often used in tropical cyclone hazard modelling in other basins, because such data are not available in those basins.

3.3.3. End-to-end validation studies

End-to-end validation studies are usually performed by comparing hazard curves developed using a stochastic modelling approach and synthetic storm track simulations with site specific hazard curves. These curves were developed using empirical (observational) data, including historical measurements of surface pressures or wind speeds. Examples of such studies are given in Refs [29, 36, 37]. The validation examples given in Refs [36, 37] compare the landfall pressure hazard curves for large regions of the US coastline, as seen, for example, in Fig. 12. James and Mason [29] made comparisons between the modelled and observed wind hazard curves using peak gust wind speed data for a number of locations in Australia. In cases where gust wind speeds associated with landfalling cyclones were not recorded, the authors supplement the measured values with best estimates obtained by modelling the historical event with a wind field model and information on central pressure, RMW and other relevant parameters.
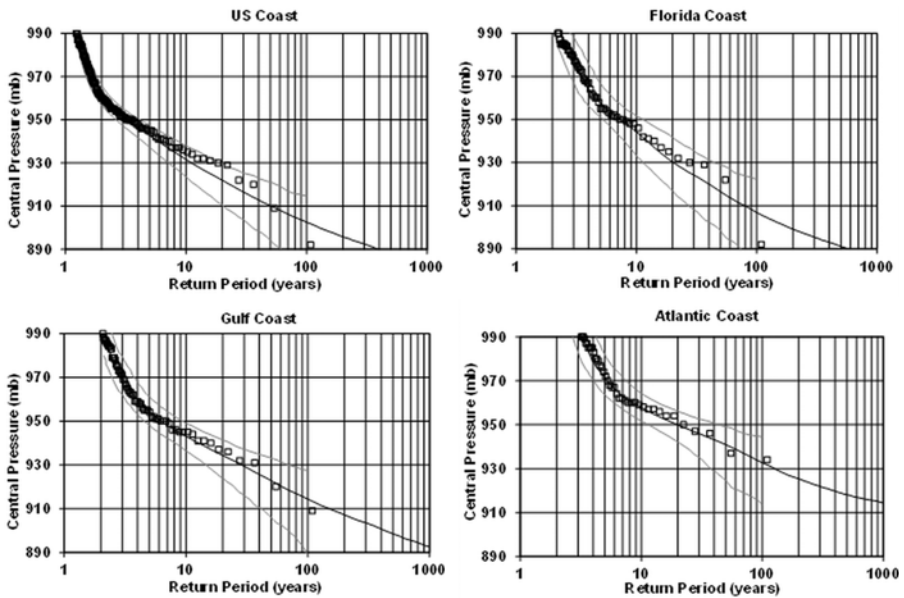
FIG. 12. Comparisons of modelled (solid line) and observed (open squares) central pressures at landfall along the full US coastline (Texas to Maine) and large segments of the coastline.

Figure 13 presents an example of a modelled (synthetic) and empirical gust wind speed hazard curve for Mobile, Alabama, USA. It can be observed that the agreement between the modelled and empirical hazard curves varies with the period of record. The modelled hazard curve was developed using the simulation model given in Ref. [37] and was developed using around 110 years of historical hurricane data. The two hazard curves agree well for wind data collected in 1990–2011 (22 years), 1970–2011 (42 years) and 1900–2011 (112 years). The agreement is not as good for the other three periods, for which the simulated hazard curves appear to overestimate those derived from empirical data. As in
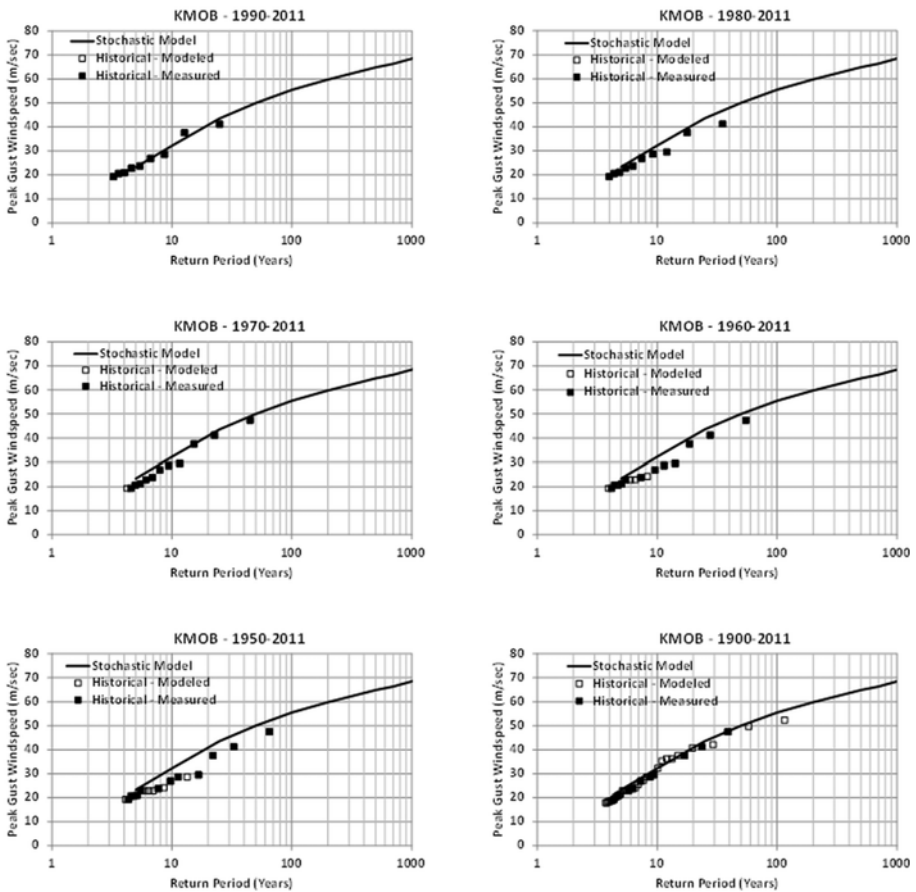
FIG. 13. Comparison of peak gust wind speed hazard curve at Mobile International Airport (KMOB) modelled from synthetic hurricane simulation with historical maxima plotted versus return period.

James and Mason [29], some of the wind speeds for the older storms had to be developed using models of the older hurricanes and are shown as open squares.

3.4. MODELLING UNCERTAINTIES

In the literature, very little attention has been paid to assessing the errors associated with the hurricane simulation process. Reference [16] used a mixture of sensitivity studies and judgement to perform a rough error study. The confidence bounds (one standard deviation) of the projected wind speeds were estimated to be about 10% (independent of return period). Twisdale, Vickery and Hardy [78] investigated the uncertainty of expected wind speeds in the Miami region and discovered a similar level of uncertainty. Later similar aspects were investigated in the USA [79]. One of the major factors affecting wind speed is the site's surface roughness.

Reference [37] used a two loop simulation to measure the uncertainty. In this two loop procedure, the outer loop represents a resampling of the parameters that form the statistical distributions employed in the N year simulation. Using this two loop strategy, the authors ran a 100 000 year simulation 5000 times (outer loop). For each new 100 000 year realization, complete related errors in the statistical distributions of landfall central pressure, Holland B parameter and occurrence rate are sampled and used to alter these key input variables. Inside the inner loop, the wind speed computed from the wind field model is multiplied by an uncorrelated wind field modelling error term (derived from Fig. 10) with a mean of zero and a coefficient of variance of 10%. Along the Gulf of Mexico coast, the outer loop uncertainty results in a coefficient of variance of about 6% for the predicted 100 year return time wind speed, rising to about 15% near Maine. The uncertainty in the wind model (considered as uncorrelated here) appears as a shift in the mean wind speed versus return time curve, rather than adding to the uncertainty in the N year wind speed. Figure 14 depicts an example of projected uncertainty in 100 year return period wind speed along the US coastline, as well as how wind field model uncertainty influences estimated N year return period gust wind speed. The instances of uncertainty given here are for wind speeds associated with landfalling storms in the USA; they do not reflect uncertainties in other places where data accuracy of the underlying pressure and wind speed is lower. For example, the landfall pressures for most US landfalling storms have been meticulously reconstructed over a 107 year period using a combination of surface and aircraft pressure measurements, whereas the Northwest pacific typhoon database is made up of a combination of aircraft and satellite estimated pressures, which are subject to large and potentially time-varying uncertainties and errors and cover a much shorter time span.
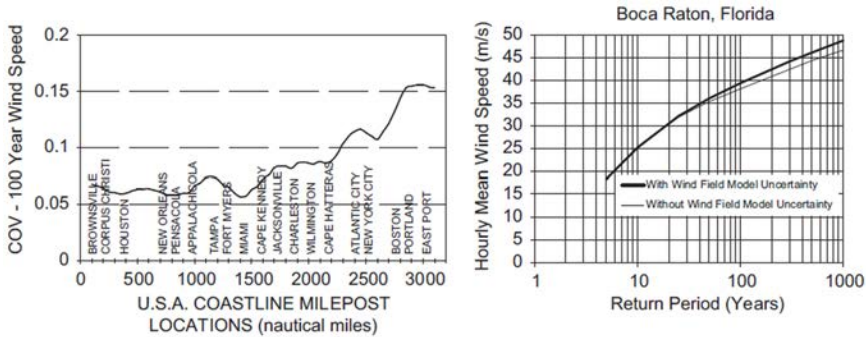
FIG. 14. Estimate coefficient of variation (smoothed) of the 100 year return period wind speed along the coastline of the USA (left plot) and effect of wind field modelling uncertainty of the predicted wind speed versus return period for a single location (reproduced from Ref. [21] with permission).

3.4.1. Historical record, climate change and long period oscillations

The accuracy of hurricane model based products would be influenced by long term trends in the frequency and intensity of tropical cyclones. Design wind speed charts by the American Society of Civil Engineers (ASCE), for example, are concentrated on annualized probabilities of exceeding peak gust thresholds (n year recurrence intervals), and these thresholds (model output) would almost certainly shift if the wind strength and/or frequency patterns changed over the many year time periods used in the model to generate such probabilities. Since tropical cyclone track and intensity databases in the Atlantic and Pacific Ocean basins (e.g. HURDAT, IBTrACS) span multiple cycles of the phenomena, the effects of annual to multi-year (El Niño/La Niña) and multidecadal oscillations are widely recognized. The effect of climate change on hurricane activity is still a hot topic of discussion, but the possible consequences need to be factored into a risk assessment.

There are also differing viewpoints on whether longer term patterns occur, as well as on their possible causes (natural versus human influenced). In an attempt to predict the effects of increased atmospheric CO_2, hurricane models have been used, but there has been no conclusive agreement among studies [80, 81]. Studies that find a connection between sea surface temperatures and hurricane power dissipation [82] draw conclusions that are scrutinized based on the quality of the historical data collection used (HURDAT). In the years 1978–1990, satellite imagery was reanalysed and revealed as many as 70 previously unidentified Category 4 and 5 cyclones [83, 84]. The existing tropical cyclone databases

(e.g. HURDAT, IBTrAC), according to these reports, are ineffective in detecting trends in the occurrence of severe cyclones.

Hurricane landfall behaviour in the USA was studied in the warm and cool phases of the El Niño–Southern Oscillation (ENSO) using historical sea surface temperature and landfall data [85, 86]. There was no noticeable difference in hurricane landfall rates between the warm period of the sea surface temperature and the overall long term average landfall rates in either study.

Figure 15 is taken from the NOAA Geophysical Fluid Dynamics Laboratory web page supplement to Ref. [87][4], where it is suggested that a mean increase in the frequency of Category 4 and 5 hurricanes could be 81%. However, in an earlier report, the Intergovernmental Panel on Climate Change reported a low confidence associated with increasing hurricane activity in a warming climate [88].

Various debates and research work are actively continuing on the future evolutions of hurricanes. As such, the science of hurricane wind modelling will need to adapt to future climate trends.
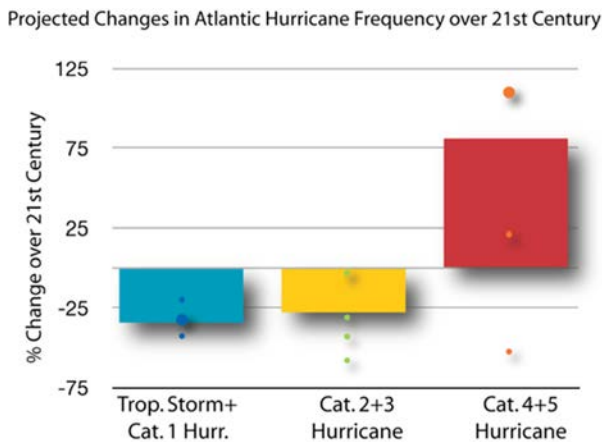
FIG. 15. Expected change in North Atlantic hurricane activity (reproduced with permission from the National Oceanic and Atmospheric Administration (NOAA)). Bars indicate 'best' estimate; dots indicate alternative estimates.

---

⁴ See http://www.gfdl.noaa.gov/21st-century-projections-of-intense-hurricanes

4. TORNADO WINDS

4.1. GENERAL CONSIDERATIONS

A tornado consists of a vortex of swirling air that spins about a vertical or nearly vertical axis between the ground and the base of a cumulo-nimbus cloud. Tornadoes are made visible by the debris and dust within the tornado. Most tornadoes occur in thunderstorm supercells and travel with the thunderstorm.

The intensity of a tornado, in terms of its maximum wind speed, is usually categorized using the Enhanced Fujita (EF) scale. The EF scale was introduced in February 2007 as a replacement for the Fujita (F) scale, which, in the judgement of many wind engineers, overstated the true maximum wind speed in a tornado. It is important to remember that the wind speeds associated with both the F and EF scales are derived from estimates of damage (e.g. to buildings, trees), and the true maximum wind speeds are rarely, if ever, measured. Table 2 presents the wind speeds associated with both the F and EF scales. In the United Kingdom (UK), tornadoes are often categorized using the Tornado and Storm Research Organization (TORRO) scale (also known as the T scale). Table 3 presents the wind speeds associated with the TORRO scale. Note that in the case of the

TABLE 2. F SCALE AND EF SCALE WIND SPEEDS VERSUS TORNADO STRENGTH CLASSIFICATION

F or EF scale classification	F scale wind speeds[a]		EF scale wind speeds[a]	
	mile/h[b]	m/s	mile/h	m/s
0	40–72	18–32	65–85	29–38
1	73–112	33–50	86–110	38–49
2	113–157	51–70	111–135	50–60
3	158–206	71–92	136–165	61–74
4	207–260	93–116	166–200	74–89
5	261–318	117–142	>200	>89

[a]   Peak gust wind speed at a height of 10 m.
[b]   1 mile/h = 1.61 km/h.

TABLE 3. T SCALE WIND SPEEDS VERSUS TORNADO STRENGTH
CLASSIFICATION

T scale classification	T scale wind speeds[a]	
	mile/h[b]	m/s
0	39–54	17–24
1	55–72	25–32
2	73–92	33–41
3	93–114	42–51
4	115–136	52–61
5	137–160	62–72
6	161–186	73–83
7	187–212	84–95
8	213–240	96–107
9	241–269	108–120
10	270–299	121–134

[a] Peak gust wind speed at a height of 10 m.
[b] 1 mile/h = 1.61 km/h.

original F scale, the wind speeds are defined as the fastest quarter-mile wind speeds; however, for tornado hazard studies, the F scale wind speeds are usually taken as representative of a 2–3 s gust wind speed [89].

Tornadoes occur in all continents except for Antarctica, but the majority of tornadoes occur in the USA. Tornadoes mostly occur between latitudes of 30 degrees and 50 degrees. The USA, on average, experiences about 1500 tornadoes per year, and Canada, with the second highest tornado rate, experiences about 100 per year. Within Europe, France has the highest annual tornado rate, with violent tornadoes (of EF 4 or 5) occurring at a rate of about once

every 15–20 years [90]. According to the European Severe Storms Laboratory, more than 450 tornadoes occurred in Europe in 2012, but only 190 of those were on land. Reference [91] provides information on the worldwide tornado risk. Figure 16 presents the average number of tornadoes per state in the USA from 1995 to 2014, and Figure 17 presents the locations of all tornadoes reported in Europe and the eastern part of the Russian Federation in the period 2000–2012.[5]

The categorization of a tornado is based on an estimate of the maximum wind speed within the tornado. This maximum wind speed occurs over a relatively small portion of the length and width of the tornado, and most of the wind speeds near the ground are much lower than the maximum. The variation of the wind speeds along the path and across the width of the tornado is a key part of any tornado risk assessment programme.
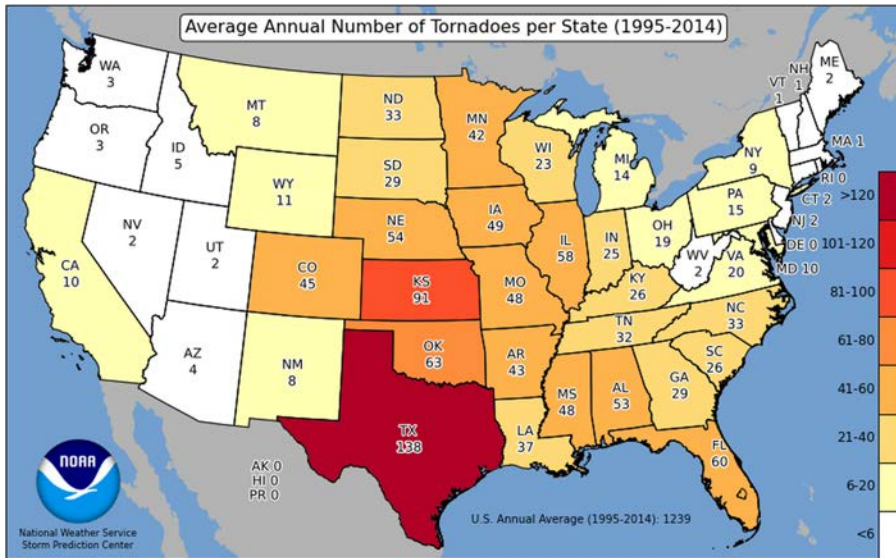
FIG. 16. *Average number of tornadoes per state per year (1995–2014) (reproduced from the NOAA web site).*

FIG. 17. European tornado occurrences during the period 2000–2012 (reproduced from the European Severe Weather Database with permission from the European Severe Storms Laboratory).

4.2. TORNADO STATISTICS AND DATABASES

A key component in the development of a tornado wind speed hazard model is a historical database containing information such as tornado intensities, path lengths, path widths and heading. In the USA, there are two such databases: the University of Chicago's Damage Area Per Path Length (DAPPLE) and the Storm Prediction Center (SPC). These data sets provide information on tornado intensity, path duration and path width, as well as path direction, geographic position parameters and time of occurrence, using the Fujita–Pearson classification method [92, 93]. Both data sets are derived from the same National Weather Service acquisition network and contain similar information. The SPC data set includes storms that have been recorded but not classified, whereas the DAPPLE data set includes storms that have been rated. DAPPLE encompasses

the period 1916–1985, whereas the SPC database includes data from 1950 to the present.

The SPC database, as well as the changes that have occurred over time, were identified in Refs [94, 95], including the effects of increased verification efforts and public awareness. The length of the tornado's path is measured in miles, the width is measured in yards, and the maximum damage is calculated using the F scale. Path width data recorded prior to 1994 refer to the mean width, and after 1994, to the maximum value associated with the tornado. In the SPC database, not all records represent individual tornadoes; often the records are of segments of the same tornado. Care needs to be taken to piece back together individual segments to ensure the proper counting of tornadoes. Once the database has been corrected to take into account the segment issue, information on path length and heading can be obtained. The data still have to be corrected for reporting biases, variations in data quality over the years, mixtures of EF and F scale classification and miscategorization of storms.

In Ref. [96], an attempt was made to resolve the discrepancies between the two data sets for F4 and F5 tornadoes. Some major biases were eliminated, especially on a state by state basis for the USA. Significant tornadoes were documented in Refs [97, 98] in the period 1880–1989. Further analyses are required to resolve the systematic and random errors inherent in the classification system. Users of the databases need to be aware of the issues, as well as the body of literature that discusses some of these errors.

4.2.1. Tornado wind speeds and the F and EF scales

A critical element in the development of a tornado hazard model is the relationship between the wind speed and the F or EF scale. Fujita's original estimates of wind speed [92] were not based on measurements or engineering calculations of damage due to high winds but were somewhat subjective. The scales have been subject to much debate and controversy since their original operational implementation by the National Weather Service. The damage associated with each of the F scale wind speed ranges is given in Table 4. Both F and EF ratings were/are made by comparing observed damage to a library of photos, each associated with an F or EF rating. In the case of the F scale, damage to individual residential structures was the key F rating indicator. The range of structure types was significantly expanded in the case of the EF scale.

Most engineering assessments of damage [99] yield estimates of the wind speeds needed to cause the observed data that are lower than those associated with the F scale winds associated with the observed damage. Twisdale updated Fujita's wind speed using previous engineering and photogrammetric analyses [100]. Although never adopted, Twisdale's F′ scale was remarkably close to the new

TABLE 4. F SCALE WIND SPEEDS AND TYPICAL DAMAGE
ASSOCIATED WITH THE INDICATED WIND SPEEDS

F scale	Wind speeds (m/s)	Damage estimates (damage applies to US construction practice)
0	18–32	Light damage: some damage to chimneys; branches broken off trees; shallow rooted trees pushed over; sign boards damaged
1	33–50	Moderate damage: the lower limit is the beginning of hurricane wind speed; surface peeled off roofs; mobile homes pushed off foundations or overturned; moving cars pushed off roads; attached garages possibly destroyed
2	51–70	Significant damage: roofs torn off frame houses; mobile homes demolished; boxcars overturned; large trees snapped or uprooted; high rise windows broken and blown in; light object missiles generated
3	71–92	Severe damage: roofs and some walls torn off well constructed houses; trains overturned; most trees in forest uprooted; heavy cars lifted off the ground and thrown
4	93–116	Devastating damage: well constructed houses levelled; structures with weak foundations blown some distance away; cars thrown and large missiles generated
5	117–142	Incredible damage: strong frame houses lifted off foundations and carried considerable distances to disintegrate; car sized missiles fly through the air in excess of 100 m; trees debarked; steel reinforced concrete structures badly damaged

EF scale for wind speeds adopted by the National Weather Service nearly 30 years later.

Table 5 presents the wind speeds associated with the three scales: F, EF and F´. Note that the upper limits of the EF and F´ scales are in the same range as the estimated maximum wind speed in a tornado of ~110 m/s [101].

The transformation of the discrete F scale classification into actual wind speeds is the single largest source of uncertainty in the development of a tornado hazard or risk model. Examples of damage were presented in Ref. [102], where in a given photograph the damage shown to a mobile home, trees and an Earth mounted satellite dish indicates an EF scale range of EF0–EF3.

In recent years, measurements of wind speeds have been taken near the ground surface in tornadoes [103–106]. Reference [106] shows some differences

TABLE 5. COMPARISON OF F, EF AND F´ SCALE WIND SPEEDS

Scale	F scale wind speeds (m/s)	EF scale wind speeds (m/s)	F´ scale wind speeds (m/s)
0	18–32	29–38	18–33
1	33–50	38–49	33–46
2	51–70	50–60	46–60
3	71–92	61–74	61–75
4	93–116	74–89	76–93
5	117–142	>89	94–124

between measured wind speeds and those estimated using the EF scale. These studies have the potential to aid in the assessment of uncertainties associated with the use of the F and EF scales.

4.3. TORNADO HAZARD MODELLING

A number of investigators in the USA have conducted tornado hazard studies for a range of purposes. Regional tornado wind speed hazard models include those developed in Refs [107–111]. Figure 18 presents the three broad tornado hazard regions given in Ref. [107]. Figure 19 presents the three hazard regions from ANSI/ANS-2.3-2011 [109], and Fig. 20 presents the wind hazard curves associated with the three zones depicted in Fig. 19. Figure 21 presents the tornado wind speed hazard associated with an annual exceedance probability of 10^{-6} from Ref. [111].

As noted in Ref. [89], these earlier vintage regional models are conservative.

Since the early 1970s, site specific hazard studies have been conducted, with hazard curves that produce lower wind speeds than those associated with general regional models. To account for the shortcomings in the tornado databases, the site specific studies have used a variety of approaches and methods. The original tornado risk models developed for point probabilities of tornado risk [112] have been enhanced through the incorporation of stochastic models (e.g. Ref. [113]), intensity path area relationships [114–116] and the effect of target size [117, 118]. Twisdale and Dunn [119] used a Monte Carlo simulation with a stochastic event

FIG. 18. Regional tornado hazard zones given in Ref. [107]. The region I wind speed is 360 mile/h (160 m/s), the region II wind speed is 300 mile/h (134 m/s) and the region III wind speed is 240 mile/h (107 m/s) (reproduced with permission from the US Nuclear Regulatory Commission).

FIG. 19. Three hazard regions given in Ref. [109]. Tornado and straight wind hazard curves are given for each region. Region II includes two hurricane hazard curves (reproduced with permission from the American Nuclear Society).
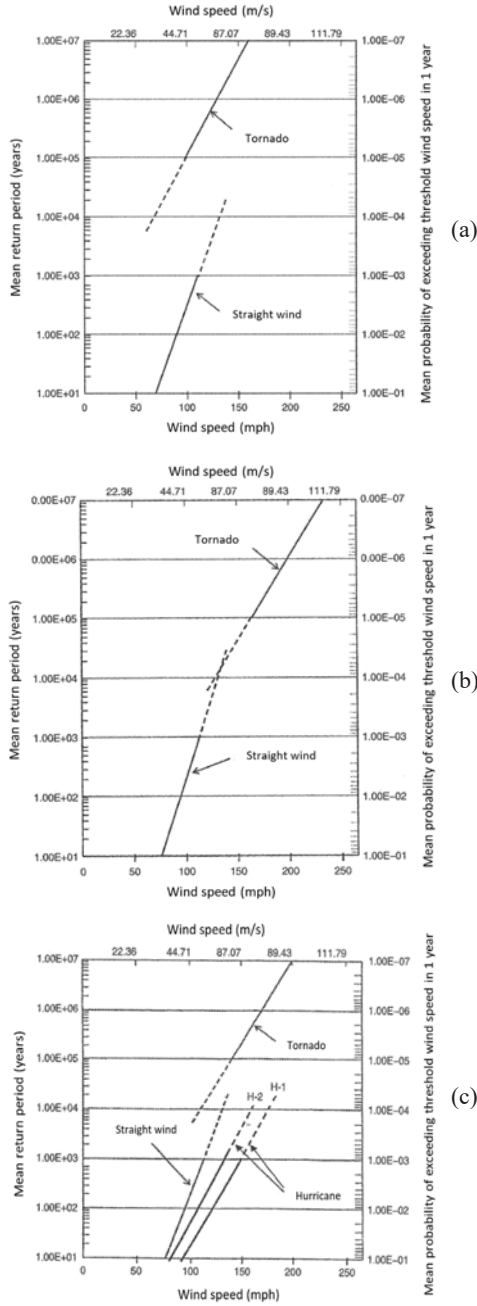
FIG. 20. Wind hazard curves for the three regions ((a) Region 1; (b) Region II; (c) Region III) given in Fig. 19 (reproduced with permission from the American Nuclear Society).

43

	124	122	120	118	116	114	112	110	108	106	104	102	100	98	96	94	92	90	88	86	84	82	80	78	76	74	72	70	68	66	
47	0	100	83	116	98	0	0	117	127	124	160	141	164	150	150	146	179	160	131										155		47
45	0	92	72	127	109	0	71	0	104	111	137	157	165	170	171	178	184	180	177	172	146	175						0	127	142	45
43	0	0	0	0	104	0	129	114	118	120	148	160	166	178	183	188	191	189	188	182	179	182		147	169	138	141	131	134	133	43
41	84	0	0	0	0	80	110	83	68	125	142	161	173	186	192	192	196	198	191	194	193	188	188	189	168	161	166	165			41
39	109	108	81	104	0	103	0	118	0	0	149	154	176	191	197	198	193	196	195	194	192	182	168	168	165	166	135				39
37		121	97	0	0	0	78	0	71	129	115	155	181	193	200	197	188	187	192	190	185	170	152	158	166	158					37
35		118	86	94	0	92	108	87	0	101	122	157	183	196	203	195	194	195	194	197	186	166	172	171	161	160					35
33			0	118	110	96	95	136	0	120	122	161	178	189	194	195	195	194	196	196	186	179	172	178	154						33
31				89	93	98	104	102	108	119	148	165	173	181	189	189	190	193	186	182	177	160	160								31
29	Region 1 – 200 mph										72	143	146	166	174	178	178	170	178	171	169	164	165								29
27	Region 2 – 170 mph													168	150	161	133					179	164								27
25	Region 3 –130 mph													144	157							196	157								25

FIG. 21. Tornado induced wind speeds associated with an annual exceedance probability of 10^{-6}; squares are 2 degrees latitude (vertical axis) by 2 degrees longitude (horizontal axis) (reproduced from Ref. [111] with permission from the US Nuclear Regulatory Commission).

model, tornado–target interaction geometry and tornado wind field probabilistic models. Reference [120] provides conditional probabilities of a secondary vortex providing tornado point strike probabilities to account for tornadoes with multiple vortices. McDonald and Fujita constructed site specific tornado wind speed hazard curves for US Department of Energy sites [121]. A site specific tornado model (TORNADO) was also developed in Ref. [122] for the US Department of Energy.

The mean tornado occurrence rate is usually used in the above mentioned tornado hazard models to establish a mean (nominal without considering uncertainties) wind speed hazard curve. The stochastic models that existed prior to 1982 are reviewed and analysed in depth in Ref. [120]. Wind speed exceedance probability for a Poissonian process is:

$$P_t(v > V) = 1 - \sum_{x=0}^{x=\infty} P(v < V|x) p_t(x)$$ (13)

where

$P(v < V|x)$ is the probability that velocity v is less than V, given that x tornadoes occur;

and $p_t(x)$ is the probability of x storms occurring during time period t.

With $p_t(x)$ defined as a Poissonian process and defining t as one year, the annual probability of exceeding a given wind speed is:

$$P_a(v > V) = 1 - \exp\left[-\lambda P(v > V \,|\, T)\right] \tag{14}$$

where λ is the mean annual occurrence rate of tornadoes and $P(v > V|T)$ is the probability of exceeding the velocity V given the occurrence of a tornado.

For annual exceedance probabilities of less than 1%, Eq. (14) can be approximated as:

$$P_a(v > V) = \lambda P(v > V \,|\, T) \tag{15}$$

To account for clustering or arrival rates, a similar expression was derived in Ref. [112] for $P_a(v > V)$ using a Pólya distribution (similar to a negative binominal distribution). Reference [89] provides similar arrival rate expressions for Weibull, Bayesian–Poisson and Bayesian–Weibull processes. The Bayesian formulation allows for the modelling of uncertainty in the incidence rate, as a gamma distribution. A fundamental expression in tornado hazard modelling is to compute $P(v > V)$ by:

$$P(v > V) = \mu_A P(v > V) / S \tag{16}$$

where $\mu_A P(v > V)$ is the mean tornado area over which $V > v$ and S is the tornado subregion area used to determine the occurrence rate λ.

Equation (16) assumes that the tornadoes over the subregion area have the same likelihood of occurrence. To take into account the area of the target facility, additional terms are needed. These additional terms are discussed in Refs [115, 117–119]. For very large target areas, the geometry of the facility is to be taken into account as discussed in Ref. [120]. Single point hazard curves developed by three different investigators, Fujita, McDonald and Twisdale for the Savannah River site in South Carolina, USA, are presented in Refs [123–125]. The differences among these curves illustrate some of the systematic differences in approaches, and hence uncertainties, in the resulting tornado hazard curves.

Regulatory Guide 1.76 (Revision 1), Design-Basis Tornado and Tornado Missiles for Nuclear Power Plants, of the US Nuclear Regulatory Commission [126],

is applied in the USA for the tornado design basis of nuclear power plants. The tornado wind speeds provided in Ref. [126] are based on NUREG/CR-4461 Revision 2 [111], which was released in February 2007 and varies from Revision 1. The EF scale [5] is used in NUREG/CR-4461 Revision 2 to compare the degree of tornado damage with the tornado maximum wind speed. The original Fujita scale was used in earlier versions of the study. The methods used in NUREG/CR-4461 Revisions 1 and 2 are identical to those used in the initial version of NUREG/CR-4461 [110], which was released in 1986, with the addition of a term to account for the finite dimensions of structures (sometimes referred to as the 'lifeline' term) and recognition of the range of wind speeds along and around the tornado footprint.

The design basis tornado wind speeds for new reactors correspond to a frequency of 10^{-7}/a (calculated as a best estimate), the same value as used in the original version of Regulatory Guide 1.76 [126]. According to the findings, a maximum wind speed of 103 m/s (230 mile/h) is appropriate for tornadoes in central USA (Region I); a maximum wind speed of 89 m/s (200 mile/h) is appropriate for a large region of the USA along the east coast, northern border and western Great Plains (Region II); and a maximum wind speed of 72 m/s (160 mile/h) is appropriate for tornadoes in western USA (Region III).

According to Regulatory Guide 1.76 [126], parameters that can be used to describe tornadoes include maximum total wind speed; radius of maximum tangential (rotational) wind speed; tornado tangential, vertical, radial and translational wind speeds; and related air pressure variations within the core.

In Ref. [126], as in its original version, the tornado is modelled as a single Rankine combined vortex to estimate the pressure drop and rate of pressure drop associated with the design basis tornado. In comparison with Fujita's model, the authors of Ref. [126] preferred the Rankine combined vortex model for its simplicity. The tornado in Fujita's model has an inner core and an annulus (outer core) where vertical motions are concentrated. Suction vortices form in the annulus between the inner core radius and the outer core radius in strong tornadoes and rotate around the parent tornado's centre. Reference [126] provides values for (i) maximum wind speed, (ii) translation speed, (iii) maximum rotational speed, (iv) radius of maximum rotational speed, (v) pressure drop and (vi) rate of pressure drop for tornadoes in each geographical area.

To ensure the safety of nuclear power plants in the event of a tornado, US Nuclear Regulatory Commission regulations require that nuclear power plant designs take into account the impact of tornado generated missiles in addition to the direct action of the tornado wind and the changing atmospheric pressure area (i.e. objects moving under the action of aerodynamic forces caused by the tornado wind). Wind speeds of more than 34 m/s (75 mile/h) can produce projectiles from objects in the tornado's path, as well as debris from nearby damaged structures. In the USA, a design basis tornado missile spectrum comprising a schedule 40 pipe,

an 'automobile' and a solid steel sphere is provided, along with maximum horizontal speeds in the three regions of the USA.

4.4. TORNADO HAZARD MODEL UNCERTAINTIES

The development of the tornado wind speed hazard model was discussed in Section 4.3 above. Uncertainties in tornado hazard modelling, both random (aleatory) uncertainties and modelling (epistemic) uncertainties, are treated in this section. A family of tornado hazard curves is developed through multiple simulations of the single point tornado wind hazard curve. In each simulation, a unique hazard curve is developed by perturbing the distributions of the key inputs to the simulation model.

The epistemic uncertainties considered in the tornado hazard analysis are the following:

(a)   Occurrence rates;
(b)   F scale probability distributions;
(c)   F scale wind speed uncertainties;
(d)   Overall modelling uncertainty factor.

The following subsections present the uncertainty models.

4.4.1. Uncertainty in occurrence rates

Assuming that tornadoes occur as a Poisson process, we can model the aleatory uncertainties in the mean occurrence rate by using the normal approximation to the Poisson process. With this assumption, the standard error of the mean is given by $\sqrt{(\lambda/N)}$ and the coefficient of variation, $\delta r = \sigma/\mu = 1/\sqrt{(\lambda N)}$.

In addition to the random uncertainty due to finite sample size, epistemic uncertainties also affect the tornado occurrence rate. Considering that tornado occurrences are not necessarily Poisson distributed, and bearing in mind tornado reporting uncertainties and climate variations, an epistemic uncertainty factor is included and made equal to three times the random standard error. Combining the two as independent random variables, the combined factor from $\sqrt{(\delta r^2 + 9\delta v^2)}$ is obtained.

4.4.2. F scale probability distributions

There is considerable uncertainty in the distribution of F or EF scales assigned to tornado events. The F scale assignments in the tornado data record

are based on interpretations of the available evidence of tornado damage characteristics. Modelled F scale uncertainties reflect a lack of knowledge and are treated as epistemic uncertainties. Storm misclassifications and non-existing or insufficient evidence of damage are potentially important factors in predicting true tornado risk [127]. A model of F scale classification errors was developed in Refs [100, 119] that accounted for misclassifications and potential underclassifications due to insufficient damage evidence at the location of maximum storm intensity.

The model uses three weighted sets for the F scale distribution to reflect the uncertainties in the true distribution of tornado intensities. The distribution as reported includes no updates or corrections to the raw, reported frequencies of F scale events in the period 1950–2012. Essentially, this record assumes that the assignments of F scale average out and that there is no inherent bias in the overall data set. The distribution is provided in the second column of Table 6.

The second F scale distribution is developed considering the potential for subjective classification errors in assigning F scales. A Bayesian updating process is applied to the data from the direct classification error model developed in Ref. [128]. Direct classification errors reflect the subjective judgement used

TABLE 6. THREE WEIGHTED SETS FOR THE F SCALE DISTRIBUTION TO REFLECT THE UNCERTAINTIES IN THE TRUE DISTRIBUTION OF TORNADO INTENSITIES

Intensity scale	As reported (wt = 0.10)	Updated direct classification error (wt = 0.25)	Reported era trend corrected (wt = 0.65)	Range (max/min)
F0, EF0	0.4203	0.4528	0.6056	1.4408
F1, EF1	0.3424	0.2779	0.2558	1.3385
F2, EF2	0.1734	0.1704	0.1069	1.6225
F3, EF3	0.0499	0.0693	0.0285	2.4284
F4, EF4	0.0140	0.0242	0.0030	8.0171
F5, EF5	0.0000	0.0054	0.0002	Undefined
All	1.0000	1.0000	1.0000	n.a.[a]

[a] n.a.: not applicable.

by National Weather Service personnel in classifying tornadoes and the use of backward classifications following the development of the F scale in the late 1960s and early 1970s. By reproducing the steps in Ref. [128], the updated F scale distribution for direct errors is computed. The direct classification error data are based on a normal distribution of errors in assigning F scale categories to actual events. That model is based on about a 50% chance of correct assignment for each of the middle F scales and about an 80% chance of correct assignment for the extreme F events (F0 and F5). Errors are distributed normally around the classified scale. The updated distribution of F scale probabilities is provided in the third column of Table 6. This model produces about a 62% increase in $\geq$ F3 tornadoes, based on potential classification errors.

The third F scale distribution is based on the updated distribution that reflects reporting eras and trends. It includes corrections that combine the early era (1950–1994) and the modern era (1995–present). It has a much higher frequency for F0 intensities and slightly reduced frequencies for $\geq$ F3, as provided in the fourth column of Table 6.

The largest weight (0.65) is applied to the trend corrected data; the second largest weight (0.25) to the updated error frequencies (somewhat higher probabilities of intense events); and the lowest weight (0.10) to the original record, which includes no corrections to early pre-F-scale reporting. These distributions provide a range that increases with EF scale, and the majority of the subjective weight is assigned to the trend corrected data.

4.4.3.   F scale wind speed uncertainties

The assignment of wind speeds to the damage scale represents the largest single modelling uncertainty in the development of tornado hazard risk. The surface roughness of the site is an important factor that influences the wind speed. The lack of direct measurements of tornadic winds and the reliance on a damage scale that is based on the maximum observed damage along the path introduce large uncertainties. Fujita's original wind speeds were developed based on judgement and a scale that connected the Beaufort wind scale to the Mach scale.

Uncertainties in F scale wind speeds are discussed in Refs [127, 128]. An F′ wind speed scale was developed that used a Bayesian updating process with engineering calculations and expert judgement. The differences between these scales represent epistemic uncertainty. Since the EF scale has been accepted by the US National Weather Service and the US Nuclear Regulatory Commission, a high weight of 0.5 was assigned to that scale. The remaining weights are assigned as 0.35 for the F′ scale and 0.15 for the F scale. This approach allows for the wind speeds of about one simulated tornado in three to follow the F′ scale and one in seven to follow the F scale. In the uncertainty simulations, a random number is

drawn, and a scale is selected for that set of model runs in the outer loop of the simulation. The sensitivity of the results to these assumptions can be evaluated by using the different uncertainty percentiles of the tornado hazard curve in the fragility analysis.

4.4.4. Overall modelling uncertainty factor

An overall modelling uncertainty factor is applied in the tornado hazard modelling to represent uncertainties in the random models for tornado wind field parameters, damage variation along the tornado path length and the subjectively estimated uncertainties. A normal distribution is used with a mean of 1.0 and a standard deviation of 0.15. This overall modelling uncertainty factor accounts for uncertainties in the random models not explicitly treated in Sections 4.4.1–4.4.3.

5. EXTRATROPICAL STORMS, THUNDERSTORMS AND OTHER WINDSTORMS

5.1. GENERAL CONSIDERATIONS

Extratropical storms are often referred to as winter storms or mid-latitude cyclones and are geographically large, covering distances of hundreds of kilometres. These storms are associated with fronts and gradients in horizontal temperatures and dew points. The most intense extratropical storms generally occur over the oceans.

Thunderstorms are produced by the rapid upward movement of warm moist air. As the warm moist air rises, it cools and forms cumulo-nimbus clouds. As the moist air reaches the dew point temperature, droplets form and begin to fall back to Earth. The falling droplets combine with other droplets and become larger, creating downdrafts of air that spread out at the ground surface. Strong winds (excluding tornadoes) are associated with gust fronts and downbursts. The majority of strong winds are associated with gust fronts, but the strongest winds are produced by downbursts. Derechos are long lines of fast moving thunderstorms that can produce very high gust wind speeds over a short period of time but covering relatively large areas. Damaging winds can cover hundreds of square kilometres, causing extensive damage to electrical transmission and distribution systems. A composite radar image of a significant derecho affecting a large region in the USA is depicted in Fig. 22.
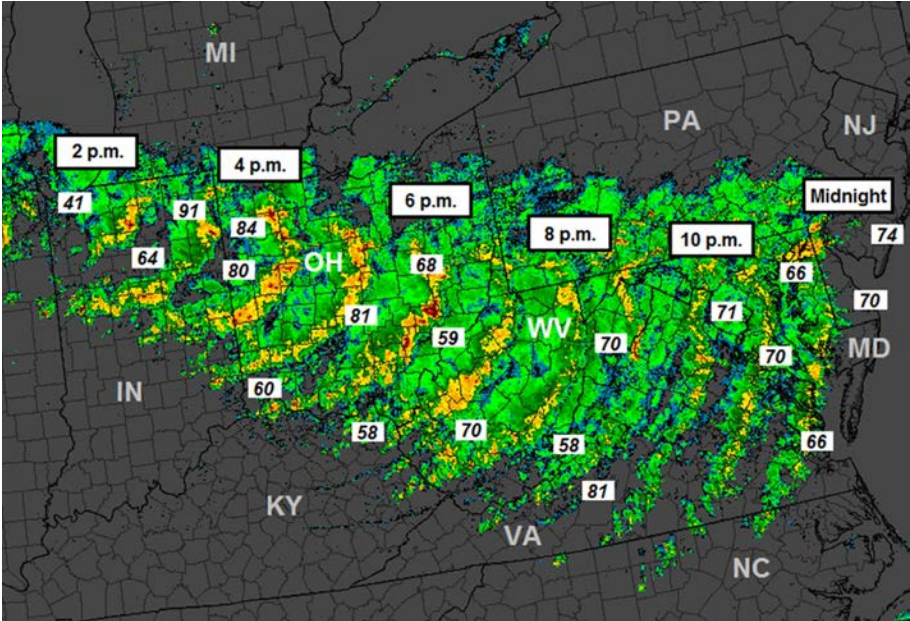
FIG. 22. Composite display of hourly radar reflectivity imagery showing the development and evolution of the derecho producing convective system that occurred on 29 June 2012, with selected observed wind gusts (italics, mile/h). Time is Eastern Daylight Time and ranges from 2.00 p.m. (6.00 p.m. Universal Time Coordinated (UTC); far left) to midnight on Friday, 29 June (4.00 a.m. UTC, 30 June; far right). Base image by G. Carbin, NOAA Storm Prediction Center (reproduced with permission from NOAA).

Other types of windstorm that can play a significant role in extreme winds include downslope winds and the shamals that occur in and around the Arabian Peninsula. These shamal windstorms are responsible for sandstorms and occur most frequently in the spring and summer months but can also occur in the winter. Other than tropical cyclones and tornadoes, these storm systems are the two main meteorological phenomena that can produce high winds.

5.2. DATA SOURCES

The primary source of wind data for use in the development of the wind hazard model is usually airport stations. As discussed in Ref. [129], many wind engineers rely on the wind speed data archived by the US National Climatic Data

Center (NCDC)[6], as the NCDC supplied data for commercial use at a moderate cost. Analyses were performed in Ref. [129] on the wind data at two stations in the UK using the wind data archived at the NCDC. It is up to the user of the data to find information on anemometer height, anemometer type, averaging times and exposure (surrounding terrain). Users of non-US data archived by the NCDC may need to perform their own quality assurance analysis. An approach to detecting artefacts in wind data was presented in Ref. [130].

The quality of wind data can vary enormously among countries. Ideally, gust wind speed measurements will be available, as these data are less sensitive to the effects of local terrain and variations in anemometer height than are wind speeds associated with longer averaging times, such as 10 min (WMO standard) or 1 h. If, for example, the terrain changes from smooth to rough, the mean wind speed decreases. This leads to an increase in turbulence, resulting in gust wind speeds that decrease by less than the mean wind speeds. Preferably, information will be available to enable thunderstorm and non-thunderstorm winds to be treated separately. In order to separate these meteorological events, the historical data need to have a data field to indicate whether thunder was heard on a given day or if a thunderstorm occurred. Such information is available in many countries, including but not limited to Australia, Canada, Germany, South Africa and the USA. If such a data field does not exist, then the analysis of the wind data progresses irrespective of the meteorological phenomena responsible for the wind gusts. If a region experiences strong winds from both thunderstorms and non-thunderstorms, analyses performed without separating the winds by storm type tend to underestimate the wind hazard.

Nuclear power plants are equipped with anemometers mounted on towers. The main purpose of these anemometers is to monitor winds in order to estimate the likely paths of airborne contaminants in the event of any type of radiation release. These anemometers are not usually positioned in ideal locations (i.e. flat, open, unobstructed terrain). On-site anemometer systems usually record and archive mean (usually 15 min and/or hourly average) wind speeds and wind directions only (no gust wind speed data). Provided that anemometers are positioned at multiple heights, they can be used to estimate the surface roughness on a direction by direction basis. This surface roughness data can then be used in conjunction with a wind fragility analysis.

The hazard curves developed from anemometers at surrounding sites (typically airport stations) can be weighted and combined to estimate the wind hazard for the nuclear power plant. The weights used in combining information

---

[6]   In 2015, the NCDC merged with the National Geophysical Data Center and the National Oceanographic Data Center to form the National Centers for Environmental Information. Reference [129] was written in 2014 and data prior to this year were used.

from various sites can be subjective (e.g. sites with fewer years of data might be given less weight than sites with more years of data), or they could be weighted as a function of distance from the site, or some other logical means could be used to assign the weights.

Some countries archive data with different averaging times. In Canada and India, the primary archive consists of 1 and/or 2 min average wind speeds recorded once per hour. Both countries have archives of peak gust wind speed data, but the periods of record are often not as long as for the 1 min wind speeds. The wind speeds at Indian airport sites are measured using a Dines anemometer, which has recently been shown to have a high bias if the assumed gust speed is representative of 3 s gust wind speeds [131]). The gust measured by the Dines anemometer is actually representative of a gust with a duration of 0.2–0.3 s. This bias needs to be taken into account when using gust wind speed data from a Dines anemometer. Wind speed data from the UK's Met Office are given as both mean (hourly mean) wind speeds and peak (3 s) gust wind speeds, as are those in South Africa.

Wind flows in mountainous terrain, valleys and other complex terrain are best dealt with through either boundary layer wind tunnel modelling [132] or through the use of mesoscale numerical weather forecasting tools, such as the Regional Atmospheric Modelling System [133]. When using these approaches to model extreme winds, the overall uncertainty in the resulting wind hazard curve will be greater than in the flat terrain case; consequently, an additional uncertainty term will be required.

5.3. STATISTICAL METHODS

The state of the art approach assumes that thunderstorm and non-thunderstorm winds can be treated as statistically independent events. Such an analysis requires a thunder day indicator in the wind speed database. If thunder day information is not available, then the winds are assumed to have been produced by the same meteorological event. In the discussion that follows, if thunderstorm winds cannot be separated, the analysis of the winds follows the approach presented for the non-thunderstorm wind case. The separation of thunderstorm and non-thunderstorm winds, treating them as statistically independent events, was first proposed in Ref. [134] for developing wind hazards in Australia. The applicability of the methodology in the USA is demonstrated in Ref. [135]. It was also shown in Refs [136, 137] that thunderstorms dominate extreme winds over most of the inland area of the USA. Interest in treating extratropical storms and thunderstorms in the USA as separate phenomena increased from the 1990s onward [138, 139].

In the USA, away from the 'hurricane coastline', a 'superstation' approach was used to develop the design wind speeds in ASCE Standard 7 on wind loading (ASCE 7) [140]. This superstation approach combined annual gust wind speeds from many neighbouring stations with similar climatology in order to create records of longer duration. The approach is valid if the distributions of extremes from the various sites are independent of one another, which was demonstrated in Ref. [140].

5.3.1. Thunderstorm winds

A thunderstorm climate model can be developed either through a standard Type I extreme value model using annual extremes or through the use of a stochastic model. In the analysis of thunderstorm winds, it is usually assumed that on days where thunder was reported in the database, the maximum gust recorded on that day was associated with a thunderstorm. The approach assumes that corrections for height and upstream terrain, made using an atmospheric boundary layer theory originally developed and validated for extratropical storms, are also valid for thunderstorm winds. This commonly used assumption has not been verified. It is likely that applying the standard correction to downburst winds will result in an overestimate of the adjustment factor associated with height and terrain corrections. The wind speeds associated with thunderstorms are generally brought about by gust front winds or downburst winds (macroburst and microbursts [141]), with the downburst winds having the potential to produce very high, short lived wind speeds.

The gust wind speeds are set to a height of 10 m using a correction factor derived from ESDU atmospheric turbulence models, for example [50, 142, 143]. Height corrections are usually carried out under the assumption that the position terrain is reflective of normal open terrain with a nominal surface roughness of 0.03 m (open terrain). This presumption of open terrain will be addressed later in this section.

Each thunder day maximum is retained and fitted to a probability distribution. In the examples that follow, data were fitted to both log-normal and Type I distributions, with the Type I distribution resulting in a better description of the peak gust wind speeds. Using the Type I distribution, the probability that the wind speed v will exceed V given the occurrence of a thunderstorm is:

$$P(v > V \mid T) = 1 - \exp\left[-\exp\left(\frac{U - v}{\alpha}\right)\right] \tag{17}$$

Figure 23 presents an example showing both linear squares fit regression and method of moments fits to a Type 1 distribution to the individual thunder

day storm maxima for a single site. Using the least squares method, the intercept of the straight line fit is the mode of the distribution U, and the slope is the dispersion $1/\alpha$. Using the method of moments, the mean values of the parameters U and α are obtained from:

$$U = \bar{x} - 0.5772\sigma_x \tag{18}$$

$$\alpha = \sigma_x \frac{\sqrt{6}}{\pi} \tag{19}$$

where $\bar{x}$ and σ_x are the mean and standard deviation of the distribution of x, the maximum wind speed.

As indicated in Fig. 23, the fit derived using the method of moments is indistinguishable from that obtained using the method of least squares, indicating that the results are not affected by the method used to determine the distribution parameters.

In Fig. 23, three anomalous gusts, or outliers, are evident in the wind speed data at this location. In this example, the three anomalous gusts were found to be associated with thunderstorm events and not erroneous entries in the database. The type of meteorological event associated with these winds can be determined by reviewing meteorological publications and newspaper archives, for example.
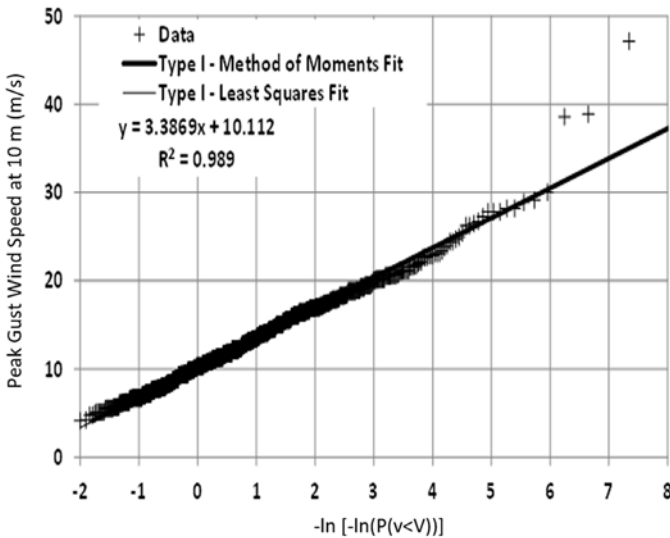

FIG. 23. *Fits of thunder day wind speed maxima to a Type I distribution.*

In the case shown here, the anomalous gusts were associated with thunderstorms and are likely to have been produced by downbursts.

The probability that the thunderstorm wind speed is exceeded during time period t is:

$$P_t(v > V) = 1 - \sum_{x=0}^{x=\infty} P(v < V|x) p_t(x) \tag{20}$$

where $P(v < V|x)$ is the probability that velocity v is less than V given that x storms occur and $p_t(x)$ is the probability of x storms occurring during time period t.

From Eq. (20), with $p_t(x)$ defined as Poissonian and defining t as one year, the annual probability of exceeding a given wind speed is:

$$P_a(v > V) = 1 - \exp[-\lambda P(v > V | T)] \tag{21}$$

where λ is the average number of thunderstorms (or thunder days) per year.

Figure 24 presents comparisons of the annual exceedance probabilities associated with thunderstorm winds computed using the stochastic modelling approach (Eqs (17–21)) with those derived using a Type I fit to the annual thunderstorm extremes only. Using all the thunder day data significantly reduces the impact of the anomalous gusts.

5.3.2. Non-thunderstorm winds

In the case of non-thunderstorm winds, the extreme wind climate can be analysed using a standard Gumbel extreme value analysis using annual extremes or a method that uses many individual storm maxima. The gust wind speeds are adjusted to a height of 10 m using a correction factor for gust wind speeds such as that derived from the ESDU model for atmospheric turbulence [50, 143]. Where upwind roughness is known, corrections for open terrain can be performed using the ESDU model. Height corrections are often performed assuming the location terrain is representative of standard open terrain (ASCE 7 Exposure C) [5] modelled with a nominal surface roughness, z_0 of 0.03 m (open terrain).
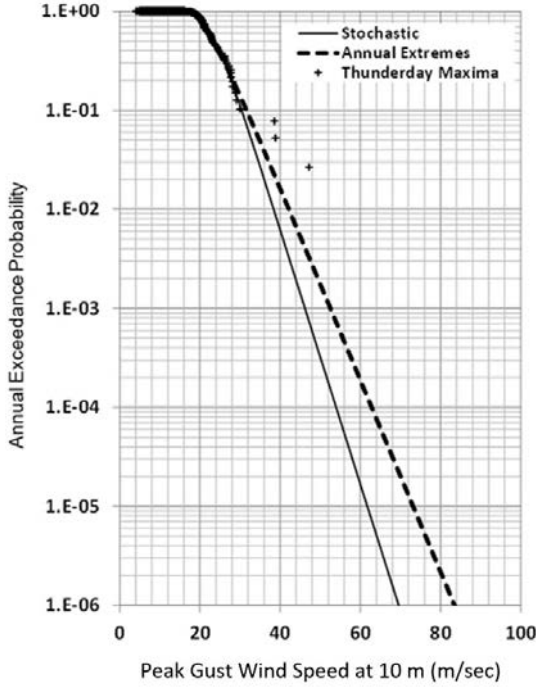
FIG. 24. Comparisons of annual exceedance probabilities of thunderstorm storm gust wind speeds derived from annual extremes and the stochastic model.

Using the method of independent storms as provided in Ref. [144], independent gust wind speeds that exceed a given threshold are extracted. These independent extremes are then modelled using an appropriate probability distribution. The annual exceedance probability of wind speed, v, is derived using:

$$P_a(v > V) = 1 - P(v < V)^r \tag{22}$$

If it is assumed that the arrival rate of extratropical storms is Poissonian, then the annual exceedance probability of the extratropical gust wind speed is:

$$P_a(v > V) = \exp[-rP(v > V)] \tag{23}$$

For practical purposes, Eqs (22) and (23) are identical for annual exceedance probabilities less than about 0.05 or $R > 20$ years.
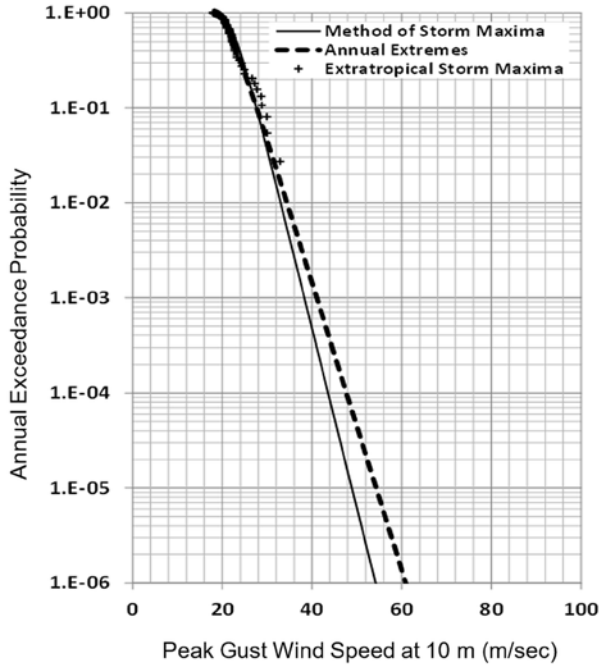
FIG. 25. *Comparisons of annual exceedance probabilities of extratropical storm gust wind speeds derived from annual extremes and the method of independent storm maxima.*

The analysis of the non-thunderstorm winds described here is an application of peaks over thresholds modelling.

Figure 25 presents comparisons of the annual exceedance probabilities associated with extratropical storm gust wind speeds derived from annual extremes and the method of independent storm maxima.

5.4. ESTIMATING UNCERTAINTIES

5.4.1. Parameter uncertainty

In this example, parameter uncertainties were estimated from the estimates in the standard errors in both the mean and standard deviations of the annual wind data that are used in the Type I parameter estimation. Errors in the mean shift the Type I fit vertically without a change in the slope. Errors in the standard deviation change the slope of the Type I fit.

Since the parameters of the Type I distribution were obtained using the method of moments, the standard errors in the estimates of the mean and standard deviation of the annual wind speed maxima were used to compute the errors in the estimates of the mode, U, and the dispersion α. Using the method of moments, the mean values of the parameters U and α are obtained from:

$$U = \bar{x} - 0.5772\sigma_x \tag{24}$$

$$\alpha = \sigma_x \frac{\sqrt{6}}{\pi} \tag{25}$$

where x represents the annual maximum gust wind speed corrected for height and gust averaging time.

The standard error in the estimate of the mean is normally distributed, unbiased, and the standard deviation is:

$$\sigma_{\bar{x}} = \frac{\sigma_x}{\sqrt{n}} \tag{26}$$

where n is the number of samples. The error in the estimate of the standard deviation is normally distributed with a mean of zero. The standard deviation of the estimate of σ_x is obtained from:

$$\sigma_{\sigma_x} = \sqrt{\frac{2\sigma_x}{n+1}} \tag{27}$$

Using the Poisson assumption whereby the mean and variance of the distribution are the same, the error in the mean value storm occurrence rate, either r in the case of extratropical storms or λ in the case of thunderstorms, is:

$$\sigma_{\bar{r}} = \frac{\sqrt{r}}{\sqrt{N_Y}} \tag{28}$$

$$\sigma_{\bar{\lambda}} = \frac{\sqrt{\lambda}}{\sqrt{N_Y}} \tag{29}$$

5.4.2. Modelling uncertainty

In addition to parameter uncertainty, additional uncertainties are treated. These additional uncertainties may include the following:

(a) Uncertainty in the correction for anemometer height;
(b) Uncertainty in the roughness of the surrounding terrain;
(c) Uncertainty in the effective gust duration for the cup anemometer era and gust wind speed averaging time (in some cases);
(d) Overall modelling uncertainty associated with the possibility of an erroneous choice of the extreme value distribution used in the study and uncertainties in the applicability of the model subcomponents (ESDU models [50, 51, 142, 143]).

5.4.2.1. Corrections for anemometer height

The ESDU models for atmospheric turbulence [50, 51, 142, 143] can be used to generate gust wind speed height correction factors. These height correction factors are applied by dividing the gust wind speed recorded at height z by the correction factor to yield an estimate of the wind speed at a height of 10 m. These correction factors are given for three different terrains (as defined by z_0) in Fig. 26.

The information given in Fig. 26 can guide the estimation of the uncertainty in the anemometer height correction. The correction ratio was modelled using a log-normally distributed multiplicative factor with a mean value of 1.0 and a standard deviation of 0.05.

5.4.2.2. Corrections for surrounding terrain

The effect of the upstream terrain on wind speed measurements at airport locations is discussed in Ref. [145], in which it is indicated that few US airport anemometer sites (located along the hurricane prone coastline) are associated with true open terrain. The median effective value of z_0 was found to be 0.07 m in Ref. [145]. A site specific effective surface roughness can be obtained by examining aerial imagery of the airport sites, attempting to find the location of the anemometer and then assessing the effective value of the surface roughness at the site. Without correcting to account for the effects of nearby terrain on the anemometer measurements, the wind hazard curve derived from the analysis will underestimate the true hazard.

The coefficient of variation can be estimated using a combination of experience and the actual surrounding terrain as indicated by the aerial photographs. Typically, the sites discussed in Ref. [145] have estimated nominal
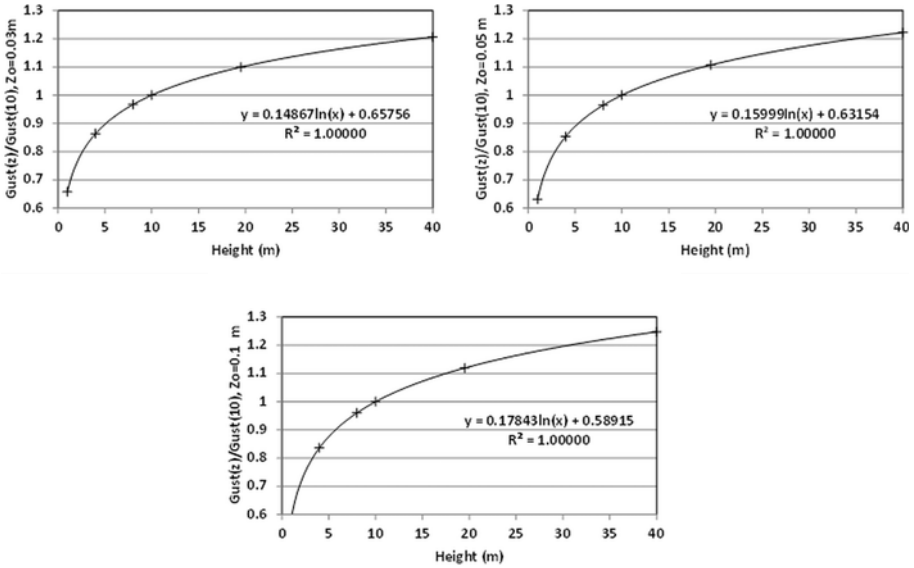
FIG. 26. *Gust wind speed adjustment factors for various anemometer heights with typical effective airport surface roughness values.*

z_0 values of around 0.06 m, and a 100% coefficient of variation yields a ±1.0 σ range of about 0.027 m < z_0 < 0.138 m (the uncertainty in z_0 is modelled using a log-normal distribution). This range seems reasonable, with the lower bound (−1.0 σ) approximately equal to open terrain and the upper bound (+1.0 σ) near the break point between the open (ASCE 7 Exposure C) and suburban (ASCE 7 Exposure B) terrains [5], which is defined using $z_0 = 0.15$ m in ASCE 7. The break point between the open and suburban type terrains in terms of a roughness length is not given in the Canadian building code. In Australian wind loading provisions, open terrain is associated with an aerodynamic roughness length of 0.02 m, and suburban terrain is characterized by a z_0 of 0.2 m. The aerodynamic roughness lengths associated with the open and rougher terrains are not specified in the Indian building code. In UK building standards, open terrain is defined as having a surface roughness, z_0, equal to 0.03 m, and the suburban terrain value of z_0 is 0.3 m. In the Eurocode, open terrain (Terrain Category II) is defined with a surface roughness of 0.05 m, and suburban terrain (Terrain Category III) is defined using a surface roughness of 0.30 m.

Figure 27 presents relationships between the effective surface roughness and the gust wind speed correction factor. One of the relationships given in Fig. 27 was derived using the ESDU models for atmospheric turbulence [50, 51], and the
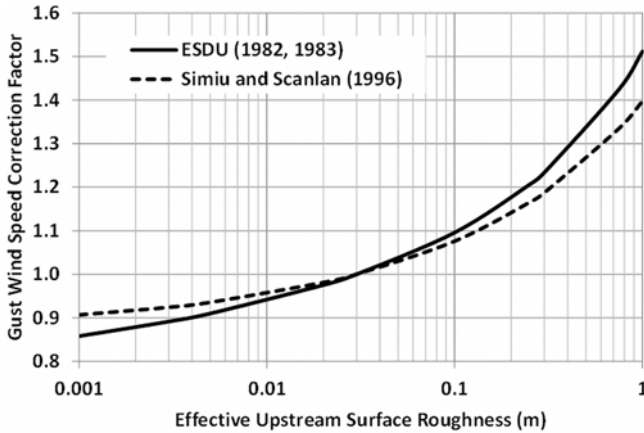
FIG. 27. Gust wind speed correction factor as a function of the effective upstream surface roughness. The correction factor is defined as the gust wind speed in open terrain ($z_0 = 0.03$ m) by the gust wind speed in the terrain with z_0, as indicated on the abscissa. For ESDU, see Refs [50, 51]; for Simiu and Scanlan (1996), see Ref. [52].

other was derived using the approach provided in Ref. [52]. As shown in Fig. 27, for a typical range (e.g. 0.010 m < z_0 < 0.20 m), and depending on the direction, the correction factor ranges between 0.94 and 1.16, or in round numbers, ±10.

5.4.2.3. Examination of outliers and the use of superstations

Thunderstorm wind speed hazard curves are generally defined by the mean, median and uncertainty bounds (5th and 95th percentile) for a site. Plots presenting the data (gust wind speeds) as a function of annual exceedance probability are derived. However, when using the stochastic modelling approach for a single airport site with limited data, more data points are observed outside the confidence bounds compared with data taken from more airport sites near the nuclear power plant. This can be done by combining the data and using a superstation approach, yielding an effective longer record length.

5.5. COMBINED STRAIGHT LINE WIND HAZARD

The approach used to combine the exceedance probabilities is to multiply the non-exceedance probabilities at each computed wind speed. Hence, the exceedance probabilities are combined as the union of statistically independent events according to:

$$P(v > V) = 1 - (1 - P_{\text{th}})(1 - P_{\text{ext}}) \tag{30}$$

where P_{th}, P_{ext} are the thunderstorm and extratropical cyclone (non-thunderstorm) annual exceedance probabilities for a given peak gust wind speed.

The separation of thunderstorms and non-thunderstorms before recombining them as statistically independent events is being implemented in the USA as a provision of ASCE 7 [146].

5.6. TAIL LIMITED DISTRIBUTIONS

Although the statistical modelling approach described above uses individual storm maxima to significantly expand the data set as compared with the more standard annual maxima approach, the methodology uses the Gumbel distribution to define the extreme value distribution, which has an infinite tail. A physical limit to the maximum gust wind speed in a thunderstorm or extratropical storm is likely, and consequently tail limited distributions have been proposed by some investigators [147, 148]. The tail limited distribution most frequently used is the generalized Pareto distribution (GPD). As discussed in Ref. [149], many methods are available to determine the parameters of the GPD. Here, two are presented, one from Simiu and Heckert [148] and the other from Holmes and Moriarty [149].

The following discussion on the use of a GPD is taken from Simiu and Heckert [148]. The GPD is a three parameter distribution given as:

$$F(y) = P(Y \le y) = 1 - \left(1 + \frac{cy}{a}\right)^{\frac{1}{c}}, \quad a > 0, \quad 1 + \frac{cy}{a} > 0 \tag{31}$$

Equation (31) can be used to express the condition cumulative distribution function for $Y = X - u$ of the variate X over the threshold value u, given $X > u$ and u is sufficiently large. The cases where $c > 0$, $c = 0$ and $c < 0$ correspond to a Type II (Frechet) distribution, a Type I (Gumbel) distribution and a Type III (reverse Weibull) distribution. The reverse Weibull distribution has a limited upper tail.

The reverse Weibull distribution is a three parameter distribution, given as:

$$F(x) = \exp\left(-\left[\frac{(\mu_{\text{W}} - x)}{\sigma_{\text{W}}}\right]^{\gamma}\right), \quad x \le \mu_{\text{W}} \tag{32}$$

The parameter σ_w is obtained from:

$$\sigma_w = \frac{s(X)}{\left[\Gamma\left(1+\frac{2}{\gamma}\right)-\Gamma^2\left(1+\frac{1}{\gamma}\right)\right]^{1/2}} \tag{33}$$

and

$$\mu_w = E(X)+\sigma_w\Gamma\left(1+\frac{1}{\gamma}\right) \tag{34}$$

The tail length parameter γ is related to the parameter c in the GPD through:

$$\gamma = \frac{1}{c} \tag{35}$$

The return period (reciprocal of the annual exceedance probability) R is obtained from the GPD using:

$$P(Y<y)=1-\frac{1}{\lambda R} \tag{36}$$

where λ is the average annual number of exceedances of the threshold wind speed u in a year.

Combining Eqs (35) and (36) yields:

$$1-\left(1+\frac{cy}{a}\right)^{\frac{1}{c}} =1-\frac{1}{\lambda R} \tag{37}$$

Equation (37) can be rearranged to yield:

$$y =-a\,\frac{1-(\lambda a)^c}{c} \tag{38}$$

The value being sought is:

$$x_R = y+u \tag{39}$$

where x_R is the R year return period wind speed.

As suggested in Ref. [148], the parameter c can be obtained using the de Haan estimation method.

Estimates of the parameters a and c are computed using:

$$c = M_n^{(1)} + 1 - \frac{1}{2\left\{1 - \dfrac{\left[M_n^{(1)}\right]^2}{M_n^{(2)}}\right\}}$$ (40)

$$a = \frac{u M_n^{(1)}}{\rho_1}, \quad \rho_1 = 1, \quad c \geq 0; \quad \rho_1 = 1(1-c), \quad c \leq 0$$ (41)

The quantities $M_n^{(r)}$ are obtained from:

$$M_n^{(r)} = \frac{1}{k} \sum_{i=0}^{k} \left[\log\left(X_{n-i}, n\right) - \log\left(X_{n-k,n}\right) \right]^r$$ (42)

where

k is the number of values above the threshold u;
n is the total number of wind speeds;

and the variate X is sorted such that $X(n)$ is the largest value.

The standard deviation of c is estimated from:

$$\mathrm{SD}(c) = \sqrt{\frac{1+c^2}{k}}, \quad c \geq 0$$ (43a)

$$\mathrm{SD}(c) = \sqrt{(1-c)^2(1-2c)\frac{4 - \dfrac{8(1-2c)}{(1-3c)} + \dfrac{(5-11c)(1-2c)}{(1-3c)(1-4c)}}{k}}, \quad c < 0$$ (43b)

Using the de Haan method selection of the appropriate value of u, and hence c, is somewhat subjective. Reference [150] presents a plot of c versus the number of threshold exceedances. The plot fluctuates significantly when the number of exceedances is small. If the number of exceedances is too large, then the values may not be associated with the tails of the distribution. As de Haan

states in Ref. [150], "It looks from the graph as if the value $c = 0$ is not a bad choice in this case."

Figure 28 presents plots of c versus the number of points above the indicated threshold value, given in m/s [148].

Figure 29 presents the point estimates of the 100, 1000 and 100 000 return period wind speeds at the same six example sites presented in Fig. 28. The return period wind speeds are plotted versus the number of exceedances and wind speed threshold values, as in Fig. 28. As may be readily seen in Fig. 28, the estimates of the N year return period wind speed vary significantly with the threshold wind speed, and judgement is required to choose the appropriate wind speed values.

Reference [148] discusses the example of Denver, for which the authors conservatively choose $c = -0.2$ (see Fig. 28(e)) and suggest that c could be lower. From the data in Fig. 29, it is suggested that Denver's 50 year return period wind speed, x_r, is about 26.8 m/s (60 mile/h, as indicated on the ordinate of Fig. 29(e)). The average number of events per year, λ, is 9.2 y^{-1}. Using Eqs (38) and (39),
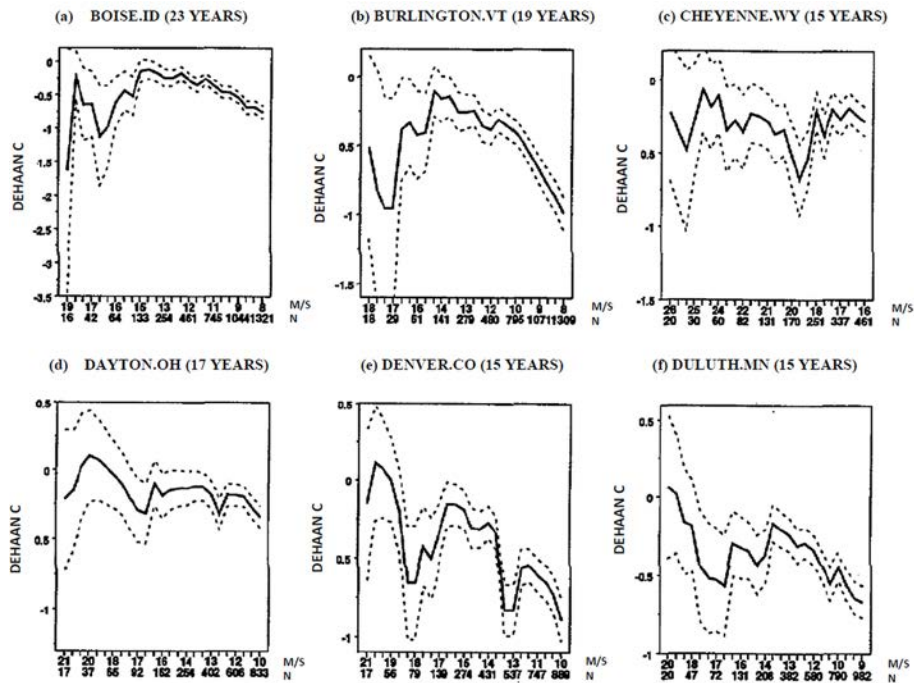
FIG. 28. *Typical plots of estimates of the parameter c and the 95th percentile confidence bounds versus threshold wind speed (m/s) and number of exceedances, N (reproduced from Ref. [148] with permission from ASCE).*
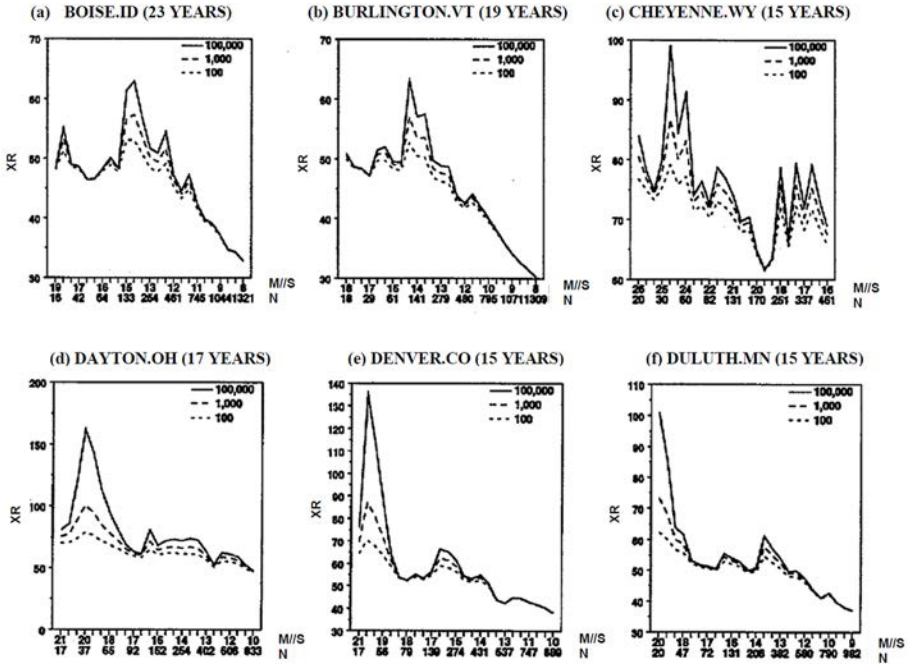
FIG. 29. Typical plots of point estimates of 100 year, 1000 year and 100 000 year wind speeds (given in mile/h) versus threshold (m/s) and number of exceedances, N (reproduced from Ref. [148] with permission from ASCE).

a was estimated to be 2.5 m/s. The estimated maximum possible wind speed at Denver, assuming $c = -0.2$, is computed as $x_{max} = u - a/c = 29.1$ m/s. The wind speeds given in Ref. [148] are fastest mile values that have effective averaging times of about 60 s. The exact value of the averaging time varies with wind speed and is equal to 3600 divided by the wind speed in mile/h. Thus, in the Denver example, the implied maximum peak gust wind speed is about $(1.25) \times 29.1 = 36.4$ m/s (81 mile/h). This value is much lower than the 90 mile/h wind speed given in the 1995–2010 editions of ASCE 7 [5].

Naess in Ref. [151] reanalysed the Simiu and Heckert wind speed data in Ref. [148] and found that by using the square of the wind speed instead of the wind speed, the transformed values were better modelled using an unbounded Type I distribution rather than a bounded distribution.

In Ref. [149], Holmes and Moriarty present an alternative method for estimating the parameters of the GPD. Reference [148] shows the mean value of:

$$Y - u|Y\rangle u = a - \left[c\left(u - u_0\right) / \left(1 + c\right) \right] \qquad (44)$$

where u_0 is the threshold wind speed.

It was noted in Ref. [149] that if the GPD is appropriate, then when the mean values of the excess over u are plotted against $u - u_0$, the points will follow a straight line with a slope of $-c/(1 + c)$ and an intercept, $a/(1 + c)$. Figure 30 presents an example for thunderstorm winds obtained from Charlotte Douglas International Airport in North Carolina, USA, developed using a threshold, u_0, of 10 m/s. The value of c obtained from the slope is 0.0928, and a is 4.014 m/s. Figure 31 presents the resulting hazard curve derived using the GPD with the above mentioned parameters and an annual occurrence rate of 23.92 thunderstorms per year.

The limiting wind speed inherent in the reverse Weibull is very sensitive to the value of c, which is a function of the threshold wind speed used in the measurement, as discussed in Ref. [152]. The results of a peak over threshold analysis when coupled with a tail limited probability distribution can lead to an underestimate of low annual frequency wind speeds, and consequently there is a possibility of underestimating extreme winds. Furthermore, when using the
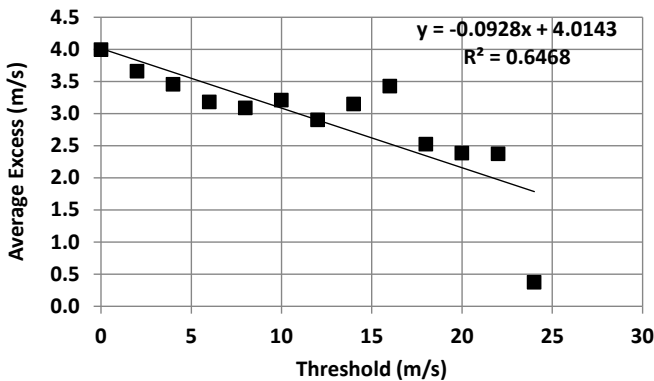
FIG. 30. Mean exceedance thunderstorm wind gusts. Plot shows data from Charlotte Douglas International Airport, North Carolina, USA.
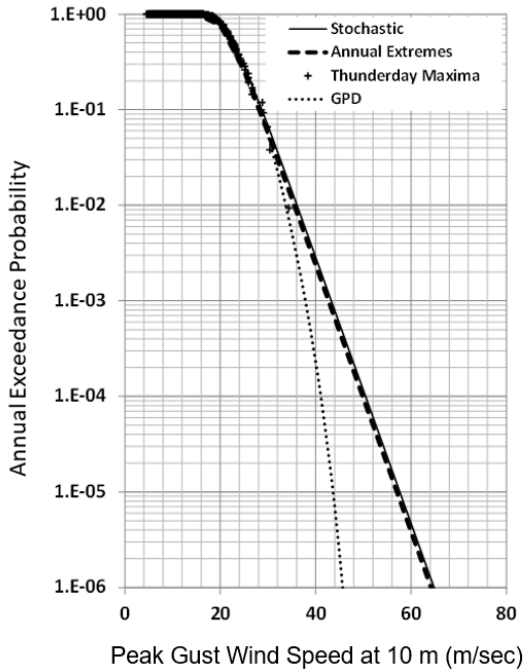
FIG. 31. *Comparison of estimates of thunderstorm wind speed versus annual exceedance probability using the Type I distribution and the bounded GPD.*

GPD, which requires the estimation of three parameters, more data are required to achieve a comparable degree of uncertainty compared with a distribution requiring only two parameters.

6. WIND-BORNE DEBRIS

6.1. GENERAL CONSIDERATIONS

High winds associated with any meteorological event may transform debris into wind-borne projectiles. High wind events, such as those associated with tropical cyclones and tornadoes, produce the most destructive, high velocity debris, but debris can be transported in any high wind event. Because of the

vertical lofting aspect of the mean wind that is not present in other windstorms, tornado winds intensify the debris issue even further.

Research into types, trajectories, speeds and other features of hurricane and tornado induced wind-borne debris has largely been handled separately and independently, with hurricane debris being the focus of more recent research. Studies on damage caused by hurricane debris began in the early 1970s, initiated by the significant debris damage brought about by Hurricane Celia in Corpus Christi, Texas, USA. In the case of tornado induced wind-borne debris, the initial research in the USA was funded by the Electric Power Institute, the US Department of Energy and the Atomic Energy Commission. The initial tornado missile models focused on debris types that were representative of those used in nuclear power plant design, including circular cylinders, pipes, rectangular parallelepipeds and shapes representative of cars and trucks. In the USA, the Tornado Missile (TORMIS) computer code methodology is currently the most readily accepted approach by the US Nuclear Regulatory Commission for performing probabilistic tornado missile risk studies. The TORMIS methodology is discussed in Refs [153, 154]. The methodology has been developed for US nuclear power plants, but the approach is valid anywhere.

Extreme winds generate aerodynamic forces that can propel objects and create missiles that can damage structures and components. The resulting impact loads are one of the three main loading effects of intense winds. Examples of wind-borne projectiles include roof gravel; building materials such as plywood panels, wood beams, steel plates, cladding and structural steel; cars; storage tanks; items of equipment; and tree branches and stems. Heavy compact missiles with low area to weight ratios usually roll or tumble along the ground. Missiles that are lighter in weight and have a higher area to weight ratio can be lifted and travel longer distances. The majority of the time, missile effects are associated with tornadoes; however, any sufficiently high wind speed (e.g. hurricanes, thunderstorms) will generate wind-borne projectiles. Window glass is also vulnerable to damage from lightweight debris (often gravel blown from a nearby building), and extensive research has been carried out on the subject. The following subsections focus on tornado missile risk analysis for nuclear power plants. Reference [89] provides a simulation of maximum missile velocities.

6.2. DETERMINISTIC AND PROBABILISTIC METHODS

Two basic approaches are used in the study of tornado missiles. The conventional deterministic approach considers a range of missile types and maximum velocities when designing structures. Maximum missile speeds for each missile class are determined using a tornado wind field model and a missile

trajectory model. A design spectrum is created with the aim of encapsulating the missile impact effects from a wide range of missiles in a conservative manner. This method is used in Simiu and Cordes [155], the US Nuclear Regulatory Commission standard configuration missile spectra [156] and the US Department of Energy specified missile approach [157]. Simplified three degrees of freedom (3-DOF) trajectory models and an average drag coefficient were used in all of these studies. The second method relies on a probabilistic analysis that covers a much wider range of possible missiles. For each structure or component, the likelihood of missile impact and damage is estimated. These findings may be specifically applied to probabilistic safety assessments. Several methodologies have been established in the USA to assess tornado missile risk for nuclear power plants [127, 128, 158–160].

To predict the characteristic velocities of missiles, both deterministic and probabilistic methods for evaluating missile impact include tornado wind field and trajectory models. Penetration, perforation and spall equations are often used to assess impact effects. A total dynamic response analysis may be needed for certain types of missiles. The following subsections discuss the most important aspects of wind-borne projectile analysis, with a focus on probabilistic approaches.

6.2.1. Tornado wind fields

With tangential, radial, vertical and translational velocity elements, tornado wind fields are 3-D. The radial inflow and vertical velocity components can be significant inside the tornado core. Tornado wind field theoretical models have been developed in a number of ways [161, 162]. However, simpler engineering models are typically used in tornado wind, missile and APC loading analyses. References [116, 155, 163, 164], as well as a model of probabilistic parameters described in Refs [127, 128], have been the most commonly used sources of information in risk assessments for nuclear power plants.

References [128, 164] provide a comparison of the tangential, radial and vertical wind field component velocity profiles for two of these models. This comparison highlights some of the fundamental characteristics of tornado wind fields, as well as the inconsistencies among models. The presence of an inner core (with no radial or vertical wind component) that extends to a radius of 90 m (300 feet) for the design basis tornado is a distinguishing feature of the Fujita tornado wind field model. For the tangential velocity field, both models show modified Rankine vortex flow. The vertical profiles of total wind speed in these and other models are steep, with more than 90% of peak winds occurring within 15 m (5 feet) above ground level. The horizontal winds just above ground level are about 65–80% of the horizontal winds at 10 m (33 feet).

Reference [128] provides details of a sensitivity study of tornado wind field model parameters in terms of tornado missile transport sensitivity, and describes the following main findings:

(a) For a given overall tornado wind speed, low translational velocity results in more missile injections and higher missile velocities.

(b) An increase in the radial inflow component relative to the tangential component increases the number of missiles injected and contributes to higher average values of maximum missile velocities, ranges and heights for a given tornado severity.

(c) Missiles injected and transported by large core tornadoes have higher maximum velocities but lower peak heights than missiles injected and transported by smaller cores. The radius of the core determines the total number of missiles made.

(d) Except for missiles injected at greater heights above ground, the slope of the core (increasing R_{max} with height) has no discernible impact on missile transport.

The study found that if the translational velocity, radial inflow parameters and core radius are all the same, missile transport predictions are not largely dependent on the tornado wind field model.

6.2.2. Hurricane wind fields as applied to wind-borne debris

The trajectories of wind-borne debris in hurricanes have received increased attention over the past 20 years because of the significant damage that the debris causes to buildings. The research has concentrated on debris from damaged residential buildings. Typical debris includes roof sheathing, roof tiles, roof shingles, roof framing and some ancillary items from a residential environment. Since the debris flight times are relatively short — a few seconds — the hurricane winds are often modelled as uniform [165], or reflecting the variation in height only [166]. Using the TORMIS trajectory models (described in the next subsection), the variation in wind speed and direction, as well as the vertical and longitudinal components of the turbulence, were modelled in their hurricane debris simulations as described in Ref. [154].

6.2.3. Trajectory models

The trajectory analysis requires a number of initial conditions, including missile mass, geometry, initial velocity and inertial orientation. The transport methodology is made up of aerodynamic models of missile shapes, governing

dynamic and kinematic interactions, and a solution scheme for the equations of motion, all of which are based on these initial conditions. The motion time history of the missile is obtained by integrating these equations, which allows for the prediction of free flight motion, maximum velocity and impact conditions. Although the following examples focus primarily on tornado wind-borne debris, the discussion on trajectory models can be applied to any storm type as long as the temporal and spatial variation of wind speed is properly modelled.

Various basic transportation models can be used to assess missile hazard. The form of motion that trajectory models represent is the most common distinction. Two degrees of freedom (2-DOF) describes particle motion in a plane; three degrees of freedom (3-DOF) describes particle motion in space; and six degrees of freedom (6-DOF) describes the translational and rotational motion of a rigid body in space. Another distinguishing characteristic is the number of aerodynamic force elements, including moments, that are taken into account.

The 2-DOF model for a mass subjected to gravity and aerodynamic drag forces is the most basic model. The resulting coupled ordinary differential equations are numerically combined to estimate the time history of debris motion. This trajectory model can be used only for straight winds and was used in the development of NUREG/CR-7004 [166]. Analysis of the hurricane wind field did not include the effect of turbulence, but it included the variation of the mean wind speed with height. A study of trajectories of spheres in strong winds described in Ref. [167] concluded that the introduction of turbulence increased the variability of flight trajectories, but the mean trajectory was similar to that determined when turbulence was ignored; thus, ignoring turbulence underestimates the extreme impact statistics.

A 3-DOF model predicts the general motion of a particle mass in space. The lift coefficient, which is often defined to account for random tumbling of the material, is also a force parameter. The 6-DOF models simulate the aerodynamics of rigid bodies that the simpler 2-DOF and 3-DOF models cannot adequately handle. The random orientation 6-DOF model takes into account drag, rise and side forces when simulating missile tumbling by periodic reorientation [168]. It has better prediction capabilities than particle models, with only a minor reduction in simulation performance. Traditional 6-DOF models [169, 170] use a system of six coupled, ordinary, non-linear differential equations to track missile translation and rotation. Aerodynamic force and moment coefficients need to be estimated for all body orientations in such models.

Deterministic 3-DOF particle models [155, 171], random orientation 6-DOF models [127, 128] and deterministic 6-DOF models [172] have all been used in the study of wind-borne missiles. Reference [168] discusses the drawbacks of 3-DOF models for predicting the motion of missiles with high aspect ratios

(e.g. beams, pipes, sticks, poles). In Refs [170, 172], the findings of wind tunnel testing of missile types used in nuclear power plant safety studies are presented.

The modelling of the trajectories of plate type debris is discussed in Refs [173, 174] and includes the impact of the Magnus effect (rotation) on the plate trajectories. The authors found that by including the Magnus effect, the agreement between the modelled and experimental trajectories was improved. It was also noted that the non-dimensional Tachikawa number [175, 176] is a key parameter for determining the trajectories of wind-borne debris of all types.

6.2.4. Characteristic tornado missile velocity statistics

Reference [128] describes a series of calculations using the random orientation 6-DOF trajectory model and a probabilistic tornado wind field model to establish statistics for maximum winds; missiles were released to the moving wind field at the time of maximum aerodynamic force [89]. To optimize the impact velocities used in a tornado missile probabilistic safety assessment, missiles are conservatively released at the time of maximum aerodynamic force. In total, 1000 trajectory analyses for each projectile, injection height and wind speed combination were used to calculate maximum velocity statistics. Reference [89] provides plots of the maximum missile velocity at any point during its flight against the maximum tornado wind field velocity. For the 30 cm (1 foot) pipe projectile, the 90th and 99th percentiles are shown. The findings also show that the maximum missile speed is highly influenced by the type of missile and the injection height. Reference [128] contains tables of comprehensive statistics.

As a percentage of the total horizontal tornado velocity, design velocities for wooden missiles are generally about 75% of the horizontal wind velocity. For steel pipe missiles, the maximum missile velocity is about 40-60% of the horizontal wind velocity. For 'automobile' missiles, the maximum missile velocity is about 18-20% of the horizontal wind velocity.

6.3. MISSILE IMPACT EFFECTS

Missile impact effects include local response effects (i.e. penetration, perforation and spall) and overall response effects (e.g. dynamic shear effects at the edge supports of the impacted wall). Local response effects are estimated by semi-empirical formulas that take into account the missile type and target materials. Overall response effects are analysed through dynamic response analysis that considers deformation of the missile and the impact force time history. The velocity and orientation of the missile are important input parameters to determine missile impact effects. In deterministic analyses, the missile impact

is assumed to have a velocity vector normal to the target surface and the missile axis to be collinear with the velocity vector. In probabilistic analyses, the velocity vector and missile obliquity are treated as random variables.

Although a wide range of literature on impact mechanics is available, few tests on wind-borne debris impact (blunt shapes and low velocities) have been conducted. Utility posts, wooden beams, steel pipes, steel rods and other projectiles have all been tested for penetration [177–181]. Reference [89] provides penetration equations for concrete and steel structures when hit by a wind-borne missile. References [182] and [183] both provide methods for dealing with complex overall response.

6.4. ATMOSPHERIC PRESSURE CHANGE LOADS

The difference in the atmospheric pressure field when a vortex passes over a system results in APC loadings. Only tornadoes, with their combination of relatively high translational storm speed (generally greater than around 13 m/s) and maximum pressure drop in the centre of a rapidly spinning vortex, have atmospheric pressure shift loads of practical engineering significance. The APC creates outward acting stresses across all of the system's surfaces for a perfectly sealed structure. A model of the tornado wind field and knowledge of the rate at which the structure can vent are needed for estimating APC loads. Since most buildings are not completely airtight, the actual pressures produced by APC can be much lower, and for structures with traditional venting features, they are often negligible.

6.4.1. Sealed buildings

The cyclostrophic equation [184] is used to develop the APC distribution:

$$\frac{dp_a}{dr} = \rho\left(V_\theta^2 / r\right) \tag{45}$$

where

dp_a/dr is the atmospheric pressure gradient at radius r from the centre of the tornado vortex;

ρ is the air density;

and V_θ is the tangential windspeed.

The pressure drop p_a is obtained by integrating Eq. (45) from infinity to r. The maximum value of p_a occurs at $r = 0$, whereas the maximum windspeed occurs at $r = R_{max}$. At R_{max}, the APC is approximately one half of its maximum value.

A commonly used expression for the maximum value of p_a is $(p_a)^{max} = \rho V_\theta^2$. Although a limiting value of APC is taken to be about 0.2 atm (20.27 kPa) [185], most tornadoes will produce a maximum APC of less than 3.5 kPa (~0.5 psi). A 90 m/s tornado produces a maximum value of p_a of about 6 kPa [107]. In a facility risk assessment, exceedance probabilities for APC may be developed from the tornado hazard curve and the tornado wind field model, using the relationships given above.

The rate at which the pressure change (dp_a/dt) occurs depends on the translation speed (V_T) of the tornado and can be estimated by:

$$\frac{dp_a}{dt} = \rho V_\theta^2 \left(V_T / R_{max} \right) \tag{46}$$

Equation (46) can be used to develop the exceedance probabilities for dp_a/dt from the tornado wind hazard curve and wind field model parameters. Maximum deterministic design basis values are given in Refs [108, 126, 157].

6.4.2. Vented buildings

The APC loading listed in Section 6.4.1 is only applicable for sealed structures built to sustain a pressure differential under extreme wind loads, such as nuclear power plant containment structures. Most other buildings will vent as a result of the building envelope being breached by wind or missile impact or as a result of the building's natural ventilation and leakage routes. Furthermore, the slower the tornado's translation speed, the more time there is for internal and external stresses to equalize. The APC loadings will apply to the affected building surfaces if the tornado core does not fully engulf the structure.

Only a few studies have been conducted on tornado venting and the amount of venting needed to prevent APC loading. Reference [186] reports of a preliminary investigation of the mechanical ventilation system of nuclear fuel cycle facilities. In Ref. [185], 0.09 m^2 (1 foot^2) of venting per 28 m^3 (1000 feet^3) of interior volume was estimated to be sufficient for effectively venting buildings from extreme tornado APC loads. Heating, ventilation and air-conditioning systems, exhaust fans, doors and cladding leakage all contribute to this amount of venting in most commercial structures. This requirement was introduced as an interim guideline for US Department of Energy facilities in Ref. [157]. To evaluate uncertainties and measure APC loadings for vented structures, no probabilistic simulations were used.

6.5. MISSILE SURVEYS

The characteristics of a site for a nuclear power plant are determined during the site evaluation stage in accordance with IAEA safety standards, and all details of the buildings and structures are available when construction has been completed. For a high wind probabilistic risk assessment, or HWPRA, to support a tornado missile risk, a site survey of the area around the plant and of the plant buildings is conducted to identify all types of missiles. This subsection discusses the procedures for conducting a site survey and a walkdown of a nuclear power plant.

During a missile survey, information on the numbers of missiles (by type), size, location, position and height is used as the basis for the TORMIS analysis. The standard characteristics include each of the seven original missiles identified by the US Nuclear Regulatory Commission [187], and each of the three updated missiles can be specified as a member of this missile spectrum by proper specification of the aerodynamic set and subset, depth dimension d, weight per unit length w and minimum cross-sectional area A_{min}. The complete set of missile aerodynamic sets and subsets is shown in Fig. 32 [127]. Reference [188] provides an overview of an approach for conducting a walkdown of a nuclear power plant and a missile survey.

6.5.1. Plant missile survey procedure

Surveys to identify potential missiles are conducted in the nuclear power plant, usually at a distance of up to 760 m (2500 ft) from fragile structures, systems and components to properly design them.

(a) Using sketches and aerial photographs of the plant, missile source zones are determined.
(b) Typically, 20–50 missile source zones are created. For each zone:
    (i) The infrastructure (e.g. houses, car parks) is recorded;
    (ii) The minimum and maximum missile injection heights are constant;
    (iii) Changes in zones are used to accommodate changes in plant grade.
(c) Once the missile source zones have been determined, walkdown notebooks are prepared to facilitate the missile survey portion of the walkdown. Notebooks contain:
    (i) A copy of the overall layout of the zones, clearly showing zone boundaries;
    (ii) For each missile zone:
        — A drawing of the zone based on plans and/or aerial photographs for note-taking regarding actual in-field conditions;
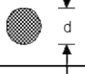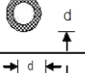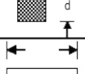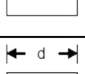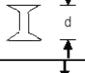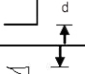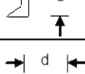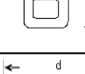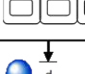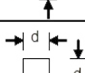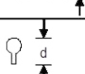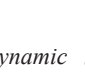
Basic Aerodynamic Shape Set	Basic Missile Sets				Subset on d (in.)
	General Description	Cross-Section b/d Variation	Impact Material	Final Set Number	a
Cylinder	Rod		Steel	1	<1
			Wood	2	<13
	Pipe		Steel	3	<3
			Concrete	4	>0
Rectangle	Box, Beam		Steel	5	<24
			Wood	6	<6
		b=d/4	Steel	7	<4
			Concrete	8	>0
			Wood	9	<12
	Plate	b=d/10	Steel	10	<24
			Wood	11	>0
		b=d/50	Steel	12	<36
			Wood	13	<48
I-Shape	Wide Flange		Steel	14	<6
Angle	Angle		Steel	15	>0
Channel	Channel		Steel	16	<8
			Concrete	17	>0
Frame, Truss	Pipe Frame		Steel	18	>0
	Rect. Frame		Steel	19	>0
	Rect. Frame		Wood	20	>0
	Pipe Frame		Steel	21	<54
	Rect. Frame	d/10	Steel	22	<48
	Rect. Frame		Wood	23	>0
Sphere	Sphere		Steel	24	>0
Vehicle	Auto, Trailer		Steel	25	>0
Tree	Tree		Wood	26	>0

FIG. 32. *Basic missile aerodynamic set and subset description (reproduced from Ref. [127] with permission from Electric Power Research Institute).*

  — A zone missile survey sheet for documenting the number of missiles and minimum and maximum injection heights for all missiles by missile type.

(iii) An ample supply of missile source building survey sheets for documenting structures that are not designed to be tornado resistant:

  — Building missile survey sheets are used to document the number of missiles and minimum and maximum injection heights for all missiles by missile type;

  — Building missile survey sheets also include a place to summarize the building characteristics (including dimensions), allowing for an estimation of missiles that may result from the failure of the building in a windstorm.

(d) The dimensions of buildings are estimated in the field and recorded with the building characteristics on the building survey sheets:

(i) If known, the exact dimensions of a building from building plans are recorded instead of in-field estimates and a note is included in this regard;

(ii) The length and width of the building can be estimated by pacing;

(iii) The height of the building can be estimated based on the number of equivalent door heights or using a similar process based on height relative to an object of known height. The number of floors is also recorded.

(e) Photographs are taken of missiles and buildings surveyed:

(i) Photograph numbers are recorded on the corresponding survey sheets (missile, building, zone or drawing) so that the photograph number can later be matched to a zone or building and vice versa;

(ii) Sufficient photographs of missiles inside each zone are taken to provide an overview of the types and quantities of missiles present in each zone;

(iii) Sufficient photographs of missiles inside missile source structures are taken to provide an overview of the types and quantities of missiles present in each missile source structure;

(iv) Sufficient photographs of each missile source structure are taken to complement the building characteristics recorded on the building survey sheets.

(f) Surveys of non-concrete frame buildings are recorded on building survey sheets but are not included on zone survey sheets, as debris from failed buildings is modelled separately from debris located in the open:

(i) The overall dimensions of the building (length, width, height) are recorded and photographs of exteriors are taken;

(ii) The location of the building is shown on the corresponding zone sketch if not shown on a drawing, and the building is given a unique name;

    (iii) The type of building is denoted (i.e. trailer, modular, wooden frame, pre-engineered frame, engineered frame or other);

    (iv) Wall and roof covering details are obtained for each building (e.g. metal siding, metal roof, shingle roof, built up roof);

    (v) Missile surveys inside buildings are required and include counts of content (e.g. office furniture, warehouse storage materials).

(g) For equipment:

    (i) If the equipment is bolted to a concrete or steel frame and is unlikely to fail in a tornado, it does not have to be counted;

    (ii) Lightweight items of equipment not bolted to a concrete or steel frame are potential missiles.

(h) For trees:

    (i) Trees with a diameter of 12 cm or greater at chest height are potential missiles and are counted as such;

    (ii) Single trees and small groups of trees will be counted as individual trees;

    (iii) For larger wooded areas within 360 m of targets, tree quantities are to be estimated as follows:

        — All trees within a predefined area are counted (generally 30 m by 30 m);

        — The total number of trees is estimated based on the tree density information gathered and the total wooded area determined from aerial photographs of the nuclear power plant and surrounding area. General characteristics of the trees (e.g. typical height, type) are recorded.

(i) For minimum and maximum missile injection heights:

    (i) The height above the base elevation of the zone or missile source system in which the centre of mass of the missiles is stored needs to be recorded;

    (ii) The minimum injection height is defined as the approximate centre of mass of the lowest missile of each type within the missile source zone or building;

    (iii) The maximum injection height is defined as the approximate centre of mass of the highest missile of each type within the missile source zone or building.

    The basic TORMIS approach, including the walkdown of the nuclear power plant, is valid in all areas in which tornadoes occur, although the model was developed for application to nuclear power plants in the USA. Furthermore, the methodology can be applied to any wind hazard, as the equations of motion for wind-borne debris are valid in any flow field.

7. GENERAL CONSIDERATIONS ON EXTERNAL FLOODING HAZARDS (EXCLUDING TSUNAMIS)

7.1. GENERAL CONSIDERATIONS

Flooding hazards result from a large set of phenomena, mainly of a natural origin but sometimes related to human activity. These phenomena may cause floods alone or in combination. High river discharges are commonly due to precipitation and snow melt on the upstream basin. Such discharges and the associated flood levels are in many cases limited by dams and dikes that have been built to control flooding. River floods may also result from dam failures not related to river discharges in the dam reservoir (e.g. failures of the Malpasset Dam, France, in 1959, or of the Teton Dam, Idaho, USA, in 1976, in which geotechnical issues played a role).

The phenomena to be considered depend first on the site environment. The list of phenomena or combinations of phenomena to be considered with respect to external flooding hazards that follows is based on SSG-18 [1] and excludes tsunamis:

(a) Wind induced coastal flooding (including storm surges and wind waves as far as coastal areas are concerned);
(b) Wind generated waves on rivers;
(c) Seiches;
(d) Extreme precipitation and runoff events;
(e) Flooding due to the sudden release of impounded water;
(f) Bores and mechanically induced waves;
(g) Tides;
(h) High groundwater levels.

Flooding can be caused by 'internal' or 'external' factors. Different methods and standards are used by Member States to describe the boundary between internal and external flooding hazards. Although there is no specific distinction between the two forms of flooding hazard, SSG-18 [1] provides the following definition:

"External events are events unconnected with the operation of a facility or the conduct of an activity that could have an effect on the safety of the facility or activity. The concept of 'external to the installation' is intended to include more than the external zone[1], since in addition to the area immediately

surrounding the site area, the site area itself may contain features that pose a hazard to the installation, such as a water reservoir.

"[1] The external zone is the area immediately surrounding a proposed site area in which population distribution and density, and land and water uses, are considered with regard to their effects on the possible implementation of emergency measures. This is the area that would be the emergency zone if the facility were in place."

This publication supports this definition and is primarily concerned with 'external' flooding risks. However internal and external flooding hazards are distinguished, the main concern in the safety assessment is to identify all potential causes of flooding, both internal and external, and to ensure that there is no gap between the two.

For the flood hazard assessment of nuclear power plants, deterministic methods have mostly been used, with statistical extrapolations being used in certain Member States. More recently, probabilistic methods have also gained acceptance for determining design basis events, which are not intended to determine the worst case scenario as a basis for design, but to state the level of risk that a chosen design would face. For the assessment of design basis floods (DBFs), the US Nuclear Regulatory Commission uses the deterministic approach but also considers probabilistic methods for flood hazard assessment and outlines the components of a formal PFHA approach [189].

Methods used to characterize hazard scenarios may be deterministic, statistical or probabilistic. These approaches are described in SSG-18 [1] as follows:

"2.22. Deterministic methods are based on the use of physical or empirical models to characterize the impact of an event in a specific scenario on a system. For a given single input value or a set of input values, including initial conditions and boundary conditions, the model will typically generate a single value or a set of values to describe the final state of the system. In this case, there is no explicit account of any annual frequency of exceedance. Appropriate extreme or conservative values of the input parameters are usually used to account for uncertainties or to provide conservative estimates."

....

"2.24. When a statistical analysis is performed, it is typically based on time series[6] analysis and synthesis. It is assumed that the series represents both deterministic components and an unknown number of random components, and that the random components are reasonably independent. By using

these methods, gaps and missing data and outliers of the available data set should be adequately taken into account."

…….

"2.27. Probabilistic hazard assessment makes use of the probabilistic descriptions of all involved phenomena to determine the frequency of exceedance of any parameter, such as tsunami wave height. It explicitly accounts for aleatory uncertainties and epistemic uncertainties."

"[6] A time series in this context is a chronological tabulation of values of a given variable measured continuously or at stated time intervals."

The remainder of this publication focuses on flooding hazards of various kinds. It presents a number of methods that are currently used in some Member States for the determination of DBF for nuclear installations, as well as a number of elements on possible developments for PFHA. It will be noted that for some Member States, DBF is associated with a frequency of exceedance in the range of 10^{-4}/a. In contrast, hazard curves for probabilistic safety assessment will cover a frequency of exceedance as low as 10^{-7}/a.

Sections 8–11 of this publication discuss the following flooding hazards:

(a) Wind induced coastal flooding;
(b) Wind generated waves on rivers;
(c) Extreme precipitation and runoff events;
(d) Floods due to the sudden release of impounded water.

Seiches, bores and mechanically induced waves and high groundwater levels are not presented in detail. The available assessment methodologies for these phenomena are so specific that general insights and possible developments for probabilistic hazard assessment are more difficult to draw. Examples of methodologies developed for DBF definition and characterization can be found in Guide No. 13, Protection of Basic Nuclear Installations Against External Flooding, issued by Autorité de Sûreté Nucléaire (ASN) [190]. Tsunami hazard assessment is also not included in this publication, as it is addressed in Ref. [191].

7.2. BASIS FOR FLOOD HAZARD ASSESSMENT

The first stage of the flood hazard assessment is to identify any water sources that could cause or contribute to flooding at the site in question, such as the following [190]:

(a) Precipitation;
(b) Groundwater;
(c) Seas and oceans;
(d) Watercourses (e.g. streams, rivers, canals);
(e) Natural reservoirs (e.g. lakes, glaciers);
(f) Artificial reservoirs (e.g. dams, tanks, water towers, pipes).

The second stage is to identify, for each of the water sources identified, any events or combinations of events that could cause damage to the installation [190].

A particular event can be characterized by the following features:

(a) Its intensity, which corresponds to physical parameters such as water volume, water height and discharge flow rate;
(b) If applicable, the frequency of exceedance of that intensity;
(c) Its duration.

For example, the 1000 year return period river flood is an event for which the discharge flow rate has a frequency of exceedance equal to 10^{-3}/a.

Flooding can be caused either by a single event or by the combination of several events (e.g. events occurring at the same time or in succession, failure of a protective structure).

The third stage is to define a set of flood scenarios based on possible, or postulated, events or combinations of events. At this stage, the scenarios are characterized by their intensity (e.g. volume, height, rate of flow, duration) and, where appropriate, by the accompanying frequency of exceedance. From a design perspective, these scenarios are used to derive the parameters of the DBF.

For estimating design bases, a traditional and commonly used deterministic method focuses on the idea of a 'probable maximum event'. The most extreme, reasonably possible occurrence at the place of interest is the probable maximum event, which is calculated by accounting for the postulated physical limits of the natural phenomenon. For example, a probable maximum flood (PMF) is the hypothetical flood that is considered to be the most extreme and reasonably possible, on the basis of a probable maximum precipitation (PMP) event and comprehensive hydrometeorological application of other factors favourable for maximum flood runoff, such as sequential storms and snow-melt. The probable

maximum storm surge is generated by either the probable maximum hurricane or the probable maximum windstorm. This approach is not presented in detail here as it is documented in many publications, in particular Refs [192, 193].

The extreme event is not correlated with any annual frequency of exceedance, as its upper limits cannot be surpassed, which is a limitation of this method. Furthermore, the degree of conservatism in the outcome appears to be variable. For example, in certain parts of the USA, far from the warm ocean moisture source, it was observed that PMP and PMF estimates are likely to have a very low frequency of exceedance, about 1×10^{-7}/a or lower [194]. In coastal regions closer to the warm ocean moisture source, the PMP, and thus PMF, frequency of exceedance estimates may be much higher, possibly between 1×10^{-3}/a and 1×10^{-5}/a. This is illustrated in a study of PMP in the Carolinas region of the USA [195], where PMP ratios to 10^{-3} annual exceedance probability 24 h rainfall were 2–6 times higher. It was also estimated that the PMP 24 h (26 km^2, 10 mile^2) annual exceedance probability ranged from 10^{-5} to $<10^{-7}$. Such observations exhibit the limitations of 'probable maximum' methods in the framework of risk informed approaches.

Statistical methods are, in most cases, included in a deterministic framework for DBF characterization. The reasons for taking such a mixed approach are, on the one hand, the limitations of physics and, on the other hand, limitations related to 'reasonable' extrapolation by statistical means. The physical limits can be illustrated by river flood characterization. The primary parameter of interest for design is flood level. Flood level results from flood discharge and the topography or roughness of the valley. Flood discharge may be approximated as an aleatory process that a statistical model is able to describe. However, the topography or roughness of the valley for a given site is unique to the site and needs to be described considering local physical parameters. Thus, river DBF is usually derived from a two step process:

(1) Flood discharge definition using statistical extrapolation or other approaches;
(2) Flood runoff using numerical models to account for local specific parameters.

How to set 'reasonable' limits to extrapolation by statistical means is a controversial topic. A practice in the hydrology community is to set such a limit on the duration of available data multiplied by a factor less than or equal to ten. Some ten years of observed data are then considered sufficient to derive a 10^{-2}/a extrapolated value. To derive a 10^{-3}/a extrapolated value, the available data need to cover more than a century. Sections 8–11 present examples of such deterministic and statistical methods, which differ from phenomenon to phenomenon because of different physics and available knowledge and data. Statistical methods are currently used in some Member States to characterize DBF for storm surge, wind

wave, precipitation, river discharge and groundwater levels. For details on the statistical methods used to derive extreme conditions, useful references include Ref. [196] for general approaches, Ref. [197] for regional approaches, and Ref. [198] for joint probability approaches. One Member State has developed Renext, an access free statistical tool based on the works of Coles [196] and programmed in the statistical programming language R[7].

Data necessary for flood hazard evaluation are presented in detail in SSG-18 [1]. Instrumental records of past events are the primary basis for flood hazard evaluation. However, records generally cover less than 100 years and provide only sparse information about extremely large floods. It is therefore necessary to expand the available series of records, to include historical data (data reported prior to the existence of the observation stations) and palaeoflood data (from geological surveys). In these approaches, attention needs to be paid to the stationarity of the data, in particular for palaeoflood data. Another efficient approach is to use data at a regional scale to expand the available information. Methods based on additional kinds of data and improved statistical tools are available for some flooding phenomena and under development for others, as described in the following sections.

Bathymetry and topography require special attention when defining the reference level (datum). The use of several reference levels needs to be avoided as far as possible. When elevation values are given, each used datum needs to be clearly defined, and if this is not possible, relationships among datums should be clearly fixed. In addition, reference levels need to be precisely defined, available and consistent over time.

7.3. UNCERTAINTIES IN FLOOD HAZARD ASSESSMENT

Classification of uncertainties varies according to different technical domains. Based on the practice for probabilistic seismic hazard assessment, a broad classification identifies 'aleatory' and 'epistemic' uncertainties (as is the case with any hazard modelling). According to para. 2.6 of IAEA Safety Standards Series No. SSG-9 (Rev. 1), Seismic Hazards in Site Evaluation for Nuclear Installations [199] (footnote and reference omitted),

"... Basically, two types of uncertainty are identified for practical application in seismic hazard assessment: (i) the aleatory variability of the seismic process, which is inherent in phenomena that occur in a random manner and as such cannot be reduced, even by collecting more data, and (ii) the

---

[7]   See http://cran.r-project.org/web/packages/renext

epistemic uncertainty, which is attributable to incomplete knowledge about a phenomenon (therefore affecting the ability to model it) and which can be reduced through the acquisition of additional data (including site specific data), further research and interaction between experts considering the diversity of their professional judgement."

Thus, epistemic uncertainties are related to any lack of knowledge arising because current scientific understanding is imperfect, but they are of a character that in principle is reducible through further research and the gathering of more and better data. Aleatory uncertainties, on the other hand, are uncertainties that for all practical purposes cannot be known in detail or cannot be reduced.

More specific to the hydrological domain, Ref. [190] addresses the uncertainties as follows:

"The uncertainties can be grouped into different types:

1) to assess the probabilities of exceedance associated with the rare events:
   a) the uncertainties in the statistical analysis input data;
   b) the uncertainties relating to the choice of statistical model;
   c) the uncertainties relating to the size of the statistical sample available;
   d) the uncertainties relating to representativeness of that sample.
2) to assess the hydraulic values of parameters relative to the rare events considered for the design of the installations:
   e) the uncertainties relating to lack of knowledge…;
   f) the uncertainties relating to the variability of the possible initial states…"

Input data are of primary importance for the study. Climatological and hydrological data are commonly recorded by national organizations based on gauge measurements at observation stations. Historical data and palaeoflood data reported prior to the existence of the observation stations are useful to expand input information and then to reduce uncertainties. Data from the region of interest are also useful to expand input information. The larger set of input data needs to be used in the study, as far as these data are reliable and representative for the site.

Expert appraisal is the current practice used to estimate uncertainties. Experts' choices need to be justified either by existing scientific consensus in the area considered or by sensitivity analysis concerning certain hypotheses to characterize the variability.

7.4. HAZARD ASSESSMENT AND PROTECTION MEASURES FOR FLOODS

Protection against flooding encompasses both hazard assessment and the definition of protection measures. In this subsection, the following are discussed:

(a) Flood effects and specificities;
(b) Protection principles;
(c) Material protection measures;
(d) Organizational protection measures.

7.4.1. Flood effects and specificities

During a flood event, the action of the water can be static, dynamic or both. Dynamic effects include, for example, waves, erosion of embankments, sediment deposition, debris jams and floating debris that can also affect the availability of certain equipment (e.g. through fouling and blockage of water intakes).

The parameters of a flood are currently expressed in terms of the following:

(a) Water level;
(b) Wave height and associated run-up;
(c) Event duration;
(d) Static and dynamic pressures (including hydrostatic uplifting forces);
(e) Additional loads due to debris.

Flooding can affect several installations at a site, if not all of them. It can also impact several lines of defence at the same time. Flooding may also influence the site's climate, leading to isolation and the loss of support functions (e.g. off-site electrical power supplies, telecommunications, off-site emergency resources, discharge facilities). Additionally, flooding may also be accompanied by extreme weather, such as strong winds and lightning. Floods may, however, be predicted in certain cases by putting in place alert systems and defining preventive safety steps, depending on the causal phenomena.

7.4.2. Protection principles

For each flooding scenario considered, measures of protection are to be put in place to preserve the safety functions that could be affected, taking into consideration the effects and specificities presented above.

Material and organizational protection measures can provide several lines of defence on different scales, including the following:

(a) The site as a whole;

(b) The buildings containing protection elements important to safety in flood scenarios;

(c) The rooms containing protection elements important to safety within these buildings;

(d) The systems or components within these rooms.

The use of several independent lines of defence, with priority given to permanent measures (that require neither human intervention nor energy supplies) is generally preferred.

7.4.3. Material protection measures

Protection of the site against flooding can be based on protective structures external to the site (e.g. dikes, drainage systems, dams, the operation of which can be modified in the event of a flood). Specific justifications need to be elaborated with the operator(s) of these structures if they are not under the full control of the licensee.

Setting the installation platform at a level above the maximum water level for all relevant flood scenarios (e.g. extreme local precipitation is not a relevant scenario) is a robust measure. The layout of the site and in particular of the platform (e.g. in terms of slopes, retention systems, water drainage systems, road development) can prevent water from flowing towards the buildings that are to be protected.

A gravity drainage system makes it much easier to handle the possible loss of off-site electrical power supplies. To prevent the ingress of water, it is good practice to place thresholds at building access points. The anticipated settlements are to be taken into account and periodically checked in situ.

The drainage system of rainfall runoff from roofs can be designed considering the potential for water ingress into buildings in the event of a system overflow, particularly through the location of water downpipes and overflows.

Particular attention can be paid, both at the design stage and during operation, to all openings (e.g. galleries, shafts, pipes, spaces between buildings) that could allow water ingress into buildings. One approach is to use a 'watertight volume', in which a volume is rendered watertight by closing off the openings in the outer walls of this volume to prevent the entry of water into rooms housing protection elements important to safety. The design of the sealing material takes into account the hydraulic pressure associated with the potential presence of water outside the watertight volume.

Passive interventions that do not require human interaction or energy sources are preferred (since off-site electrical power supplies to the site could be

lost). At sites relying on human interaction or energy sources, it is important to consider the difficulty of predicting flooding events and their kinetics. A warning system is needed when provisions for the protection of installations require human intervention, to ensure that sufficient advance warning is provided to allow the implementation of all necessary protection measures. The monitoring system associated with the warning system can also be used for situation tracking.

The loss of support functions as a result of flooding at the site and in the site region (e.g. loss of electrical supply, unavailability of cooling water, site isolation), or correlated phenomena (e.g. lightning and wind for flooding initiated by storms), is considered at the design phase of the protection measures. The conceivable duration of loss of a support function is taken into account, as well as the availability and reliability of equipment involved in maintaining safety functions in such situations.

Data acquisition continues during the operation of the installation in order to consolidate the characteristics of the various flood scenarios and identify changes resulting from climatic changes or modifications of the site environment. In the case of a significant flooding event near the site, this continuous monitoring is supplemented by the collection and analysis of data specific to the event (e.g. hydrograph, flooded zones, observed levels, debris jams). This information is used to enhance knowledge of the site and improve future studies, by helping, for example, to improve the calibration of a model.

7.4.4. Organizational protection measures

A monitoring and maintenance policy for all passive and active material protection measures needs to be defined and implemented. Organizational measures, such as provisioning of means, periodic verification of availability, alert procedures and training, are formalized and implemented to ensure the correct performance of these actions at the planned times. To ensure the effective implementation of the warning and situation monitoring systems, the monitored quantities and the associated benchmark values need to be defined.

Organizational measures such as emergency plans also need to be defined for the mitigation of the consequences of situations (e.g. water detection in the installation). The potential for site isolation (i.e. cut off from outside) needs to be prevented by measures that aim to guarantee the presence of required personnel and material resources as well as the permanence of the communication means necessary to manage the emergency. Ensuring that conditions will allow for vehicle and personnel movement at the site is essential for the implementation of these procedures.

7.5. BACKGROUND ELEMENTS FOR PROBABILISTIC FLOOD HAZARD ASSESSMENT

Probabilistic hazard assessment makes use of the probabilistic descriptions of all involved phenomena to determine the frequency of exceedance of any parameter of interest for design and assessment. This approach has been developed and is currently applied in many Member States to assess seismic hazards. To introduce their guide to probabilistic seismic hazard analysis (PSHA), Baker et al. [200] state:

"With PSHA … we will consider all possible earthquake events and resulting ground motions, along with their associated probabilities of occurrence, in order to find the level of ground motion intensity exceeded with some tolerably low rate. At its most basic level, PSHA is composed of five steps.

1. Identify all earthquake sources capable of producing damaging ground motions.
2. Characterize the distribution of earthquake magnitudes (the rates at which earthquakes of various magnitudes are expected to occur).
3. Characterize the distribution of source-to-site distances associated with potential earthquakes.
4. Predict the resulting distribution of ground motion intensity as a function of earthquake magnitude, distance, etc.
5. Combine uncertainties in earthquake size, location and ground motion intensity, using a calculation known as the total probability theorem.

"The end result of these calculations will be a full distribution of levels of ground shaking intensity, and their associated rates of exceedance."

Moreover, the use of expert judgement has been studied extensively in the PSHA field, and a structured process known as the Senior Seismic Hazard Analysis Committee process has been developed and has been applied in some Member States.

An examination of the possible transposition of these approaches to flooding hazards appears particularly useful, considering the various sources and involved phenomena for flooding and the weight of uncertainties in hazard assessment.

One of the key issues for such a transposition is the capability to define 'hazard curves' that cover a frequency of exceedance as low as 10^{-7}/a, when current practices to define DBF frequency of exceedance are limited to an order of magnitude of 10^{-4}/a. This challenge is illustrated in Fig. 33.
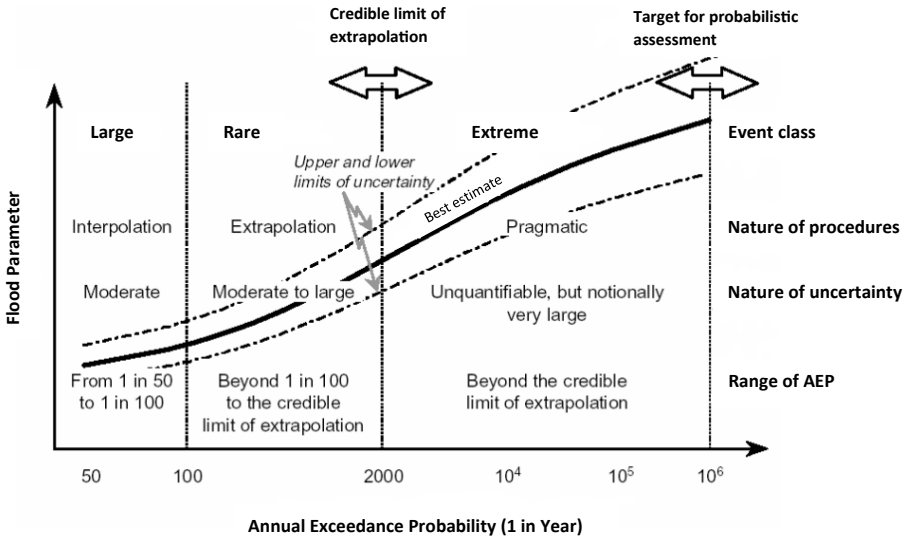
FIG. 33. *Hazard curve — potential and limits for rare and extreme event characterization considering annual exceedance probability (AEP).*

Because of differences in the state of the art and the methods applied for the flooding hazards considered here, separate discussions are necessary. The following sections present elements of a probabilistic hazard assessment specific to each flooding hazard, based on ongoing developments that aim to expand the domain of frequency of exceedance.

8. WIND INDUCED COASTAL FLOODING

8.1. GENERAL CONSIDERATIONS

Storms occurring over seas or oceans cause a rise in the sea level (storm surge) and wind waves. The potential of these phenomena to cause flooding in a coastal area generally depends on the sea level due to tide. Wind induced coastal flooding results from the combination of tide level (astronomical and seasonal), and storm surges and waves (owing to storms) and their associated effects (e.g. wave set-up, run-up).

Storm surges are caused by moving atmospheric pressure deficits and by the wind stress accompanying moving storm systems. Wind waves are caused by the friction of wind across a water body.

Wind induced coastal flooding can also occur on the coast of a large lake or an estuary. The effects of a storm on such a water body can be the same as for a sea or ocean. The reference water level to consider in studies of flooding can depend on phenomena other than the tide (e.g. river discharge, control by dams).

8.2. DATA SOURCES

National organizations estimate the theoretical tide using a set of measurements taken at tidal gauges, available in harbours. Correction may be required for a site located far from the reference harbour to account for the difference in theoretical tides between the site and the reference harbour.

Long series of measurements at tidal gauges are also necessary to compute a series of observed storm surges (set-up). In the described approach, the set-up is considered equivalent to a storm surge; other existing approaches also include wind wave effects in the definition of a storm surge. Set-up is, by definition, equal to the difference between the observed sea level and the predicted tide level at a given time. For simplification reasons, and also to obtain further relevant data regarding the high water level, set-up is often defined as the difference between the highest observed sea level and the highest predicted tide level at a given tide cycle (see Fig. 34) [201].

Series of measurements of waves can be obtained using wave buoys or from satellite derived data. Usually, such series cover a period that is too short to perform statistical extrapolation to a frequency of exceedance lower than 10^{-2}/a. A current practice is therefore to supplement the wave measurements using meteorological series to derive wave characteristics from wind data (see Sections 3 and 5).

Meteorological data can also be used to derive storm surge. These data are related to storm characterization (see Sections 3 and 5).
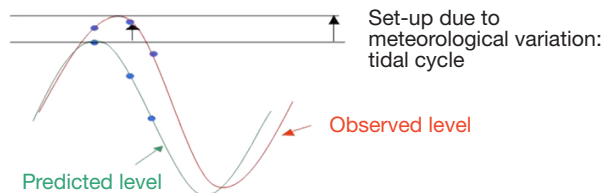

FIG. 34. Definition of set-up (adapted from Ref. [201] with permission from the authors).

8.3. DETERMINISTIC ASSESSMENT (USING STATISTICAL ANALYSIS)

8.3.1. Scenario definition

The following scenarios are described in Ref. [190] and are based on engineering judgement and a probabilistic objective (i.e. frequency of exceedance of 10^{-4}/a, in order of magnitude and covering associated uncertainties).
The reference high sea water level is the sum of the following:

(a) The maximum height of the theoretical tide;
(b) The 1000 year storm surge (upper limit of the 70% confidence interval), increased to take account of uncertainties associated with the evaluation of rare storm surges and resulting from outliers;
(c) The change in mean sea water level extrapolated until the next periodic safety review.

As an alternative to the first two points above, two statistical analyses may be carried out addressing (i) tide levels and (ii) storm surges. By combining the two phenomena (joint probability method), the probability of exceedance of the water level can be worked out, considering a 10 000 year return period.
Wave conditions at a coastal site depend on ocean waves and waves generated by the local wind. The reference waves are characterized from the 100 year return period significant height[8] wave conditions (upper limit of the 70% confidence interval) determined offshore of the site and propagated over the reference high sea level. The duration of this scenario is determined from the variations in sea level caused by the tide.

8.3.2. Guidance for scenario characterization

8.3.2.1. Reference high sea water level

The series of observations used for sea level analysis is selected taking account of duration (i.e. as long as possible), the reliability of the values (particularly for the highest instantaneous sea water levels) and how representative they are of the site. The existence of any bias linked to changes in the sea water level needs to be investigated in order to apply any necessary corrections [190].

---

[8]   In a field of waves, the wave heights (between the peaks and troughs) vary. The significant height is the average of the wave heights whose heights lie in the upper third of the population of wave heights.

The values of historical storm surges are inventoried and taken into account in the statistical analysis. In many cases, the traditional approach that considers measured storm surges at a unique reference station does not allow sufficient account for exceptional events (outliers) observed at several monitoring stations. An additional increase in reference sea level of 1 m is applied to allow for this.

A different approach for calculating the 1000 year storm surge, such as one based on a regional analysis, may be used provided that the statistical extrapolation model is shown to be appropriate and right for the outliers observed at different monitoring stations. In this case, no extra increase needs to be applied.

Regional frequency analyses were carried out for the surges along the French coast of the Atlantic Ocean and the Channel [201, 202]. These analyses aim to cope with the outlier issue in surge series. This methodology is not the current approach used to estimate extreme surges. First results showed that the extreme events identified as outliers during these analyses do not appear to be outliers in the regional empirical distribution (see Fig. 35). Indeed, the regional distribution presents a curve to the top with these extreme events that extrapolation distribution seems to recreate. This regional approach has the benefit of allowing more observations than the commonly used local approach. Thus, the regional approach appears to be more reliable for some sites than at-site analyses.

The change in mean sea water level can be extrapolated on the basis of Intergovernmental Panel on Climate Change reports, supplemented by regional studies to address regional trends and by statistical analysis of local observations to take account of observed trends. This could be used for extrapolation to evaluate extreme parameters in the short term. Figure 36 provides an example of observed trends at Brest, the longest series of sea level data for France.
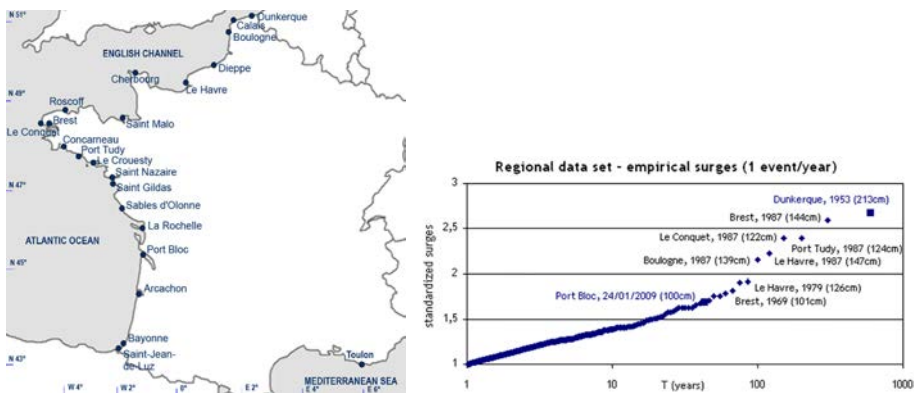

FIG. 35. Locations of sites studied in Ref. [201] and empirical distribution of the surges of the corresponding regional data set (reproduced from Ref. [201] with permission from the authors).
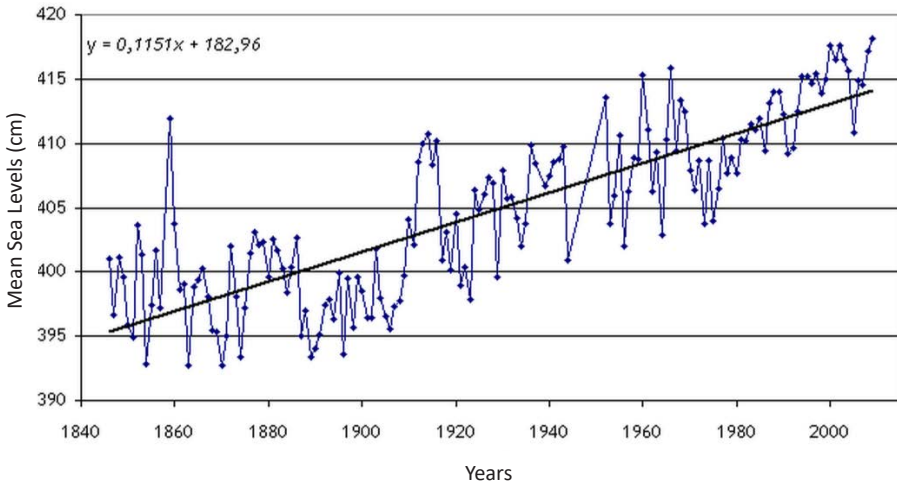
FIG. 36. Evolution of observed annual mean sea levels (cm) at Brest, France (1846–2009) (adapted from Ref. [201] with permission from the authors).

8.3.2.2. *Wind waves*

In the first step of the study, the 'offshore' reference ocean waves are defined at a distance from the coast sufficient to avoid any influence from the effects of physical processes occurring in shallow water, such as shoaling or the breaking of waves.

In the second step of the study, offshore waves are propagated to the site (considering specific site features such as harbour basins or water intake or outlet channels) by means of modelling (numerical and physical). Wave propagation is simulated for stationary conditions and considers constant unfavourable boundary conditions.

One or more unfavourable offshore wave directions are used to determine the risk of overspill over the various structures protecting the site (e.g. protective dikes, structures inside channels).

Where the waves are sufficiently steep that the conditions in which they break are reached or exceeded, the waves are defined by the waves with characteristics at the limit of the wave breaking.

The assessment of the stability of protective structures requires the definition of dynamic loads due to waves, including duration. When the waves cause the overtopping of protective structures, the overtopping water volume is

estimated. A large set of methods is provided in Ref. [203]. The effect of local wind on the overtopping water volumes is also taken into account.

8.4. ELEMENTS OF PROBABILISTIC ASSESSMENT

As indicated in Ref. [204],

"The [US Army Corps of Engineers] has developed a probabilistic–deterministic methodology for storm surge hazard assessment… The methodology utilizes an integrative, interdisciplinary approach that incorporates state-of-the-art knowledge in hurricane science, hydrology, and probabilistic methods. This methodology involves the following steps:

(1)   Selection of a stochastic set of simulated storm tracks affecting the region of interest.
(2)   Hydrodynamic simulation of the region of interest using a high-resolution surge model and the simulated storm tracks to generate time histories of wind speeds and corresponding time histories of storm surge heights at sites within the affected region.
(3)   Use of wind speed and storm surge height information generated in Steps (1) and (2) to develop probabilistic information on the joint probability of wind speed and storm surge height events [205]."[9]

A key issue for the development of such an approach is the capacity to run a large number of simulations with a high resolution surge model.

9. WIND GENERATED WAVES ON RIVERS

9.1. GENERAL CONSIDERATIONS

Wind blowing over rivers may raise wind waves if the length of action of the wind (fetch) is sufficient. This length could be significantly increased during river flood conditions. Generally, wind waves have a potential for flooding a river

---

[9]   The reference number has been updated to align with the reference list in this publication.

site only during a river flood event that increases the water level and expands the water covered area.

9.2. DATA SOURCES

Series of measurements of waves on rivers are rarely available and cannot be a reliable basis for extreme wave characterization. The current practice is to use meteorological series to derive wave characteristics from wind data (see Sections 3 and 5).

9.3. HAZARD ASSESSMENT

As an example of deterministic assessment (using statistical analysis), the following scenario is defined in ASN Guide No. 13 [190]. The field of waves generated by a 100 year return period wind (upper limit of the 70% confidence interval) propagated over a 1000 year return period river flood is referred to as the reference local wind waves (upper limit of the 70% confidence interval). It is characterized by a large wave height, a representative period and a dominant propagation direction. The duration of the scenario is extracted from data on the durations of major wind events.

According to Ref. [190], the wind speed is an average wind speed over 10 min, measured at a height of 10 m. In a deterministic framework, wind speeds are usually considered irrespective of their direction, and the reference wind is not associated with a prevailing direction. Local parameters that can significantly influence the wind flow at the site are site topography and surface roughness.

Generation and propagation of local wind waves is first based on the characterization of the zones in which local wind waves can develop. These characteristics are determined considering the geometry of the body of water around the site, taking in all the areas displaying a sufficient length (fetch) for significant local wind waves to be generated. The reference wind speed is the input to derive local wind waves on each fetch, generally using empirical methods. Wave propagation to the site can be derived using empirical methods such as those outlined in Ref. [206], where bathymetric conditions are simple, or using numerical methods.

The action of the current on the propagation of local wind waves is considered, as it can increase or decrease the local wind waves. If the steepness of the waves is such that the conditions of wave breaking are reached or exceeded, the reference local wind waves are defined by the local wind waves whose characteristics are at the limit of breaking.

Overtopping of dikes or other protective structures may result from wind waves. The overtopping water volumes are estimated for each fetch, taking wind direction into account.

9.4. ELEMENTS OF PROBABILISTIC ASSESSMENT

As wind waves generally have the potential for flooding a river site only during a river flood event, wind waves are usually considered in combination with river flooding. It is therefore a prerequisite to be able to define river flood conditions in a probabilistic framework (elements of this topic are presented in Section 10.4). On this basis, it could be possible to derive wind wave characteristics from wind conditions. However, it would be necessary to estimate the probability of joint occurrence of flood and other potential events.

10. EXTREME PRECIPITATION AND RUNOFF EVENTS

10.1. GENERAL CONSIDERATIONS

The most common flood hazard, irrespective of the site location, is runoff from precipitation. To assess this risk, a variety of methods have been developed. They vary primarily in terms of the scale of the drainage basin under consideration. Small drainage basins are the domain of methods focused primarily on precipitation characterization, whereas broad drainage basin studies benefit from discharge observations. Precipitation falling on the site and in upstream drainage basins necessitates various flood mitigation measures (typically, a site grading design to monitor the flow path and drainage system for local precipitation, and site elevation to prevent flooding caused by precipitation in rivers or nearby drainage basins), as well as different hazard criteria for the designs.

10.2. DATA SOURCES

National meteorological organizations that collect long historical series of measurements currently hold precipitation data. Some of these organizations also provide assessments of extreme precipitation, which can be useful for nuclear power plants. Comprehensive information on WMO defined meteorological data and guidance is offered in SSG-18 [1].

Operators typically make assumptions about discharge measurements based on their particular needs (e.g. hydroelectrical production, navigation, flood risk assessment or forecast). It is important to note that discharge calculation entails some uncertainty in determining a relationship between water depth and discharge, and that extra care is required.

Topography, roughness in the flood plain, 'water loss' by infiltration and vegetal interception, groundwater flow and hydraulic controlling structures are the most important data needed for the description and modelling of drainage basins. These data are currently available from national organizations and hydroelectric plant operators, but they are incomplete and need to be supplemented with precise surveys (e.g. of the local detailed topography). Furthermore, roughness and penetration parameters are derived from estimates (hydraulic model calibration) or expert judgement, rather than direct measurements. These parameters are then calculated based on the study's objectives.

10.3. HAZARD ASSESSMENT

As examples of deterministic assessment (using statistical analysis), scenarios for local rainfall, flooding in a small drainage basin and flooding in a large drainage basin are defined in Ref. [190] and discussed below.

10.3.1. Local rainfall

10.3.1.1. Characterizing the reference rainfall events

A rainfall event is traditionally described by the cumulative amount of precipitation that falls within a given period of time. The upper limit of the 95% confidence interval for 100 year rainfall events calculated from data from a representative station is used to describe the reference rainfall events in Ref. [190].

The reference rainfall events are defined for all durations necessary for the development of one or more conservative rainfall scenarios for the areas of the site with equipment or premises that require protection. The Montana formula[10] is an

---

[10] The Montana formula links the average intensity i, the duration t and the exceedance frequency F of a rainfall event of duration t, as a function of two parameters a and b that depend on the exceedance frequency F considered:

$$i(t,F) = a(F)t^{b(F)}$$

This model is to be used with caution, because a particular pair of parameters a and b does not give a satisfactory fit if the range of rainfall event durations is too great.

acceptable method for determining the intensity of the reference rainfall events. The biases due to the use of 'non-centred' rainfall data are corrected. The validity of the 100 year reference rainfall value is substantiated notably by examining the values measured in stations in the region other than the reference station, or by comparison with the values calculated using a regionalized approach.

10.3.1.2. Quantification of runoff flow rates

The runoff flow rates are quantified by a rainfall runoff transformation method. Reference [190] recommends performing detailed digital modelling of the local drainage basins for this purpose. The rainfall events are modelled by design rainfall events (typically, Keiffer or double triangle rainfall patterns are considered appropriate) and are associated with one or more periods of intense rainfall, in order to obtain worst case rainfall event scenarios for those areas of the site with equipment or premises that require protection. The infiltration losses are accounted for by considering the behaviour of the soils during extreme rainfall events.

Other methods, such as the rational method, can, however, be used in certain simple cases. Only three parameters are used to define rainfall and drainage basins in this system: (i) the uniform rate of rainfall intensity, (ii) the drainage area, and (iii) the runoff coefficient.

10.3.1.3. Study of the behaviour of the water drainage system

According to Ref. [190], the model of the installation's water drainage system needs to be preferably integrated into a model of the site water drainage system to account for interactions among the different components of the site system.

The friction coefficients used for the system are representative of the wear and state of maintenance of the pipes. As a general rule, the unfavourable nature of the drainage system behaviour model is justified by setting the model parameters to increase the overflows, or — when possible — by calibration using measured flow rates.

The study of the behaviour of the water drainage system considers the continuous flow rate discharged into the system in normal operation. When the design of the water drainage system requires the definition of a water level at the outlet, this level is defined considering possible dependencies between local rainfall events and the high water level at the outlet.

On completion of the site development work, an on-site verification is carried out to validate the hypotheses used in the study of the behaviour of the water drainage system. This verification can be supported by as-built drawings,

topographical surveys, and runoff and drainage tests corresponding to normal rainfall situations.

The installation can cope with a surface water runoff scenario when its local water drainage system is fully blocked, taking into account first the potential for obstruction of the water drainage system during severe events, and second the potential for events rarer than those described in the reference rainfall events. The one hour return time rainfall event (value of the upper limit of the 95% confidence interval) is used to describe this reference surface water runoff scenario [190].

Additional studies for the drainage basins upstream of the installation are carried out using a similar method.

10.3.2. Flooding in a small drainage basin

The reference small drainage basin flooding is defined by an instantaneous peak flow rate for a 10 000 year return period in Ref. [190].

10.3.2.1. Determining the reference flood events

The reference small drainage basin flooding is preferably assessed using a method that models the asymptotic behaviour of the mean rainfall runoff transformation for a time step suitable for the drainage basin's concentration time, such as the semi-continuous rainfall runoff simulation for extreme flood estimation (SCHADEX) method for drainage basins with a surface area of 10–5000 km^2. The reference instantaneous peak flow rate is calculated as follows:

(a) Extrapolating from a sample of daily flow rates.
(b) Multiplying the resulting flow rate by a shape factor. The shape factor is the average of the ratios of the peak flood flow rate to the mean daily flow rate for a selection of measured floods.

The reference flow rate for drainage basins with a surface area of 10–100 km^2 can be calculated by multiplying the resulting flow by a factor of two based on 100 year rainfall events (upper limit of the 95% confidence interval).

10.3.2.2. Quantification of runoff flow rate

Runoff modelling takes into account the behaviour of the soil during extreme rainfall events. When the flow rate at the site is determined by the watercourse's downstream condition (at the drainage basin outlet), the downstream condition

is determined by considering the probability of concurrent flooding of the watercourse and an unfavourable water level at the drainage basin outlet.

The points at which debris jams that could aggravate the effects of the reference flood on the site might occur are considered.

If determining the water level from the reference flow rate requires the use of a local flood propagation model, the recommendations relative to flood propagation on a large drainage basin apply (see the next subsection).

10.3.3. Flooding in a large drainage basin

A drainage basin is considered to be large if it covers an area greater than around 5000 km^2 [190]. A large drainage basin flooding is characterized by a reference flow rate, a reference water level and the associated flood plain.

The reference flow rate corresponds to the peak flow rate associated with the 1000 year return period flood, taking the upper limit of the 70% confidence interval and increased by 15%. This approach implies that flow rates have been measured for decades [190]. The reference water level is the maximum level on the site resulting from the reference flow rate or a lower flow rate (e.g. if the water level decreases because of levee failure during the increasing flow rate phase). The behaviour and functioning of installed equipment along engineered watercourses are considered (e.g. head loss due to friction on bridge pillars, operation rules in flood conditions). The proximity of a confluence of watercourses to the site may require that the flood study takes this confluence into account.

10.3.3.1. Processing the flow data

The reference flow rate is quantified from a statistical analysis of the flood flow rates measured at the hydrological station that is representative of the site's conditions [190]. The representativeness of the station for the site can be substantiated by comparing the size of the drainage basins at the station and at the site. Before the statistical analysis, the quality of the flow rate data is reviewed based on information on data acquisition at the station and comparison with data from other stations situated in the vicinity.

In the case of a lack of good quality data for the representative station, it is acceptable to take data from other stations to reconstitute a representative sample of data. Recommendations are provided in Ref. [190] related to checking, and if necessary correcting, the effect on measured flow rates of hydraulic structures such as water retaining structures. If the flow rate sample is significantly heterogeneous, it can be divided into subsamples, subject to justifications.

10.3.3.2. Extrapolation of the flow rates to the extreme flow rates

The choice of the extrapolation law adopted by fitting it to the flow rate sample needs to be justified, in particular by presenting a visual check and a test on the goodness of fit of the chosen law against the empirical distribution in Ref. [190]. The reference peak flow rate can be obtained by (i) extrapolating from a sample of daily flow rates, and (ii) multiplying the resulting flow rate by a shape factor. The shape factor is the average of the ratios of the peak flood flow rate to the mean daily flow rate for a selection of measured floods.

10.3.3.3. Reference water level

The reference water level is a benchmark that can be easily used to characterize a site [190]. It is deduced from the study of the flood plain around the site corresponding to a flood whose maximum flow rate equals the chosen flow rate (i.e. the reference flow rate, or a lower flow rate if it leads to a higher water level). The flood plain is defined considering the following:

(a) Steady flow rate conditions, unless transient flow rate conditions are justified;
(b) An unfavourable value for the identified influencing parameter(s), whose variations have a significant impact on the calculation results (e.g. roughness coefficient or criteria for dike failure).

10.3.3.4. Modelling the flood plain

The flood plain is preferably defined on the basis of a numerical model of the site [190]. The main data required to develop this model include the following:

(a) Topographical and bathymetric information;
(b) Land cover database necessary to determine the roughness coefficients considered for the different plain areas;
(c) The geometrical characteristics of the structures (e.g. bridges, dikes, plants, dams) and the hydraulic laws of the structures through which the flows pass;
(d) Hydraulic information (e.g. flood marks, monitoring station recordings and water level–discharge relation).

The model covers an area that extends laterally to include the entire extent of the extreme flood plain, unless it is proved that the chosen limits are unfavourable for the hazard assessment. The longitudinal extension of the

model is defined in order that both downstream and upstream conditions have a negligible impact on the water levels at the site.

The model grid is refined in the zones of hydraulic interest (e.g. dikes, particular features such as bridges, weirs). Hydraulic laws can also be used to integrate the particular features of the model.

The model is calibrated based on the available data relative to severe floods. When calibration is impossible because of a shortage of data, the values of the parameter(s) of the model that cannot be adjusted, such as the roughness coefficient in the flood plain, can be characterized by expert judgement. If the calculations are carried out for transient flow rate conditions, the model is validated in such conditions.

The flooding characteristics can depend on the behaviour of dikes that could be eroded during the flood. In this case, the behaviour scenario adopted for these structures (i.e. breach or resist) needs to be justified based on its unfavourable nature or by a specific study considering water velocities during extreme flows. In addition, the potential for jams resulting from ice or from an accumulation of debris and, where applicable, their impact on the water levels at the site, is analysed.

10.3.3.5. Specific case of confluences

When a confluence has to be taken into account to evaluate the flood plain around the site, the flow rates are characterized for each of the three branches (i.e. two upstream and one downstream). For the downstream branch, the flow rate Q is the reference flow rate, as defined in Section 10.3.3.2. The flow rate adopted for the upstream branches is the distribution of the worst case flow rates, without exceeding the reference flow rate in each branch, and ensuring that the sum of the two flow rates equals the downstream flow rate Q.

When the extreme flood leads to a significant overflow in the confluence zone, the calculation of the water levels around the site is preferably based on 2-D modelling.

10.4. ELEMENTS OF PROBABILISTIC ASSESSMENT

Stream flow based statistical approaches and rainfall based statistical approaches augmented by runoff modelling are two types of methods that can be used to calculate severe flood conditions caused by precipitation.

Runoff modelling is used in both methods to determine flood parameters for the site. Many sources of uncertainty need to be dealt with in runoff modelling. Furthermore, some of them are dispersed around the globe

(e.g. topography, roughness). Probabilistic flood hazard assessment would need to develop approaches to deal with these uncertainties, such as sensitivity analysis. Sensitivity analysis methods are valuable tools because they allow for the verification of model predictions and the identification of input parameter influences. To propagate uncertainties, the Monte Carlo method is widely used. The effect of parameters on outcome variability can then be ranked using a variety of methods. The entire procedure is known as a global sensitivity analysis [207], and it consists of the following steps (see Fig. 37):

(i)   Determine the hydraulic code input parameters of interest and assign a probability density function to them;
(ii) Propagate uncertainties within the model;
(iii) Establish the impact of input parameter variability on the output of interest variance.

In practice, such a method is of great interest, but it is still in the early stages of use in river flood studies.

Recent developments in 2-D hydraulic modelling applications are presented in Ref. [208]. This paper brings to light the promising possibilities of the approach for the identification of the most influential uncertainty input parameters. It also identifies that efforts are required for the characterization of the spatial variability of input parameters and that the computational resources required to process this type of study are considerable.

Stream flow based statistical approaches could be enforced by the use of historical and palaeoflood information. However, such necessary information
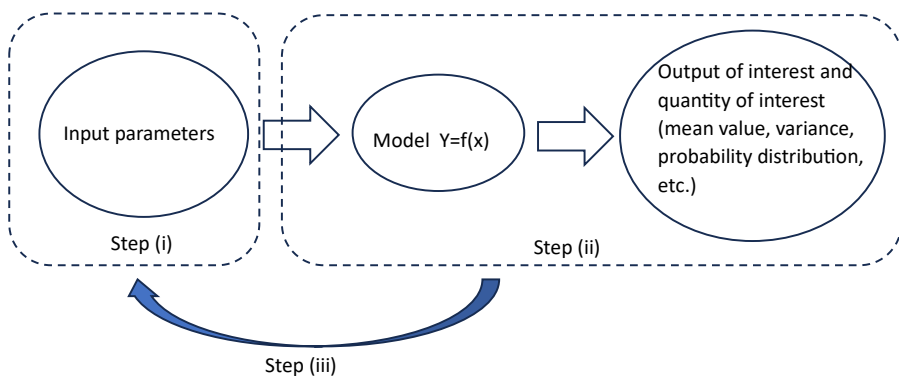

FIG. 37. Global sensitivity analysis approach.

only provides an incomplete view of meteorological, hydrological and hydraulic variability.

Because they take into account meteorological and hydrological simulations of extreme flooding, rainfall based statistical methods seem to be a more suitable way to derive flood hazard curves. Such approaches also provide more opportunities to incorporate regional data. Using rainfall models and hydrological models, methods for stochastically simulating large numbers of floods have been developed. However, as previously noted, these methods are currently restricted to catchment areas of less than 5000 km^2. Dam operators, for example, use SCHADEX [208] and the Stochastic Event Flood Model (SEFM) [209].

A key issue for the development of the PFHA approach is the capacity to run a large number of simulations with a high resolution runoff model.

11. FLOODS DUE TO THE SUDDEN RELEASE OF IMPOUNDED WATER

11.1. GENERAL CONSIDERATIONS

Water may be impounded by human-made structures, such as a dam, a dike or a tank, or by natural causes, such as an ice jam or debris dam that causes an obstruction in a river channel. The failure of such water retaining structures may induce floods in the site area. Failures can occur as a result of hydrological, seismic, geotechnical or other causes.

11.2. DATA SOURCES

The owners and operators of water controlling structures are the primary sources of data regarding structure characteristics and operating conditions.

National organizations and hydroelectric plant operators currently have the data needed to study flood propagation from the structure to the site, but these data are inadequate and need to be supplemented by specialized surveys (e.g. of local detailed topography). In addition, roughness and infiltration parameters are calculated (hydraulic model calibration) or based on expert judgements rather than direct measurements. These parameters then need to be calculated in the light of the objectives of the study.

11.3. HAZARD ASSESSMENT

Hazard assessment in the domain is currently based, as indicated in SSG-18 [1], on an approach that opens two possibilities: either the failure of water retaining structures is postulated under conservative hypotheses, or survival can be demonstrated with the required degree of confidence. As an example of deterministic assessment using the first possibility, Ref. [190] defines the following scenario for dam failure.

11.3.1. Scenario definition

Water retaining systems that lie across watercourses, such as dams, are among the failure scenarios. The most disastrous scenario for the site will be caused by the failure of the water retaining structure in the watercourse. The highest water level on the site as a result of the flood wave's propagation is the reference water level associated with this structure's failure.

The watercourse on which the site is located, as well as the numerous valleys that open up near the site, are taken into account in the flooding scenario analysis. The behaviour and operation of mounted equipment along engineered watercourses are taken into account (e.g. head loss due to friction on bridge pillars, operation rules in flood conditions). For a site near a confluence of watercourses, the flooding scenario analysis may need to account for the impact of the flood wave propagation in each tributary.

11.3.2. Guidance for scenario characterization

11.3.2.1. General

The choice of the structure representing the highest potential hazard needs to be justified by expert opinion, supported wherever necessary by flood calculations for several structures.

The assessment of the flooding scenario can be based on a two step approach: first, calculation of flood wave propagation from the structure to immediately upstream of the site, and second, calculation of the water levels around the site by means of a local model.

The aim of studying the flood wave is to determine the flow characteristics in the area surrounding the site as a function of time (i.e. time for the wave to arrive, speed and flow rate, duration of the flood) and to quantify the flooding scenario (i.e. flood plain and reference level).

11.3.2.2. Hypotheses associated with the failure

Failure of the structure inducing the flood wave is postulated in Ref. [190]; it is assumed that the failure leads to complete emptying of the reservoir. The reservoir is assumed to be filled to the maximum level at the time of failure (the different ways to define this maximum level are detailed in Ref. [190]).

The failure is assumed to occur as instantaneous and total destruction for concrete or masonry structures. For rock or earthfill structures, failure is gradual as a result of progressive erosion development.

11.3.2.3. Propagation of the flood wave

The flood wave propagation study distinguishes two zones in Ref. [190]. Generally, in the upstream zone, the flood wave is propagated on a dry bed; in the downstream zone, it is propagated on the mean interannual flow rate[11] of the watercourse. However, the function of the retaining structure (e.g. a flood retention structure) can make it necessary to use different initial flow rates. The limit between the upstream zone and the downstream zone corresponds to the point at which the level reached by the wave propagated on a dry bottom is equal to the one reached by the 100 year return period flood, or the worst known flood if the latter is higher.

Recommendations related to the hypotheses that are adopted regarding domino effect (cascading) failures and the numerical simulation of the flow (e.g. wave front propagation, torrential flow) are provided in Ref. [190].

11.3.2.4. Reference level

The flood plain around the site is calculated from the flood wave hydrograph obtained after propagation up to the numerical model input point used to represent the site and the surrounding area (local model) [190]. In order to cover uncertainties in the first step of flood wave propagation, the flood wave hydrograph is increased by 15%. Generally, the initial flow rate in the local model is the mean interannual flow rate of the watercourse. However, the function of the retaining structure (e.g. a flood retention structure) can make it necessary to use a higher initial flow rate.

Analyses of the modelling of the flood plain around the site are carried out in accordance with the recommendations presented in Section 10.3.

---

[11] The mean interannual flow rate is the arithmetic mean of the mean annual flow rates calculated over a period of at least 30 consecutive years. The mean annual flow rate is the arithmetic mean of all the flow rates for the year considered.

11.4. ELEMENTS OF PROBABILISTIC ASSESSMENT

Databases on large dam failures have been implemented in several countries and by the International Commission on Large Dams (ICOLD). Bulletin 111 of ICOLD [210] presents a statistical analysis of historical dam failures. On the basis of the ICOLD international database and considering the number of dams and failures, the mean failure rate per year is 10^{-4} per dam. The analysis emphasizes the diversity of failure causes and the significant role of dam age and structural type. For example, Ref. [210] mentions that the largest number of failures is among new dams (failure frequently occurs during the first 10 years after dam construction) and that dams built in 1910–1920 have the largest number of failures in terms of percentage. Thus, it appears that such databases provide information that cannot be directly used to derive failure probability for a specific dam. For a specific dam, probabilistic analysis requires detailed evaluations, including engineering, geotechnical and hydrological aspects.

For dam safety assessment, the approach in many countries is deterministic and aims to demonstrate that the dam will not cause unacceptable situations in the case of the occurrence of a set of scenarios (e.g. considering dam operation conditions, hydrology, earthquakes). Developments towards a more risk informed approach are ongoing.

Probabilistic flood hazard assessment related to the sudden release of impounded water for nuclear installations thus appears related to ongoing developments in the dams and levees domain. Furthermore, flood routing between dam(s) and the nuclear site needs to address specific uncertainties (see Section 10.4).

REFERENCES

[1]   INTERNATIONAL ATOMIC ENERGY AGENCY, WORLD METEOROLOGICAL ORGANIZATION, Meteorological and Hydrological Hazards in Site Evaluation for Nuclear Installations, IAEA Safety Standards Series No. SSG-18, IAEA, Vienna (2011).

[2]   WEINKLE, J., MAUE, R., PIELKE, R., Jr., Historical global tropical cyclone landfalls, J. Clim. **25** (2012) 4729–4735, https://doi.org/10.1175/JCLI-D-11-00719.1

[3]   AMERICAN NATIONAL STANDARDS INSTITUTE, Minimum Design Loads for Buildings and Other Structures, ANSI A58.1, ANSI, New York (1982).

[4]   AMERICAN SOCIETY OF CIVIL ENGINEERS, ASCE 7 Minimum Design Loads for Buildings and Other Structures, ASCE, New York (1990).

[5]   AMERICAN SOCIETY OF CIVIL ENGINEERS, ASCE 7 Minimum Design Loads for Buildings and Other Structures, ASCE, New York (1996).

[6]   CARIBBEAN COMMUNITY SECRETARIAT, Caribbean Uniform Building Code (cubic), Structural Design Requirements. Wind Load, Part 2, Section 2, CARICOM, Georgetown, Guyana (1985).

[7]   STANDARDS AUSTRALIA, Structural Design Actions Part 2: Wind Actions, Australian/New Zealand Standard, AS/NZS 1170.2:2011, Standards Australia, Sydney (2011).

[8]   RUSSELL, L.R., Probability Distribution for Texas Gulf Coast Hurricane Effects of Engineering Interest, PhD Thesis, Stanford Univ. (1968).

[9]   RUSSELL, L.R., Probability distributions for hurricane effects, J. Waterw. Port Coast. Ocean Eng. **97** (1971) 139–154, https://doi.org/10.1061/AWHCAR.0000056

[10]   TRYGGVASON, V.J., DAVENPORT, A.G., SURRY, D., Predicting wind-induced response in hurricane zones, J. Struct. Eng. **102** (1976) 2333–2350, https://doi.org/10.1061/JSDEAG.0004496

[11]   MARKS, F.D., KAPPLER, G., DEMARIA, M., "Development of a tropical cyclone rainfall climatology and persistence (R-CLIPER) model", 25th Conf. on Hurricanes and Tropical Meteorology, American Meteorological Society, San Diego, CA, 2002.

[12]   VICKERY, P.J., LIN, J.X., SKERLJ, P.F., TWISDALE, L.A., Jr., HUANG, K., HAZUS-MH hurricane model methodology, Part I: Hurricane hazard, terrain and wind load modelling, Nat. Hazards Rev. **7** (2006) 82–93, https://doi.org/10.1061/(ASCE)1527-6988(2006)7:2(82)

[13]   LONFAT, M., ROGERS, R., MARCHOK, T., MARKS, F.D., Jr., A parametric model for predicting hurricane rainfall, Mon. Weather Rev. **135** (2007) 3086–3097, https://doi.org/10.1175/MWR3433.1

[14]   LANGOUSIS, A., VENEZIANO, D., Long-term rainfall risk from tropical cyclones in coastal areas, Water Resour. Res. **45** (2009), https://doi.org/10.1029/2008WR007624

[15]   VICKERY, P.J., WADHERA, D., TWISDALE, L.A., Technical Basis for Regulatory Guidance on Design-Basis Hurricane Wind Speeds for Nuclear Power Plants, Rep. NUREG/CR-7005, Nuclear Regulatory Commission, Washington, DC (2011).

[16]   BATTS, M.E., CORDES, M.R., RUSSELL, L.R., SHAVER, J.R., SIMIU, E., Hurricane Wind Speeds in the US, National Bureau of Standards, Rep. No. BSS-124, US Department of Commerce (1980),
https://doi.org/10.6028/NBS.BSS.124

[17]   GEORGIOU, P.N., DAVENPORT, A.G., VICKERY, B.J., Design wind speeds in regions dominated by tropical cyclones, J. Wind Eng. Ind. Aerodyn. **13** 1–3 (1983) 139–152,
https://doi.org/10.1016/0167-6105(83)90136-8

[18]   GEORGIOU, P.N., Design Windspeeds in Tropical Cyclone-Prone Regions, PhD Thesis, Univ. of Western Ontario (1985).

[19]   NEUMANN, C.J., The National Hurricane Centre Risk Analysis Program (HURISK), NOAA Technical Memorandum NWS NHC 38, National Oceanic and Atmospheric Administration (NOAA), Washington, DC (1991).

[20]   VICKERY, P.J., TWISDALE, L.A., Jr., Prediction of hurricane wind speeds in the United States, J. Struct. Eng. **121** (1995) 1691–1699,
https://doi.org/10.1061/(ASCE)0733-9445(1995)121:11(1691)

[21]   VICKERY, P.J., MASTERS, F.J., POWELL, M.D., WADHERA, D., Hurricane hazard modeling: The past, present, and future, J. Wind Eng. Ind. Aerodyn. **97** (2009) 392–405,
https://doi.org/10.1016/j.jweia.2009.05.005

[22]   JARVINEN, B.R., NEUMANN, C.J., DAVIS, M.A.S., A Tropical Cyclone Data Tape for the North Atlantic Basin 1886–1983: Contents, Limitations and Uses, NOAA Technical Memorandum NWS NHC 22, US Department of Commerce, Washington, DC (1984).

[23]   DARLING, R.W.R., Estimating probabilities of hurricane wind speeds using a large-scale empirical model, J. Clim. **4** (1991) 1035–1046,
https://doi.org/10.1175/1520-0442(1991)004<1035:EPOHWS>2.0.CO;2

[24]   EMANUEL, K.A., The maximum intensity of hurricanes, J. Atmos. Sci. **45** (1988) 1143–1155,
https://doi.org/10.1175/1520-0469(1988)045<1143:TMIOH>2.0.CO;2

[25]   VICKERY, P.J., SKERLJ, P.J., STECKLEY, A.C., TWISDALE, L.A., Jr., Hurricane wind field model for use in hurricane simulations, J. Struct. Eng. **126** 10 (2000),
https://doi.org/10.1061/(ASCE)0733-9445(2000)126:10(1203)

[26]   HOLLAND, G.J., An analytic model of the wind and pressure profiles in hurricanes, Mon. Weather Rev. **108** (1980) 1212–1218,
https://doi.org/10.1175/1520-0493(1980)108<1212:AAMOTW>2.0.CO;2

[27]   POWELL, M.D., et al., State of Florida hurricane loss projection model: Atmospheric science component, J. Wind Eng. Ind. Aerodyn. **93** (2005) 651–674,
https://doi.org/10.1016/j.jweia.2005.05.008

112

[28] HALL, T., JEWSON, S., Statistical modelling of North American tropical cyclone tracks, Tellus **59A** (2007) 486–498, https://doi.org/10.1111/j.1600-0870.2007.00240.x

[29] JAMES, M.K., MASON, L.B., Synthetic tropical cyclone database, J. Waterw. Port Coast. Ocean Eng. **131** (2005) 181–192, https://doi.org/10.1061/(ASCE)0733-950X(2005)131:4(181)

[30] ARTHUR, W.C., SCHOFIELD, A., CECHET, R.P., SANABRIA, L.A., "Return period cyclonic wind hazard in the Australian region", 28th Conf. on Hurricanes and Tropical Meteorology, American Meteorological Society, Orlando, FL, 2008.

[31] GRAF, M., NISHIJIMA, K., FABER, M.H., "A probabilistic typhoon model for the northwest Pacific region", Proc. 7th Asia-Pacific Conf. on Wind Engineering (APCWE-VII), Taipei, 2009, IAWE (2009).

[32] YIN, J., WELCH, M.B., YASIRO, H., SHINOHAR, M., "Basin wide typhoon risk modelling and simulation for western north Pacific basin", Proc. 7th Asia-Pacific Conf. on Wind Engineering (APCWE-VII), Taipei, 2009, IAWE (2009).

[33] EMANUEL, K.A., RAVELA, S., VIVANT, E., RISI, C., A statistical deterministic approach to hurricane risk assessment, Bull. Am. Meteorol. Soc. **87** (2006) 299–314, https://doi.org/10.1175/BAMS-87-3-299

[34] LEE, K.H., ROSOWSKY, D.V., Synthetic hurricane wind speed records: development of a database for hazard analyses and risk studies, Nat. Hazard. Rev. **8** (2007) 23–34, https://doi.org/10.1061/(ASCE)1527-6988(2007)8:2(23)

[35] EMANUEL, K.A., DES AUTELS, C., HOLLOWAY, C., KORTY, R., Environmental control of tropical cyclone intensity, J. Atmos. Sci. **61** (2004) 843–858, https://doi.org/10.1175/1520-0469(2004)061<0843:ECOTCI>2.0.CO;2

[36] VICKERY, P.J., SKERLJ, P.F., TWISDALE, L.A., Jr., Simulation of hurricane risk in the US using an empirical track model, J. Struct. Eng. **126** (2000) 10, https://doi.org/10.1061/(ASCE)0733-9445(2000)126:10(1222)

[37] VICKERY, P.J., WADHERA, D., TWISDALE, L.A., Jr., LAVELLE, F.M., U.S. hurricane wind speed risk and uncertainty, J. Struct. Eng. **135** (2009) 301–320, https://doi.org/10.1061/(ASCE)0733-9445(2009)135:3(301)

[38] NIEDORODA, A.W., et al., Analysis of the coastal Mississippi storm surge hazard, Ocean Eng. **37** 1 (2010) 82–90, https://doi.org/10.1016/j.oceaneng.2009.08.019

[39] TORO, G.R., RESIO, D.T., DIVOKY, D., NIEDORODA, A., REED, C., Efficient joint-probability methods for hurricane surge frequency analysis, Ocean Eng. **37** 1 (2010) 125–134, https://doi.org/10.1016/j.oceaneng.2009.09.004

[40] NUCLEAR REGULATORY COMMISSION, Guidance for Performing a Tsunami, Surge, or Seiche Hazard Assessment, Interim Staff Guidance, Rep. JLD-ISG-2012-06, NRC, Washington, DC (2013).

[41] THOMPSON, E.F., CARDONE, V.J., Practical modelling of hurricane surface wind fields, J. Waterw. Port Coast. Ocean Eng. **122** (1996) 195–205, https://doi.org/10.1061/(ASCE)0733-950X(1996)122:4(195)

[42] SCHWERDT, R.W., HO, F.P., WATKINS, R.W., Meteorological Criteria for Standard Project Hurricane and Probable Maximum Hurricane Wind Fields, Gulf and East Coasts of the US, NOAA Tech. Rep. NWS 23, US Department of Commerce, Washington, DC (1979).

[43] HARPER, B.A., Numerical modelling of extreme tropical cyclone winds, J. Wind Eng. Ind. Aerodyn. **83** (1999) 35–47,
https://doi.org/10.1016/S0167-6105(99)00059-8

[44] SHAPIRO, L.J., The asymmetric boundary layer flow under a translating hurricane, J. Atmos. Sci. **40** (1983) 1984–1998,
https://doi.org/10.1175/1520-0469(1983)040<1984:TABLFU>2.0.CO;2

[45] VICKERY, P.J., WADHERA, D., POWELL, M.D., CHEN, Y., A hurricane boundary layer and wind field model for use in engineering applications, J. Appl. Meteor. **48** (2009b) 381–405,
https://doi.org/10.1175/2008JAMC1841.1

[46] FOSTER, R.C., Why rolls are prevalent in the hurricane boundary layer, J. Atmos. Sci. **62** (2005) 2647–2661,
https://doi.org/10.1175/JAS3475.1

[47] SPARKS, P.R., HUANG, Z., Gust factors and surface-to-gradient wind speed ratios in tropical cyclones, J. Wind Eng. Ind. Aerodyn. **89** (2001) 1470–1058,
https://doi.org/10.1016/S0167-6105(01)00098-8

[48] SPARKS, P.R., Wind speeds in tropical cyclones and associated insurance losses, J. Wind Eng. Ind. Aerodyn. **1215** (2003) 1731–1751,
https://doi.org/10.1016/j.jweia.2003.09.018

[49] POWELL, M.D., VICKERY, P.J., REINHOLD, T.A., Reduced drag coefficient for high wind speeds in tropical cyclones, Nature **422** (2003) 279–283,
https://doi.org/10.1038/nature01481

[50] ENGINEERING SCIENCES DATA UNIT, Strong Winds in the Atmospheric Boundary Layer, Part 1: Mean Hourly Wind Speed, ESDU Rep. 82026, ESDU, London, UK (1982).

[51] ENGINEERING SCIENCES DATA UNIT, Strong Winds in the Atmospheric Boundary Layer, Part 2: Discrete Gust Speeds, ESDU Rep. 83045, ESDU, London, UK (1983).

[52] SIMIU, E., SCANLAN, R.H., Wind Effects on Buildings and Structures: Fundamentals and Applications to Design, 3rd edn, Wiley-Interscience, Hoboken, NJ (1996) 688 pp.

[53] KEPERT, J., The dynamics of boundary layer jets within the tropical cyclone core, Part I: linear theory, J. Atmos. Sci. **58** (2001) 2469–2484,
https://doi.org/10.1175/1520-0469(2001)058<2469:TDOBLJ>2.0.CO;2

[54] LARGE, W.G., POND, S.A., Open ocean momentum flux measurements in moderate to strong winds, J. Phys. Oceanography **11** (1981) 324–336,
https://doi.org/10.1175/1520-0485(1981)011<0324:OOMFMI>2.0.CO;2

[55]   BLACK, P.G., et al., Air–sea exchange in hurricanes: Synthesis of observations from coupled boundary layer air–sea transfer experiment, Bull. Am. Meteorol. Soc. **20** (2007) 357–374,
https://doi.org/10.1175/BAMS-88-3-357

[56]   DURST, C.S., Wind speeds over short periods of time, Meteorol. Mag. **89** (1960) 181–186.

[57]   KRAYER, W.R., MARSHALL, R.D., Gust factors applied to hurricane winds, Bull. Am. Meteorol. Soc. **73** (1992) 270–280,
https://doi.org/10.1175/1520-0477(1992)073<0613:GFATHW>2.0.CO;2

[58]   SCHROEDER, J.L., CONDER, M.R., HOWARD, J.R., "Additional insights into hurricane gust factors", 25th Conf. on Hurricanes and Tropical Meteorology, American Meteorological Society, San Diego, CA, 2002.

[59]   SCHROEDER, J.L., SMITH, D.A., Hurricane Bonnie wind flow characteristics as determined from WEMITE, J. Wind Eng. Ind. Aerodyn. **91** (2003) 767–789,
https://doi.org/10.1016/S0167-6105(02)00475-0

[60]   SPARKS, P.R., HUANG, Z., "Wind speed characteristics in tropical cyclones", Wind Engineering into the 21st Century (Proc. 10th Int. Conf. on Wind Engineering, Copenhagen, 21–24 June, 1999), CRC Press, Boca Raton, FL (1999) 343–350.

[61]   VICKERY, P.J., SKERLJ, P.F., Hurricane gust factors revisited, J. Struct. Eng. **131** (2005) 828–832,
https://doi.org/10.1061/(ASCE)0733-9445(2005)131:5(825)

[62]   MILLER, C.A., "Gust factors in hurricane and non-hurricane conditions", 27th Conf. on Hurricanes and Tropical Meteorology, American Meteorological Society, Monterey, CA, 2006.

[63]   MASTERS, F., "Measurement of tropical cyclone surface winds at landfall", 59th Interdepartmental Hurricane Conf., Jacksonville, FL, 2005.

[64]   POWELL, M.D., HOUSTON, S.H., Hurricane Andrew's landfall in South Florida, Part II: Surface wind fields and potential real-time applications, Weather Forecast. **11** (1996) 329–349,
https://doi.org/10.1175/1520-0434(1996)011<0329:HALISF>2.0.CO;2

[65]   WURMAN, J., WINSLOW, J., Intense sub-kilometer-scale boundary layer rolls observed in Hurricane Fran, Science **280** (1998) 555–557,
https://doi.org/10.1126/science.280.5363.555

[66]   McCONOCHIE, J.D., HARDY, T.A., MASON, L.B., Modelling tropical cyclone over-water wind and pressure fields, Ocean Eng. **31** 14–15 (2004) 1757–1782,
https://doi.org/10.1016/j.oceaneng.2004.03.009

[67]   VICKERY, P.J., TWISDALE, L.A., Jr., Wind field and filling models for hurricane wind speed predictions, J. Struct. Eng. **121** (1995) 1700–1709,
https://doi.org/10.1061/(ASCE)0733-9445(1995)121:11(1700)

[68]   WILLOUGHBY, H.E., RAHN, M.E., Parametric representation of the primary hurricane vortex, Part I: Observations and evaluation of the Holland (1980) model, Mon. Weather Rev. **132** (2004) 3033–3048,
https://doi.org/10.1175/MWR2831.1

[69]   VICKERY, P.J., WADHERA, D., Statistical models of the Holland pressure profile parameter and radius to maximum winds of hurricanes from flight-level pressure and H*Wind data, J. Appl. Meteor. Climatol. **47** (2008) 2497–2517, https://doi.org/10.1175/2008JAMC1837.1

[70]   HARPER, B.A., HOLLAND, G.J., "An updated parametric model of tropical cyclone", Proc. 23rd Conf. on Hurricanes and Tropical Meteorology, American Meteorological Society, Dallas, TX, 1999.

[71]   WILLOUGHBY, H.E., DARLING, R.W.R., RAHN, M.E., Parametric representation of the primary hurricane vortex, Part II: A new family of sectional continuous profiles, Mon. Weather Rev. **134** (2006) 1102–1120, https://doi.org/10.1175/MWR3106.1

[72]   KAPLAN, J., DEMARIA, M., A simple empirical model for predicting the decay of tropical cyclone winds after landfall, J. Appl. Meteorol. Climatol. **34** (1995) 2499–2512, https://doi.org/10.1175/1520-0450(1995)034<2499:ASEMFP>2.0.CO;2

[73]   VICKERY, P.J., Simple empirical models for estimating the increase in the central pressure of tropical cyclones after landfall along the coastline of the United States, J. Appl. Meteorol. Climatol. **44** (2005) 1807–1826, https://doi.org/10.1175/JAM2310.1

[74]   WONG, P.W., LIU, K.S., CHAN, J.C.L., CHENG, W.C., TAI, S.L., Distribution of convection associated with tropical cyclones making landfall along the South China coast, Meteorol. Atmos. Phys. **97** (2007) 57–68, https://doi.org/10.1007/s00703-006-0244-1

[75]   VELDEN, C., et al., The Dvorak tropical cyclone intensity estimation technique: A satellite-based method that has endured for over 30 years, Bull. Am. Meteorol. Soc. **87** 9 (2006) 1195–1210, https://doi.org/10.1175/BAMS-87-9-1195

[76]   KNAPP, K.R., KRUCK, M., LEVINSON., D.H., DIAMOND, H.J., NEUMANN, C.L., The International Best Track Archive for Climate Stewardship (IBTRACS) — unifying tropical cyclone data, Bull. Am. Meteorol. Soc. **91** (2010) 363–376, https://doi.org/10.1175/2009BAMS2755.1

[77]   WORLD METEOROLOGICAL ORGANIZATION, Guidelines for Converting Between Various Wind Averaging Periods in Tropical Cyclone Conditions, WMO/TD No. 1555, WMO, Geneva (2010).

[78]   TWISDALE, L.A., VICKERY, P.J., HARDY, M.B., "Uncertainties in the prediction of hurricane windspeeds", Proc. ASCE Conf. on Hurricanes of 1992, Miami, FL, 1993.

[79]   VICKEREY, P.J., TWISDALE, L.A., Prediction of hurricane wind speeds in the United States, J. Struct. Eng. **12** 11 (1995), https://doi.org/10.1061/(ASCE)0733-9445(1995)121:11(1691)

116

[80]   KNUTSON, T.R., TULEYA, R.E., Impact of CO_2-induced warming on simulated hurricane intensity and precipitation: Sensitivity to the choice of climate model and convective parameterization, J. Clim. **17** (2004) 3477–3495,
https://doi.org/10.1175/1520-0442(2004)017<3477:IOCWOS>2.0.CO;2

[81]   WEBSTER, P.J., HOLLAND, G.J., CURRY, J.A., CHANG, H.R., Changes in tropical cyclone number, duration, and intensity in a warming environment, Science **309** (2005) 1844–1846,
https://doi.org/10.1126/science.1116448

[82]   EMANUEL, K.A., Increasing destructiveness of tropical cyclones over the past 30 years, Nature **436** (2005) 686–688,
https://doi.org/10.1038/nature03906

[83]   LANDSEA, C.W., HARPER, B.A., HOARAU, K., KNAFF, J.A., Can we detect trends in extreme tropical cyclones? Science **313** (2006) 452–454,
https://doi.org/10.1126/science.1128448

[84]   LANDSEA, C.W., Counting Atlantic tropical cyclones back to 1900, Eos Trans. Am. Geophys. Union **88** (2007) 197–208,
https://doi.org/10.1029/2007EO180001

[85]   DAILEY, P.S., ZUBA, G., LJUNG, G., DIMA, I.M., GUIN, J., On the relationship between North Atlantic sea surface temperatures and US hurricane landfall risk, J. Appl. Meteor. **48** (2009) 111–129,
https://doi.org/10.1175/2008JAMC1871.1

[86]   VICKERY, P.J., LAVELLE, F.M., "The effects of warm Atlantic Ocean sea surface temperatures on the ASCE 7–10 design wind speeds", Advances in Hurricane Engineering: Learning from Our Past (Proc. ATC–SEI Advances in Hurricane Engineering Conf., Miami, 2012) (JONES, C.P, GRIFFIS, L.G., Eds), ASCE, Reston, VA (2012) 13–22,
https://doi.org/10.1061/9780784412626.002

[87]   BENDER, M.A., et al., Modeled impact of anthropogenic warming on the frequency of intense Atlantic hurricanes, Science **327** 5964 (2010) 454–458,
https://doi.org/10.1126/science.1180568

[88]   INTERGOVERNMENTAL PANEL ON CLIMATE CHANGE, Climate Change 2013 — The Physical Science Basis. Working Group I Contribution to the Fifth Assessment Report of the Intergovernmental Panel on Climate Change (STOCKER, T.F., et al., Eds), Cambridge University Press, Cambridge (2013) 1535 pp,
https://doi.org/10.1017/CBO9781107415324

[89]   TWISDALE, L.A., VICKERY, P.J., "Extreme-wind risk assessment", Probabilistic Structural Mechanics Handbook, Van Nostrand Reinhold, New York (1995) Ch. 20,
https://doi.org/10.1007/978-1-4615-1771-9_20

[90]   BROOKS, H., DOSWELL, C.A., Some aspects of the international climatology of tornadoes by damage classification, Atmos. Res. **56** (2001) 191–201,
https://doi.org/10.1016/S0169-8095(00)00098-3

[91]   CHRISTOPHER, C.B., Extreme Weather: A Guide and Record Book, W.W. Norton, New York (2007).

[92]   FUJITA, T.T., Proposed Characterization of Tornadoes and Hurricanes by Area and Intensity, SMRP Research Paper No. 91. Univ. of Chicago, Chicago, IL (1971).

[93]   FUJITA, T.T., PEARSON, A.D., "Results of FPP classification of 1971 and 1972 tornadoes", Proc. 8th Conf. on Severe Local Storms, American Meteorological Society, Boston, MA, 1973.

[94]   SCHAEFER, J.T., EDWARDS, R., "The SPC tornado/severe thunderstorm database", Proc. 11th Conf. on Applied Climatology, American Meteorological Society, Dallas, TX, 1999, 215–220.

[95]   McCARTHY, D.W., "NWS tornado surveys and the impact on the national tornado database", 1st Symp. on F-Scale and Severe-Weather Damage Assessment, American Meteorological Society, Long Beach, CA, 2003.

[96]   GRAZULIS, T.P., Violent Tornado Climatography, 1880–1982, Rep. NUREG/CR-3670, Nuclear Regulatory Commission, Washington, DC (1984).

[97]   GRAZULIS, T.P., Significant Tornadoes, 1880–1989, Vol. II: A Chronology of Events, The Tornado Project of Environmental Films, St. Johnsburg, VT (1990).

[98]   GRAZULIS, T.P., Significant Tornadoes, 1880–1989, Vol. I: Discussion and Analysis, The Tornado Project of Environmental Films, St. Johnsburg, VT (1990).

[99]   MEHTA, K.C., "Windspeed estimates: Engineering analysis", Symposium on Tornadoes: Assessment of Knowledge and Implications for Man (Proc. Symp. on Tornadoes, Lubbock, 1976) (PETERSON, R.E., Ed.), Texas Tech. Univ. (1976) 89–103.

[100]   TWISDALE, L.A., Tornado data characterization and windspeed risk, J. Struct. Eng. **104** 10 (1978) 1611–1630,
         https://doi.org/10.1061/JSDEAG.0005009

[101]   FIEDLER, B.H., ROTUNNO, R., A theory for the maximum windspeeds in tornado-like vortices, J. Atmos. Sci. **43** (1986) 2328–2340,
         https://doi.org/10.1175/1520-0469(1986)043<2328:ATOTMW>2.0.CO;2

[102]   EDWARDS, R., et al., Tornado intensity estimation: Past, present, and future, Bull. Am. Meteorol. Soc. **94** (2013) 641–653,
         https://doi.org/10.1175/BAMS-D-11-00006.1

[103]   BLUESTEIN, H.B., WEISS, C.C., PAZMANY, A.L., The vertical structure of a tornado near Happy, Texas, on 5 May 2002: High-resolution, mobile, W-band, Doppler radar observations, Mon. Weather Rev. **132** (2004) 2325–2337,
         https://doi.org/10.1175/1520-0493(2004)132<2325:TVSOAT>2.0.CO;2

[104]   BURGESS, D.W., MAGSIG, M.A., WURMAN, J., DOWELL, D.C., RICHARDSON, Y., Radar observations of the 3 May 1999 Oklahoma City tornado, Weather Forecast. **17** (2002) 456–471,
         https://doi.org/10.1175/1520-0434(2002)017<0456:ROOTMO>2.0.CO;2

[105]   WURMAN, J., ALEXANDER, C., ROBINSON, P., RICHARDSON, Y., Low-level winds in tornadoes and potential catastrophic tornado impacts in urban areas, Bull. Am. Meteorol. Soc. **88** (2007) 31–46,
         https://doi.org/10.1175/BAMS-88-1-31

[106] WURMAN, K., KOSIBA, K., ROBINSON, P., In situ, Doppler radar, and video observations of the interior structure of a tornado and the wind–damage relationship, Bull. Am. Meteorol. Soc. **94** 6 (2013) 835–946, https://doi.org/10.1175/BAMS-D-12-00114.1

[107] MARKEE, E.H., BECKERLEY, J.G., Technical Basis for Interim Regional Tornado Criteria.,WASH-1300, US Atomic Energy Commission, Washington, DC (1974).

[108] AMERICAN NUCLEAR SOCIETY, Standard for Estimating Tornado and Extreme Wind Characteristics at Nuclear Power Sites, ANSI/ANS-2.3, ANS, La Grange Park, IL (1983).

[109] AMERICAN NUCLEAR SOCIETY, Estimating Tornado, Hurricane, and Extreme Straight Line Wind Characteristics at Nuclear Facility Sites, ANSI/ANS-2.3-2011, ANS, La Grange Park, IL (2011).

[110] RAMSDELL, J.V., ANDREWS, G.L., Tornado Climatology of the Contiguous United States, Rep. NUREG/CR-4461; PNNL-5679, Nuclear Regulatory Commission, Washington, DC (1986).

[111] RAMSDELL, J.V., RISHELL, J.P., Tornado Climatology of the Contiguous United States, Rep. NUREG/CR-4461, Rev. 2; PNNL-15112, Rev. 1, Nuclear Regulatory Commission, Washington, DC (2007).

[112] THOM, H.C.S., Tornado probabilities, Mon. Weather Rev. **91** (1963) 730–736, https://doi.org/10.1175/1520-0493(1963)091<0730:TP>2.3.CO;2

[113] WEN, Y.-K., CHU, S.-L., Tornado risks and design wind speed, J. Struct. Div. **99** 12 (1973) 2409–2421, https://doi.org/10.1061/JSDEAG.0003666

[114] ABBEY, R.F., Jr., FUJITA, T.T., "Use of tornado path lengths and gradations of damage to assess tornado intensity probabilities", Proc. 9th Conf. on Severe Local Storms, Norman, 1975, American Meteorological Society, Boston, MA (1975) 286–293.

[115] GARSON, R.C., CATALAN, J.M., CORNELL, C.A., Tornado risk evaluation using wind speed profiles, J. Struct. Eng. **101** 5 (1975) 1167–1171, https://doi.org/10.1061/JSDEAG.0004068

[116] McDONALD, J.R., MEHTA, K.C., MINOR, J.E., BEASON, L., Development of a Windspeed Risk Model for the Argonne Natl Lab. Site, Texas Tech.l Univ., Lubbock, TX (1975).

[117] GARSON, R.C., CATALAN, J.M., CORNELL, C.A., Tornado design winds based on risk, J. Struct. Eng. **101** 9 (1975b) 1883–1897, https://doi.org/10.1061/JSDEAG.0004161

[118] WEN, Y.-K., ANG, A.H.E., "Tornado risk and wind loading effects on structures", Proc. 4th Int. Conf. on Wind Effects on Buildings and Structures, London, 1975, Cambridge University Press, Cambridge (1975) 63–74.

[119] TWISDALE, L.A., DUNN, W.L., Probabilistic analysis of tornado wind risks, J. Struct. Eng. **109** 2 (1983) 468–488, https://doi.org/10.1061/(ASCE)0733-9445(1983)109:2(468)

[120]   TWISDALE, L.A., DUNN, W.L., Wind loading risks from multi vortex tornadoes, J. Struct. Eng. **109** 8 (1983) 2016–2022,
https://doi.org/10.1061/(ASCE)0733-9445(1983)109:8(2016)

[121]   COATS, D.W., MURRAY, R.C., Natural Phenomena Hazards Modeling Project: Extreme Wind/Tornado Hazard Models for Department of Energy Sites, UCRL-53526, Rev. 1, Lawrence Livermore Natl Lab., Livermore, CA (1985),
https://doi.org/10.2172/5331368

[122]   BOISSONNADE, A., HOSSAIN, Q., KIMBALL, J., MENSING, R., SAVY, J., Development of a Probabilistic Tornado Wind Hazard Model for the Continental US: Volume I: Main Report, Rep. UCRL-ID-140922, Lawrence Livermore Natl Lab., USDOE (2000),
https://doi.org/10.2172/15013402

[123]   FUJITA, T.T., Tornado and High-Wind Hazards at Savannah River Plant, South Carolina, Lawrence Livermore Natl Lab., Livermore, CA (1980).

[124]   McDONALD, J.R., Assessment of Tornado Mid Straight Wind Risks at the Savannah River Plant Site, Aiken, South Carolina, Lawrence Livermore Natl Lab., Livermore, CA (1982).

[125]   TWISDALE, L.A., HARDY, M.B., Tornado Windspeed Frequency Analysis of the Savannah River Plant, E.I. Dupont de Nemours and Co., Aiken, SC (1985).

[126]   NUCLEAR REGULATORY COMMISSION, Design-Basis Tornado and Tornado Missiles for Nuclear Power Plants, Regulatory Guide 1.76 Revision 1, NRC, Washington, DC (2007).

[127]   TWISDALE, L.A., DUNN, W.L., Tornado Missile Risk Analysis, Rep. EPRI-NP-769, Vols I and II, Electric Power Research Inst., Palo Alto, CA (1978).

[128]   TWISDALE, L.A., DUNN, W.L., Tornado Missile Simulation and Design Methodology, Vol. 1: Simulation Methodology, Design Applications, and TORMIS Computer Code, Rep. EPRI-NP-2005, Electric Power Research Inst., Palo Alto, CA (1981).

[129]   COOK, N.J., Review of errors in archived wind data, Weather **69** 3 (2014) 72–78,
https://doi.org/10.1002/wea.2148

[130]   COOK, N.J., Detecting artefacts in analyses of extreme wind speeds, Wind Struct. **19** 3 (2014) 271–294,
https://doi.org/10.12989/was.2014.19.3.271

[131]   MILLER C., HOLMES, J., HENDERSON, D., GINGER, J., MORRISON, M., The response of the dines anemometer to gusts and comparisons with cup anemometers, J. Atmos. Oceanic Technol. **30** (2013) 1320–1336,
https://doi.org/10.1175/JTECH-D-12-00109.1

[132]   CHOCK, G.Y.K., COCHRAN, L., Erratum to modeling of topographic wind speed effects in Hawaii, J. Wind Eng. Ind. Aerodyn. **93** 8 (2005) 623–638,
https://doi.org/10.1016/j.jweia.2005.06.002

[133] De WEKKER, S.F.J., STEYN, D.G., FAST, J.D., ROTACH, M.W., ZHONG, S., The performance of RAMS in representing the convective boundary layer structure in a very steep valley, Environ. Fluid Mech. **5** (2005) 35–62, https://doi.org/10.1007/s10652-005-8396-y

[134] GOMES, L., VICKERY, B.J., On thunderstorm wind gusts in Australia, Civ. Eng. Trans. Inst. Eng. **18** (1976) 33–39.

[135] GOMES, L., VICKERY, B.J., Extreme wind speeds in mixed wind climates, J. Wind Eng. Ind. Aerodyn. **2** (1977/78) 331–344, https://doi.org/10.1016/0167-6105(78)90018-1

[136] TWISDALE, L.A., VICKERY, P.J., Research on thunderstorm wind design parameters, J. Wind Eng. Ind. Aerodyn. **41–44** (1922) 545–556, https://doi.org/10.1016/0167-6105(92)90461-I

[137] TWISDALE, L.A., VICKERY, P.J., "Analysis of thunderstorm occurrences and windspeed statistics", Proc. 7th US National Conf. on Wind Engineering, Los Angeles, CA, 1993.

[138] LETCHFORD, C., GHOSALKAR, M., "Extreme wind speed climatology in the United States Mid-West", 6th UK Conf. on Wind Engineering, Cranfield Univ., UK, 2004.

[139] LOMBARDO, F.T., MAIN, J.A., SIMIU, E., Automated extraction and classification of thunderstorm and non-thunderstorm wind data for extreme-value analysis, J. Wind Eng. Ind. Aerodyn. **97** (2009) 120–131, https://doi.org/10.1016/j.jweia.2009.03.001

[140] PETERKA, J.A., SHAHID, S., Design gust wind speeds in the United States, J. Struct. Eng. **124** 2 (1998) 207–214, https://doi.org/10.1061/(ASCE)0733-9445(1998)124:2(207)

[141] FUJITA, T.T., The Downburst: Microburst and Macroburst, Department of Geophysical Sciences, Univ. of Chicago, Chicago, IL (1985).

[142] ENGINEERING SCIENCES DATA UNIT, Strong Winds in the Atmospheric Boundary Layer, Part 1: Mean Hourly Wind Speeds, ESDU Rep. 82026, ESDU, London (1993).

[143] ENGINEERING SCIENCES DATA UNIT, Strong Winds in the Atmospheric Boundary Layer, Part 2: Discrete Gust Speeds, ESDU Rep. 83045, ESDU, London (1993).

[144] COOK, N.J., Towards better estimation of extreme winds, J. Wind Eng. Ind. Aerodyn. **9** (1982) 295–323, https://doi.org/10.1016/0167-6105(82)90021-6

[145] MASTERS, F., VICKERY, P.J., BACON, P., RAPPAPORT, E.N., Toward objective standardized intensity estimates from surface wind speed observations, Bull. Am. Meteorol. Soc. **91** (2010) 1665–1681, https://doi.org/10.1175/2010BAMS2942.1

[146] AMERICAN SOCIETY OF CIVIL ENGINEERS, ASCE (7–16) Minimum Design Loads for Buildings and Other Structures, ASCE, New York (2017).

[147]   LECHNER, J.A., LEIGH, S.D., SIMIU, E., Recent approaches to extreme value estimation with application to wind speeds. Part I: The Pickands method, J. Wind Eng. Ind. Aerodyn. **41–44** (1992) 509–519,
https://doi.org/10.1016/0167-6105(92)90457-L

[148]   SIMIU, E., HECKERT, N.A., Extreme wind distribution tails: A "peaks over threshold" approach, J. Struct. Eng. **122** (1996) 539–547,
https://doi.org/10.1061/(ASCE)0733-9445(1996)122:5(539)

[149]   HOLMES, J.D., MORIARTY, W.W., Application of the generalized Pareto distribution to extreme value analysis in wind engineering, J. Wind Eng. Ind. Aerodyn. **83** (1999) 1–10,
https://doi.org/10.1016/S0167-6105(99)00056-2

[150]   DE HAAN, L., "Extreme value statistics", Extreme Value Theory for Applications Vol. 1 (GALAMBOS, J., LECHNER, J., SIMIU, E., Eds), Kluwer, Dordrecht (1994),
https://doi.org/10.1007/978-1-4613-3638-9_1

[151]   NAESS, A., Statistical extrapolation of extreme value data based on the peaks over threshold method, J. Offshore Mech. Arct. Eng. **120** (1998) 91–96,
https://doi.org/10.1115/1.2829529

[152]   COOK, N.J., HARRIS, R.I., Discussion on Application of the generalized Pareto distribution to extreme value analysis in wind engineering by J.D. Holmes, W.W. Moriarty, J. Wind Eng. Ind. Aerodyn. **89** (2001) 215–224,
https://doi.org/10.1016/S0167-6105(00)00063-5

[153]   TWISDALE, L.A., DUNN, W.L., Tornado Missile Simulation and Design Methodology, Vol. 2: Model Verification and Database Updates, Rep. EPRI-NP-2005, Electric Power Research Inst., Palo Alto, CA (1981).

[154]   TWISDALE, L.A., VICKERY, P.J., STECKLEY, A.C., Analysis of Hurricane Windborne Debris Impact Risk for Residential Structures, Rep. 5303, Applied Research Associates, Raleigh, NC (1996).

[155]   SIMIU, E., CORDES, M., Tornado Borne Missile Speeds, NBSIR 76-1050, National Bureau of Standards, Washington, DC (1976),
https://doi.org/10.6028/NBS.IR.76-1050

[156]   NUCLEAR REGULATORY COMMISSION, Missiles Generated by Natural Phenomena Standard Review Plan 3.5.1.4, Rep. NUREG-0800, NRC, Washington, DC (1981).

[157]   KENNEDY, R.P., et al., Design and Evaluation Guidelines for Department of Energy Facilities Subjected to Natural Phenomena Hazards, USDOE, Washington, DC (1989),
https://doi.org/10.2172/6461594

[158]   TWISDALE, L.A., Probability of facility damage from extreme wind effects, J. Struct. Eng. **114** (1989) 2190–2209,
https://doi.org/10.1061/(ASCE)0733-9445(1988)114:10(2190)

[159]   GOODMAN, J., KOCH, J.E., The probability of a tornado missile hitting a target, Nucl. Eng. Des. **75** (1982) 125–155,
https://doi.org/10.1016/0029-5493(83)90086-9

[160] JOHNSON, B., et al., Tornado Hazard to Production Reactors at Savannah River Plant, Science Applications International, San Diego, CA (1985).

[161] LEWELLEN, W.S., "Theoretical models of the tornado vortex", Symposium on Tornadoes: Assessment of Knowledge and Implications for Man (Proc. Symp. on Tornadoes, Lubbock, 1976) (PETERSON, R.E., Ed.), Texas Tech. Univ. (1976) 107–144.

[162] DAVIES-JONES, R.P., "Tornado dynamics", Thunderstorm Morphology and Dynamics (KESSLER, E., Ed.), Univ. of Oklahoma Press, Norman, OK (1986) 197–236.

[163] ROTZ, J.V., LINDERMAN, R.B., YEH, G.C.K., Design of Structures for Missile Impact, Tech. Rep. BC-TOP-9, Rev. 2, Bechtel Power Corp., San Francisco, CA (1974) 88 pp,
https://doi.org/10.2172/4242097

[164] FUJITA, T.T., Workbook of Tornadoes and High Winds, SMRP Research Paper 165, Univ. of Chicago, Chicago, IL (1978).

[165] GRAYSON, M., PANG, W., SCIFF, S., Three-dimensional probabilistic wind-borne debris trajectory model for building envelope impact risk assessment, J. Wind Eng. Ind. Aerodyn. **102** (2012) 22–35,
https://doi.org/10.1016/j.jweia.2012.01.002

[166] SIMIU, E., POTRA, F., Technical Basis for Regulatory Guidance on Design-Basis Hurricane-Borne Missile Speeds for Nuclear Power Plants, Rep. NUREG/CR-7004, Office of Nuclear Regulatory Research, Nuclear Regulatory Commission Washington, DC (2011).

[167] HOLMES, J.D., Trajectories of spheres in strong winds with application to windborne debris, J. Wind Eng. Ind. Aerodyn. **92** (2004) 9–22,
https://doi.org/10.1016/j.jweia.2003.09.031

[168] TWISDALE, L.A., DUNN, W.L., DAVIS, T.L., Tornado missile transport analysis, Nucl. Eng. Des. **51** (1979) 295–308,
https://doi.org/10.1016/0029-5493(79)90096-7

[169] ETKIN, B., Dynamics of Atmospheric Flight, John Wiley and Sons, New York, NY (1972).

[170] REDMANN, G.H., RADBILL, J.R., MARTE, J.E., DERGARABEDIAN, P., Wind Field and Trajectory Models for Tornado-Propelled Objects, Rep. EPRI-NP-748, Electric Power Research Inst., Palo Alto, CA (1978).

[171] McDONALD, J.R., "Incredible tornado-generated missiles", Proc. 4th US National Conf. on Wind Engineering, Seattle, WA, 1981.

[172] REDMANN, G.H., RADBILL, J.R., MARTE, J.E., DERGARABEDIAN, P., FENDELL, F.E., Wind Field and Trajectory Models for Tornado Propelled Objects, Tech. Rep. 1, Electrical Power Research Institute, Palo Alto, CA (1976).

[173] LIN, N., LETCHFORD, C.W., HOLMES, J.D., Investigation of plate-type windborne debris. Part I: Experiments in wind tunnel and full scale, J. Wind Eng. Ind. Aerodyn. **94** (2006) 51–76,
https://doi.org/10.1016/j.jweia.2005.12.005

[174]   HOLMES, J.D., LETCHFORD, C.W., LIN, N., Investigations of plate-type windborne debris. Part II: Computed trajectories, J. Wind Eng. Ind. Aerodyn. **94** (2006) 21–39,
https://doi.org/10.1016/j.jweia.2005.10.002

[175]   TACHIKAWA, M., A method for estimating the distribution range of trajectories of wind-borne missiles, J. Wind Eng. Ind. Aerodyn. **29** (1988) 175–184,
https://doi.org/10.1016/0167-6105(88)90156-0

[176]   HOLMES, J.D., BAKER, C.J., TAMURA, Y., Tachikawa number: a proposal, J. Wind Eng. Ind. Aerodyn. **94** (2006) 41–47,
https://doi.org/10.1016/j.jweia.2005.10.004

[177]   STEPHENSON, A.E., Full-Scale Tornado-Missile Impact Tests, Rep. EPRI-NP-440, Electric Power Research Inst., Palo Alto, CA (1977).

[178]   BERRIAUD, C., SOKOLOVSKY, A., DULAC, J., GUERAUD, R., LABROT, R., Local behaviour of reinforced concrete walls under missile impact, Nucl. Eng. Des. **45** (1978) 457–469,
https://doi.org/10.1016/0029-5493(78)90235-2

[179]   VASSOLLO, F.A., Missile Impact Testing of Reinforced Concrete Panels, prepared for Bechtel Power Corp., Calspan Corp., Buffalo, NY (1975).

[180]   ROTZ., J.V., "Results of missile impact tests on reinforced concrete panels", Proc. 2nd Specialty Conf. on Structural Design of Nuclear Plant Facilities, New Orleans, LA, Vol. 1A (1975) 720–738.

[181]   McDONALD, J.R., "Impact resistance of common building materials to tornado missiles", Proc. 6th US National Conf. on Wind Engineering, Houston, TX, 1989, J. Wind Eng. Ind. Aerodyn. **36** (1990) 717–724,
https://doi.org/10.1016/0167-6105(90)90069-O

[182]   AMERICAN SOCIETY OF CIVIL ENGINEERS, Structural Analysis and Design of Nuclear Plant Facilities, ASCE58, New York (1980).

[183]   AMERICAN SOCIETY OF CIVIL ENGINEERS, Impactive and Impulsive Loads (Proc. 2nd ASCE Conf. on Civil Engineering and Nuclear Power, Knoxville, TN, 1980), Vol. 4, ASCE, New York (1980).

[184]   SIMIU, E., SCANLAN, R.H., Wind Effects on Structures, 2nd edn, Wiley-Interscience, New York (1986).

[185]   MINOR, J.E., McDONALD, J.R., MEHTA, K.C., Tornado: An Engineering-Oriented Perspective, Tech. Memo. ERL-NSSL-82, NOAA, Boulder, CO (1977),
https://doi.org/10.2172/6624980

[186]   GREGORY, W.S., SMITH, P.R., DUERRE, K.H., "Effects of tornadoes on mechanical systems", Symposium on Tornadoes: Assessment of Knowledge and Implications for Man (Proc. Symp. on Tornadoes, Lubbock, 1976) (PETERSON, R.E., Ed.), Texas Tech. Univ. (1976) 313–328.

[187]   NUCLEAR REGULATORY COMMISSION, Standard Review Plan for the Review of Safety Analysis Reports for Nuclear Power Plants: LWR Edition, Rep. NUREG-0800, Section 3.5.1.4, Missiles Generated by Tornadoes and Extreme Winds, Rev.0, NRC, Washington, DC (1975).

[188]   SCIAUDONE, J.C., TWISDALE, L.A., BANIK, S.S., MIZZEN, D.R., "High wind PRA plant walkdown insights and recommendations", Proc. Int. Topical Mtg on Probabilistic Safety Assessment and Analysis (PSA 2015), Sun Valley, ID (2015).

[189]   NUCLEAR REGULATORY COMMISSION, Design-Basis Flood Estimation for Site Characterization at Nuclear Power Plants in the USA, Rep. NUREG/CR-7046, NRC, Washington, DC (2011).

[190]   AUTORITÉ DE SÛRETÉ NUCLÉAIRE, Protection of Basic Nuclear Installations Against External Flooding, Guide No. 13, ASN, Montrouge, France (2013).

[191]   INTERNATIONAL ATOMIC ENERGY AGENCY, Tsunami and Seiche Hazards in Site Evaluation for Nuclear Installations, Safety Reports Series No. 116, IAEA, Vienna (2021).

[192]   AMERICAN NATIONAL STANDARDS INSTITUTE/AMERICAN NUCLEAR SOCIETY, Determining Design Basis Flooding at Power Reactor Sites, Rep. ANSI/ANS-2.8-1992, ANSI/ANS, New York (1992).

[193]   WORLD METEOROLOGICAL ORGANIZATION, Manual on Estimation of Probable Maximum Precipitation (PMP), Rep. No. 1045, WMO, Geneva (2009).

[194]   LORD, D.W., "FERC need for probabilistic flood hazard analysis (PFHA) — journey from deterministic to probabilistic", Proc. Workshop on Probabilistic Flood Hazard Assessment (PFHA), Maryland, 2013.

[195]   CALDWELL, R., SANKOVICH, V., ENGLAND, J., Synthesis of Extreme Storm Rainfall and Probable Maximum Precipitation in the South Eastern US Pilot Region, US Department of the Interior, Bureau of Reclamation, Technical Service Centre, Denver, CO (2011).

[196]   COLES, S., An Introduction to Statistical Modeling of Extreme Values, Springer Series in Statistics, Springer, Berlin (2001),
https://doi.org/10.1007/978-1-4471-3675-0

[197]   HOSKING, J.R.M., WALLIS, J.R., Regional Frequency Analysis — An Approach Based on L-Moments, Cambridge University Press, Cambridge (1997),
https://doi.org/10.1017/CBO9780511529443

[198]   DIXON, M.J., TAWN, J.A., Extreme Sea-Levels at UK A-Class Sites: Site-by-Site Analyses, Internal Document No. 65, Proudman Oceanographic Laboratory, UK (1997).

[199]   INTERNATIONAL ATOMIC ENERGY AGENCY, Seismic Hazards in Site Evaluation for Nuclear Installations, IAEA Safety Standards Series No. SSG-9 (Rev.1), IAEA, Vienna (2022).

[200]   BAKER, J.W., BRADLEY, B.A., STAFFORD, P.J., Seismic Hazard and Risk Analysis, Cambridge University Press, Cambridge (2021),
https://doi.org/10.1017/9781108425056

[201]   BARDET, L., DULUC, C.-M., REBOUR, V., L'HER, J., Regional frequency analysis of extreme storm surges along the French coast, Nat. Hazards Earth Syst. Sci. **11** (2011) 1627–1639,
https://doi.org/10.5194/nhess-11-1627-2011

[202]   BERNARDARA, P., ANDREEWSKY, M., BENOIT, M., Application of regional frequency analysis to the estimation of extreme storm surges, J. Geophys. Res. **116** C2 (2011),
https://doi.org/10.1029/2010JC006229

[203]   EurOtop, Manual: Wave Overtopping of Sea Defences and Related Structures, 2nd edn (2018),
www.overtopping-manual.com

[204]   NUCLEAR REGULATORY COMMISSION, Guidance for Performing a Tsunami, Surge, or Seiche Hazard Assessment, Interim Staff Guidance, JLD-ISG-2012-06, NRC, Washington, DC (2013).

[205]   NUCLEAR REGULATORY COMMISSION, The Estimation of Very-Low Probability Hurricane Storm Surges for Design and Licensing of Nuclear Power Plants in Coastal Areas, Rep. NUREG/CR-7134, Office of Nuclear Regulatory Research, NRC, Washington, DC (2012).

[206]   US ARMY COASTAL ENGINEERING RESEARCH CENTER, Shore Protection Manual, 4th edn, US Army Coastal Engineering Research Center, Washington, DC (1984).

[207]   ABILY, M., et al., "Global sensitivity analysis with 2D hydraulic codes: Applied protocol and practical tool", Proc. SimHydro 2014: Modelling of Rapid Transitory Flows, Sophia Antipolis, France, 2014,
https://doi.org/10.1051/lhb/20150050

[208]   PAQUET, E., GARAVAGLIA, F., GARÇON, R., GAILHARD, J., The SCHADEX method: A semi-continuous rainfall–runoff simulation for extreme flood estimation, J. Hydrol. **495** (2013) 23–37,
https://doi.org/10.1016/j.jhydrol.2013.04.045

[209]   SCHAEFER, M.G., BARKER, B.L., Stochastic Event Flood Model — User Manual, MGS Engineering Consultants, Olympia, WA (2009).

[210]   INTERNATIONAL COMMISSION ON LARGE DAMS, Dam Break Flood Analysis — Review and Recommendations, Bulletin 111, ICOLD, Paris (1998).

ABBREVIATIONS

APC	atmospheric pressure change
ASCE	American Society of Civil Engineers
DAPPLE	Damage Area Per Path Length
DBF	design basis flood
DOF	degrees of freedom
EF scale	Enhanced Fujita scale
ESDU	Engineering Sciences Data Unit
F scale	Fujita scale
GPD	generalized Pareto distribution
HURDAT	hurricane database
IBTrACS	International Best Track Archive for Climate Stewardship
PFHA	probabilistic flood hazard assessment
PMF	probable maximum flood
PMP	probable maximum precipitation
PSHA	probabilistic seismic hazard analysis
RMW	radius to maximum winds
SPC	Storm Prediction Center
TORMIS	tornado missile computer code
WMO	World Meteorological Organization

CONTRIBUTORS TO DRAFTING AND REVIEW

Abe, H.	Nuclear Regulation Authority, Japan
Agrawal, M.K.	Bhabha Atomic Research Centre, India
Ahmad, M.	Pakistan Atomic Energy Commission, Pakistan
Altinyollar, A.	International Atomic Energy Agency
Basu, P.C.	Consultant, India
Blahoianu, A.	Consultant, Canada
Chokshi, N.C.	Consultant, United States of America
Contri, P.	International Atomic Energy Agency
Cook, C.B.	United States Nuclear Regulatory Commission, United States of America
Devlin, S.	United States Nuclear Regulatory Commission, United States of America
Ebisawa, K.	Central Research Institute of Electric Power Industry, Japan
Fleming, K.N.	KNF Consulting Services LLC, United States of America
Freijo, J.L.	Comisión Nacional de Energía Atómica, Argentina
Guohan, C.	National Nuclear Safety Administration, China
Hibino, K.	International Atomic Energy Agency
Holmes, J.	JDH Consulting, Australia
Jimenez, A.	Consejo de Seguridad Nuclear, Spain
Katona, T.	Consultant, Hungary
Letchford, C.	Rensselaer Polytechnic Institute, United States of America

Lonkhuyzen, W.V.	Authority for Nuclear Safety and Radiation Protection, Kingdom of the Netherlands
Lusse, L.	South African Nuclear Energy Corporation, South Africa
Madona, A.	ITER-Consult, Italy
Mahmood, H.	Consultant, Pakistan
Malleron, N.	Électricité de France, France
Munson, C.	United States Nuclear Regulatory Commission, United States of America
Nefedov, S.S.	Rosenergoatom, Russian Federation
Nomura, S.	Nuclear Regulation Authority, Japan
Peterka, J.A.	Jon Peterka Engineering LLC, United States of America
Pino, G.S.	ITER-Consult, Italy
Pisharady, A.S.	Atomic Energy Regulatory Board, India
Ravikiran, A.	Bhabha Atomic Research Centre, India
Ravindra, M.K.	MK Ravindra Consulting, United States of America
Rebour, V.	Institut de Radioprotection et de Sûreté Nucléaire, France
Roshan, A.D.	Atomic Energy Regulatory Board, India
Roy, S.M.	Atomic Energy Regulatory Board, India
Samaddar, S.K.	International Atomic Energy Agency
Sanchez-Cabanero, J.	Consejo de Seguridad Nuclear, Spain
Sorel, V.	Électricité de France, France
Ulla, V.	Radiation and Nuclear Safety Authority, Finland
Välikangas, P.	Radiation and Nuclear Safety Authority, Finland
Vickery, P.J.	Applied Research Associates, Australia
Yamanaka, Y.	Tokyo Electric Power Company, Japan

Consultants Meetings

Vienna, Austria: 5–8 March 2013
Rockville, Maryland, United States of America: 11–14 June 2013
Monaco: 21–24 October 2013

IAEA
International Atomic Energy Agency

ORDERING LOCALLY

IAEA priced publications may be purchased from the sources listed below or from major local booksellers.

Orders for unpriced publications should be made directly to the IAEA. The contact details are given at the end of this list.

NORTH AMERICA

Bernan / Rowman & Littlefield
15250 NBN Way, Blue Ridge Summit, PA 17214, USA
Telephone: +1 800 462 6420 • Fax: +1 800 338 4550
Email: orders@rowman.com • Web site: www.rowman.com/bernan

REST OF WORLD

Please contact your preferred local supplier, or our lead distributor:

Eurospan Group
Gray's Inn House
127 Clerkenwell Road
London EC1R 5DB
United Kingdom

Trade orders and enquiries:
Telephone: +44 (0)176 760 4972 • Fax: +44 (0)176 760 1640
Email: eurospan@turpin-distribution.com

Individual orders:
www.eurospanbookstore.com/iaea

For further information:
Telephone: +44 (0)207 240 0856 • Fax: +44 (0)207 379 0609
Email: info@eurospangroup.com • Web site: www.eurospangroup.com

Orders for both priced and unpriced publications may be addressed directly to:
Marketing and Sales Unit
International Atomic Energy Agency
Vienna International Centre, PO Box 100, 1400 Vienna, Austria
Telephone: +43 1 2600 22529 or 22530 • Fax: +43 1 26007 22529
Email: sales.publications@iaea.org • Web site: www.iaea.org/publications

In recent years, significant experience of the effects of high wind and flooding on nuclear installations has been gained worldwide. These phenomena may simultaneously affect all the structures, systems and components important to safety at a nuclear installation site. By detailing the methodologies and providing case studies for the evaluation of meteorological and hydrological hazards, this publication supports IAEA Safety Standards Series No. SSG-18, Meteorological and Hydrological Hazards in Site Evaluation for Nuclear Installations. In the first part of the publication, wind hazards relating to tropical cyclones, tornadoes, extratropical storms, thunderstorms and wind-borne debris are discussed. The second part covers external flooding hazards (excluding tsunamis) relating to wind induced coastal flooding, wind generated waves on rivers, extreme precipitation and runoff events and the sudden release of impounded water.